OXYCOMBUSTION OF SYNTHETIC GAS IN AN OXYGEN TRANSPORT REACTOR (OTR)

BY

SALAUDEEN SHAKIRUDEEN ALADE

A Thesis Presented to the
DEANSHIP OF GRADUATE STUDIES

KING FAHD UNIVERSITY OF PETROLEUM & MINERALS

DHAHRAN, SAUDI ARABIA

In Partial Fulfillment of the
Requirements for the Degree of

MASTER OF SCIENCE

In

MECHANICAL ENGINEERING

OCTOBER, 2015

KING FAHD UNIVERSITY OF PETROLEUM AND MINERALS

DHAHRAN 31261, SAUDI ARABIA

DEANSHIP OF GRADUATE STUDIES

This thesis, written by **Salaudeen Shakirudeen Alade** under the direction of his thesis advisor and approved by his thesis committee, has been presented to and accepted by the Dean of Graduate Studies, in partial fulfillment of the requirements for the degree of **MASTER OF SCIENCE in MECHANICAL ENGINEERING**.

Thesis committee

Dr. Mohamed A. Habib (Advisor)

Dr. Esmail M. A. Mokheimer (Member)

Dr. Rached Ben-Mansour (Member)

Dr. Zuhair Gasem

Department Chairman

Dr. Salam A. Zummo

Dean of Graduate Studies

22/12/15

Date

Dedicated to

My beloved parents, siblings for their constant supports

And to

The less privileged in the whole world

ACKNOWLEDGEMENTS

All approbations and adorations are due to Almighty Allah, who, in His infinite mercy has made it possible for me to go this far in life. I thank Him for making it possible to conclude my Masters in King Fahd University of Petroleum and Minerals, Saudi Arabia successfully.

I would like to deeply extend my appreciation to my parents Mr. and Mrs. Salaudeen. I am nothing without them. They expended a lot on me from my childhood despite the family background. They are the best. Their moral, spiritual and financial supports are highly appreciated. I will also like to show my sincere gratitude to my siblings, Mr. AbdulGaniy Salaudeen, Mr. Sharafadeen Salaudeen, Mr. Ismaheel Salaudeen and Miss Basirah Salaudeen.

My thesis advisor, Dr. Mohamed Habib is more than just an advisor. His guide, moral, spiritual and financial supports, motivations, understanding, recommendations, criticisms and corrections are far more than expectations. Despite his tight schedules, he made my thesis research a reality. My appreciations to him cannot be overemphasized. Similarly, my thesis work will not be possible without the immense contributions of my MS thesis committee members, Dr. Esmail M. A. Mokheimer and Dr. Rached Ben-Mansour. I so much appreciate their contributions in my research. Furthermore, I will like to appreciate all my professors in KFUPM, who taught me various courses during my Masters. Many thanks is due to the combustion group of KFUPM especially Dr. Medhat Nemitallah, who gave a lot of assistance during my research. In addition, Dr. Yinka Sanusi is highly appreciated for all his assistance in my work.

I would also like to acknowledge the support from King Fahd University of Petroleum and Minerals, Saudi Arabia for giving me the opportunity to study for free, and the Kingdom of Saudi Arabia for allowing these initiatives.

TABLE OF CONTENTS

LIST OF TABLES

LIST OF FIGURES

THESIS ABSTRACT (ENGLISH)

Full Name: Salaudeen Shakirudeen Alade

Thesis Title: Oxycombustion of synthetic gas in an oxygen transport reactor (OTR)

Major Field: Mechanical Engineering

Date of Degree: October, 2015

Fossil fuels are used by mankind to satisfy energy demands and they provide very significant fraction of the world energy. The use of fossil fuels involves some adverse effects which include the emission of CO_2. Oxyfuel combustion is a very promising technology compared to other carbon capture methods. It involves combustion with only oxygen, resulting in exhaust gas that comprises CO_2 and H_2O. H_2O can be easily separated using condensation, which is a simple cooling process. To avoid the energy penalties associated with cryogenic air separation, oxygen separation is achieved with the use of oxygen transport reactor with dense, nonporous, mixed ionic-conducting membrane. The present work provides a study of the permeation potential of LSCF-6428 membrane with a reactive gas, syngas, which comprises CO and H_2.

The present work utilizes syngas generated from solar thermal reforming of methane and then burn the syngas in an Oxygen Transport Reactor (OTR). Computational Fluid Dynamic (CFD) calculations were performed using FLUENT 14.0 software, where UDF that enables the transfer of oxygen from the feed to the sweep zone was written in C++, then compiled and hooked to the FLUENT software. Two models were utilized to study the oxycombustion characteristics of synthetic gas, which serves as the fuel in addition to CO_2 in the reactor, serving as the diluent. The first model is for the permeation (UDF) while the second model is for the syngas reaction kinetics.

The models of oxygen permeation and reaction kinetics have been validated against the available experimental data under similar oxycombustion conditions, and there are very good agreements between the numerical results and recorded experimental data. A selective wall serves as the dense, non-porous membrane (ITM), and it separates the two computational zones considered in this work, the feed and sweep zones. Permeation of oxygen appears from region of higher partial pressure to region of lower partial pressure. The performance of the membrane is affected by temperature, gas flow rates and the differences in partial pressures of oxygen across the membrane.

Considering reactive flow conditions, the effects of inlet temperature, CO_2 circulation, fuel composition and sweep gas flux on oxygen permeation and combustion temperature are studied. Comparison between the reactive and non-reactive case showed that the reactive has more oxygen permeation potential than the non-reactive case, with flux of about four times the non-reactive case. It was also found that increase in inlet temperature, inlet fuel concentration, inlet hydrogen concentration and sweep flow rate result in high combustion temperature and improved oxygen permeation flux.

THESIS ABSTRACT (ARABIC)

ألاسم: صلاح الدين شاكر الدين ألادي

عنوان الرسالة:الحرق بواسطة الاوكسجين للغاز الصناعي في مفاعل نقل الاوكسجين (OTR)

التخصص: هندسة ميكانيكية

التاريخ: أكتوبر 2015

استخدمت البشرية الوقود الاحفوري لتلبية الطلب على الطاقة ويوفر الوقود الاحفوري جزءا كبير جدا من الطاقة في العالم. يحتوي استخدام الوقود الاحفوري على بعض الاثار السلبية التى تشمل انبعاثات ثاني اكسيد الكربون. يعتبر احتراق الوقود بالأوكسجين تقنية واعدة جدا مقارنة مع الطرق الاخرى لاحتجاز الكربون. بحيث يكون فيها الاحتراق مع الاوكسجين فقط مما يؤدي الى غاز عادم يحتوي على ثانى أكسيد الكربون و بخار الماء. يمكن فصل بخار الماء بسهولة باستخدام ألتكثيف وهي عملية تبريد بسيطة. لتجنب عقوبات الطاقة المرتبطة بفصل الهواء ألبارد تم تحقيق فصل الأكسجين باستخدام مفاعل نقل الأكسجين بواسطة غشاء ايوني خلط كثيف و مسامي. يقدم العمل الحالي دراسة لإمكانية تخلل غشاء LSCF-6428 باستخدام غاز نشت غاز صناعي الذي يضم أول أكسيد الكربون الهيدروجين.

يستخدم العمل الحالي يستخدم الغاز الصناعي المتولد من الطاقة الشمسية الحرارية من اعادة تكوين الميثان ثم حرق الغاز الصناعي في مفاعل نقل الأكسجين (OTR). أجريت حسابات الموائع الحركية حاسوبيا (CFD) باستخدام برنامج FLUENT 14.0, حيث تم كتابة UDF التي تمكن من نقل الأكسجين من منطقة التغذية إلى منطقة الازالة بلغة C ++، ثم تم تجميعها ودمجها إلى برنامج FLUENT. وتم استخدام نموذجين لدراسة خصائص الحرق بواسطة الاوكسجين للغاز ألصناعي والتي هي بمثابة الوقود بالإضافة إلى ثانى أكسيد الكربون في ألمفاعل بوصفه مخفف. النموذج الأول هو نفاذية (UDF) في حين أن النموذج الثاني هو لحركية التفاعل للغاز الصناعي.

تم التحقق من صحة نماذج نفاذية الأكسجين وحركية التفاعل بمقارنتها مع البيانات التجريبية المتاحة في نفس ألظروف وهناك تشابه جيد جدا بين النتائج العددية والبيانات التجريبية المسجلة. يخدم جدار انتقائية كغشاء (ITM) كثيف غير قابل للاختراق ويفصل بين المنطقتين الحسابيتين المعتبرتين في هذه ألدراسة وهما منطقة التغذية ومنطقة الازالة. يبدأ ظهور تخلل الأكسجين من المنطقة عالية الضغط الجزئي الى المنطقة منخفضة الضغط الجزئي. يتأثر أداء الغشاء بدرجات الحرارة ومعدلات تدفق الغاز والاختلاف في الضغط الجزئي للأكسجين عبر الغشاء.

وبالنظر إلى ظروف التدفق ألنشط تم دراسة تأثيرات درجة الحرارة الداخلة وتدوير ثانى أكسيد الكربون و احتراق الوقود وتدفق الغاز المطرود على نفاذ الأكسجين ودرجة حرارة احتراقه. وأظهرت المقارنة بين الحالة النشطة والغير نشطة أن في الحالة النشطة احتمالية تخلل الاكسجين اكبر بحوالي أربعة أضعاف من

الحالة غير النشطة. وتبين أيضا أن زيادة درجة الحرارة في المدخل و تركيز الوقود الداخل و تركيز الهيدروجين الداخل و معدل تدفق الازالة يؤدي الى ارتفاع درجة حرارة الاحتراق وتحسين تدفق تخلل الأوكسجين.

CHAPTER 1

INTRODUCTION

Energy is vital to human existence and indispensable for socio-economic development of any nation. It is the bedrock of industrialization and development, fossil fuels are used by mankind basically to satisfy energy demands and they provide very significant fraction of the world energy demands. Although fossil fuels are in abundant supply and are used by man in heating, transportation and energy generation, unfortunately, the use of fossil fuels involve some adverse effects. Prominent among which is the emission of green-house gases, predominantly carbon dioxide (CO_2). It significantly contributes to global warming and consequently causing climatic change. This has called for international policies like the Kyoto protocol and Copenhagen summit that set limits on greenhouse gases (GHG) emission [1]**.**

Alternative energy sources like nuclear power and renewable energy are carbon neutral and can present a favourable condition by reducing CO_2 emissions to the atmosphere. Unfortunately, they are not yet in abundant supply to meet mankind's demand. Extensive research and work are still needed to make them available in ample quantity to cater for our energy demands. Fossil fuels are, therefore, likely to remain as our major energy sources.

Carbon capture technologies are needed to enable the continuing usage of fossil fuels, yet decreasing the CO_2 emitted to the atmosphere, and thereby mitigating climatic changes. Many methods have been proposed for carbon capture both numerically and experimentally [2] **.** Some involve the separation of CO_2 from the flue gases after combustion process. This is referred to post combustion carbon capture. Others involve decarbonation process that involves the removal of

carbon before the combustion process commence. Hence, the name pre-combustion carbon capture, and thus resulting in zero carbon dioxide formation during the combustion step. In this case, the fuel reacts with air or oxygen to produce synthetic gas (CO and H_2). The gas mixture is further passed through a shift reaction to produce CO_2 and H_2 as the products at high pressure and temperature. The produced hydrogen can be used as fuel elsewhere like in a plant for generating electricity, while CO_2 is separated for sequestration.

Among the methods available for carbon capture, oxyfuel combustion is a very promising technology [3]. It finds ready application in power generation plants. It involves burning of fuel in pure oxygen. The oxygen is separated from air using different methods like cryogenics air separation or using membrane. The exhaust gases from oxyfuel combustion contain mainly CO_2 and H_2O; which can be separated by condensation processes and the CO_2 can be stored for other purposes.

1.1 Problem Statement

This thesis research aimed at studying the oxycombustion characteristics of synthetic gas in an oxygen transport reactor (OTR). The OTR has a tubular shape and is surrounded by air in an annulus. A mixture of synthetic gas (CO/H_2) and CO_2 (both serving as sweep gas) is introduced from one side (permeate side) and air is introduced from the other side (feed side) of the membrane. Oxygen, then, separates from the air; the separated O_2 permeates through the membrane wall of the reactor and reacts with the fuel mixture. Thereby, leads to oxycombustion of syngas in the combustion chamber. The combustion products (CO_2 and H_2O) are produced at the permeate side of the combustor. The current work focuses on the following:

1. Investigating oxycombustion of syngas numerically in an oxygen transport reactor

2. Investigating the influence of combustion of syngas in the OTR on O_2 permeation flux through the membrane.

3. Investigating the effect of radiation on the temperature field and oxygen permeation flux.

1.2 Objectives

The specific objectives of this research work are listed below:

1. To study the characteristics of oxycombustion of syngas

2. To develop a numerical model for oxygen permeation in a syngas oxygen transport reactor.

3. To study the effects of reaction on the oxygen permeation flux across the membrane.

4. To study the effects of inlet temperature on the oxycombustion.

5. To study the effects of syngas composition (hydrogen and CO contents) on the oxygen permeation.

6. To study the effects of air and permeate gas flow rates on the O_2 permeation flux.

7. To study the effects of CH_4 inclusion in the syngas.

CHAPTER 2

LITERATURE REVIEW

2.1 Carbon capture and CO_2 storage

Various techniques are used in carbon capture as well as geographical storage. Gibbins and Chalmers [4] identified three main ways through which carbon capture can be achieved: pre-combustion, post combustion and oxyfuel combustion capture. Although energy required for pre-combustion capture is lower than post-combustion, but the post-combustion has been studied to have higher thermal efficiency for electricity generation.

Pre-combustion carbon capture can be achieved from the partial oxidation of fuel and then shift reaction. As the name implies, it involves decarbonation of the fuel by removing carbon from fuel before combustion process, this results in no CO_2 during the combustion stage. The gas mixture formed (CO and H_2) is then passed through shift reaction to produce H_2 and CO_2 at elevated pressure and temperature, from which the CO_2 can be captured. The processes involved in pre-combustion are shown in Figure 1.

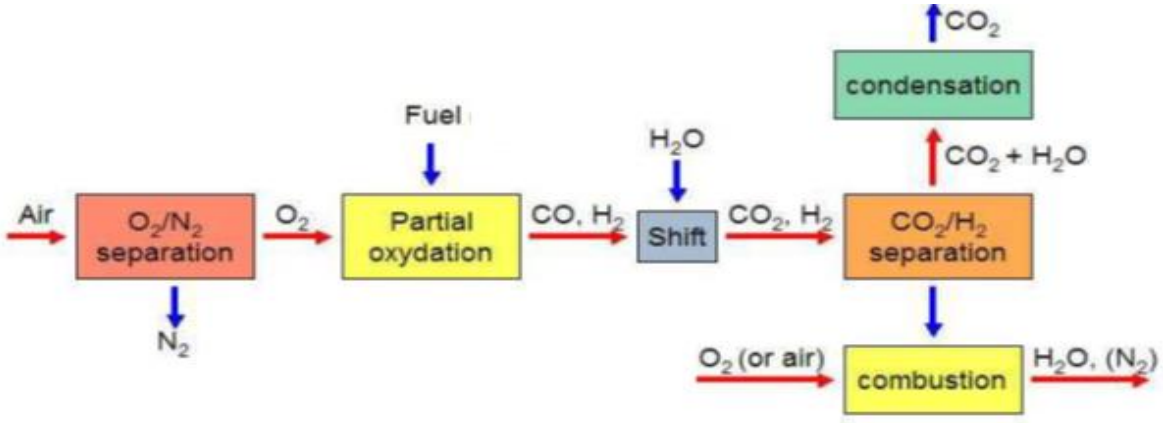

Figure 1: Pre-combustion processes

In post-combustion, the CO_2 removal occurs by chemical absorption [5] after the combustion process. The absorption process involves scrubbing the flue gas with an amine solution (alkanolamine). This forms an amine-CO_2 complex. The complex formed is, then, heated to release pure CO_2. Oxyfuel combustion capture on the other hand is realized by first separating oxygen from air, and then combustion takes place to produce CO_2 and H_2O. The capture efficiency of oxyfuel combustion is around 90% [6]. To completely explore the oxycombustion potential, it is suggested that further research will still be necessary on some factors and effects of oxyfuel combustion like level of corrosion at different temperatures, oxygen concentration levels, quality of ash, prediction of the amount of oxides of sulphur and nitrogen emitted, and also operability [6].

Storage of the captured carbon is also very important in reducing carbon emissions to the environment. Carbon storage can be achieved in oil fields, abandoned gas fields or into saline aquifers [4]. The use of the mineral called serpentinite, which reacts with CO_2 and produce a magnesium compound, is also a good form of storing CO_2 [7]. The principles of operations of the three main CO_2 capture technologies are summarized as shown in Figure 2.

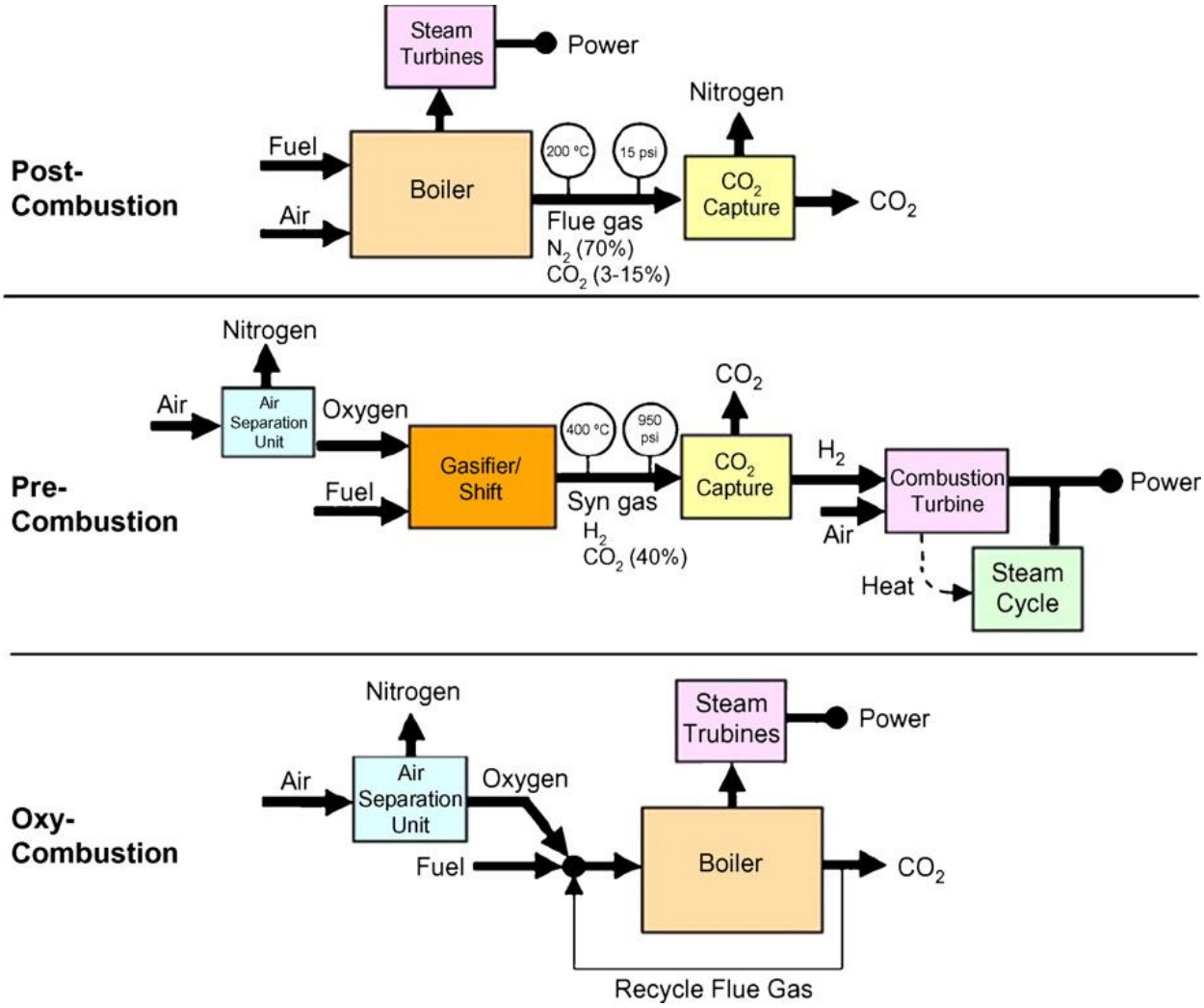

Figure 2: CO_2 capture techniques [8]

2.2 Oxyfuel Combustion

Oxycombustion is an effective means of CO_2 capture. Unlike air, oxycombustion requires the fuel to burn in the presence of pure oxygen to generate CO_2 and H_2O. This increases the concentration of CO_2 for easy capture after separation of H_2O by condensation. It also enables the reduction in emission of oxides of nitrogen (NO_x) due to absence of nitrogen during combustion. Compare to air combustion, NO_x emission decreases to about one-third (1/3) and emissions of SO_x also reduces by about 30% [6]. Oxyfuel combustion is a very important carbon capture technology because

almost all clean energy technologies require O_2 as their feed gas [9]. The basic principles of oxyfuel combustion are shown in Figure 3.

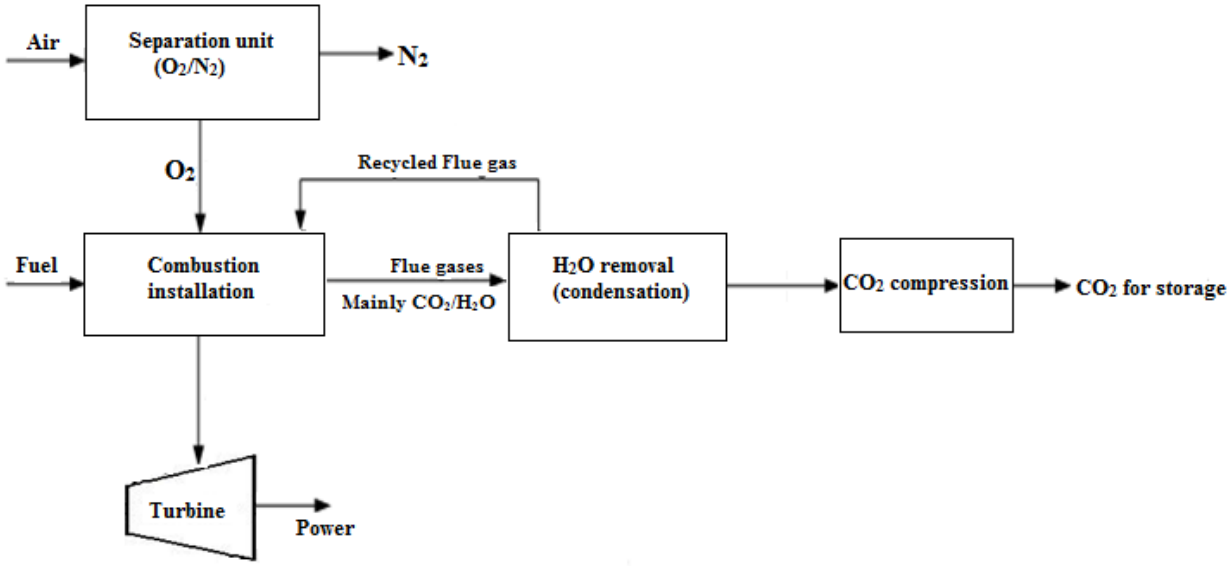

Figure 3: Basic principles of oxyfuel combustion

The combustion behaviour and characteristics of oxyfuel flames have been investigated by various researchers. Kutne et al. [10] performed experiments to study the flame structure and stability of oxyfuel combustion in a gas turbine, for oxygen at mole fraction of 20% - 40%, equivalence ratio of 0.5 – 1.0 and powers of 10-30 kW. The authors pointed out that if the mole fraction of oxygen is less than 22%, the burner will be impossible to operate, as it will result in unstable operation and blow out even if the equivalence ratio is 1.0 and at powers of 20 and 30kW, the results of Nemitallah and Habib [11] also indicated extinction of the flame if the oxygen in the mixture is less than 21%. Hence, flame stability will only be possible if the mole fraction of oxygen is more than 21%. The authors also found that heat loss in the CH_4/oxycombustion was more as compared to CH_4/air flames when operated in the same burner.

Realistically, oxycombustion will not be possible if oxygen, fuel and diluent are not supplied properly [12]. Increase in the initial O_2 percentage of the oxidizer mixture (which implies reduction in the concentration of CO_2) improves combustion stability, increases H_2O concentration of the exhaust gas [11]. Also, at a certain ratio of oxygen/diluent of oxyfuel combustion, flames will be stable and low emissions will be made [12].

The influence of equivalence ratio on H_2O concentration and the oxidizers is very significant. When the equivalence ratio is increased, keeping the ratio of O_2/CO_2 % and fuel volume flow rate constant, the concentration of H_2O increases, whereas the availability of oxygen is reduced [11]. The effects of pressure on the combustion products are also significant. At high pressure, it was realized that the CO emissions and O_2 level in the flue gases were higher than at lower pressure [12]. This is due to incomplete combustion, which also leads to lower combustion temperature.

2.3 Synthetic gas

Syngas comprises basically H_2 and CO, with little amount of CO_2, H_2O, CH_4 and N_2. The composition of syngas depends on the fuel sources for its generation as well as the processing conditions [13]. Basically, it is generated by gasification or reforming of carbon containing materials like natural gas, coal, and biomass or even from wastes. If produced from biological origin such as organic waste, the syngas produced is considered to be a renewable fuel and the power produced by its combustion is also considered renewable.

2.3.1 Synthetic gas production

Syngas can be produced from gasification or reforming of carbonaceous materials. Production by steam and CO_2 reforming was demonstrated by Rostrup-Nielsen et al. [14] in the presence of catalysts like Nickel, Cobalt and the group 8 metals, though the group 8 metals are active but very

expensive. Nickel based catalysts when compared to mineral catalysts have better performance in the production of syngas [15]. The findings by Rostrup-Nielsen et al. [14] also indicated that steam reforming is an effective way of producing syngas, with ratio of H_2/CO very close to 3. The reforming process requires high temperature for maximum CH_4 conversion. It was also noted that the steam can be replaced with CO_2 but with outcome of H_2/CO ratio reduced to 1. The authors also indicated that for the formation of H_2, water gas shift reaction follows the reforming process in the presence of copper as catalyst, and this leads to complete conversion of carbon monoxide.

Partial oxidation is another means of generating syngas. The non-catalytic type of this method is a thermal process using high temperature for complete CH_4 conversion and reduction in soot formation, the non-catalytic process usually produce syngas with H_2/CO ratio of about 1.7-1.8 [14]. The auto-thermal reforming (ATR) type works by hybridizing partial oxidation and steam reforming, utilizing a fixed catalyst bed as well as a burner. This results in a lower maximum temperature, improved efficiencies and lower oxygen consumption. Catalytic partial oxidation (CPO) type takes place without a burner [16], with all the reactants premixed, and all the reactions take place in a catalytic reactor, the CPO produces H_2/CO with ratio of 2, and with low heat of reaction [14].

Table 1: The major reactions taking place in syngas production [14,17]

Process	ΔH (kJ/mol)
Steam Reforming	
1. $CH_4 + H_2O \rightleftharpoons CO + 3H_2$	-206
2. $C_nH_m + nH_2O \rightleftharpoons nCO + (n+0.5m)H_2$	-1179 (for n-C_7H_{16})
3. $CO + H_2O \rightleftharpoons CO_2 + H_2$	41
CO_2 Reforming	
4. $CH_4 + CO_2 \rightleftharpoons 2CO + 2H_2$	-247
Autothermal Reforming (ATR)	
5. $CH_4 + 1.5O_2 \rightleftharpoons CO + 2H_2O$	520
6. $CH_4 + H_2O \rightleftharpoons CO + 3H_2$	-206
7. $CO + H_2O \rightleftharpoons CO_2 + H_2$	41
Catalytic Partial Oxidation (CPO)	
8. $CH_4 + 0.5O_2 \rightleftharpoons CO + 2H_2$	38

Another means of producing syngas is through gasification of coal, where coal is gasified at high temperature, and the gasifiers are steam and oxygen or air as shown in Table 2.

Table 2: Syngas production through coal gasification

Gasification of Coal in the presence of steam and air or oxygen	ΔH (kJ/mol)
$C + H_2O \rightleftharpoons CO + H_2$	-131

Biomass gasification is another way of producing syngas. Biomass is a carbon containing renewable source, and unlike fossil fuels, it is a CO_2 neutral resource because they only emit the carbon absorbed during their growing process and the emitted carbon are further absorbed by the growth of new biomass and thereby not contribute to the emission of the greenhouse gas, CO_2.

Lv et al. [17] produced syngas from biomass with a single stage process by direct catalytic gasification. In their experiments, they used two reactors: fluidized bed gasifier with dolomite based catalyst, and downstream fixed bed reactor utilizing Nickel based catalyst. The gasifying agents used in their experiments were steam and air. The outcome of their experiments indicated that the application of more catalyst enhanced the production of more H_2 of about 52.47% by volume, and hence high H_2/CO ratio between 1.87 and 4.45, with optimum value occurring at 750^{o}C temperature of the fixed bed reactor. They also noted that rise in temperature enhance production of more hydrogen, while production of CO reduces initially but later increases with temperature. The authors also found that the CO_2 and CH_4 contents of the syngas produced were high. This, they believe will be solved with proper operating conditions and more catalyst usage.

Production of syngas from biomass can also be realized by catalytic pyrolysis of the biomass with gasification, this can yield syngas of about 3.29 Nm^3/kg. Xie et al. [15] worked on a 2-stage technology for producing syngas by applying catalytic pyrolysis and gasification processes. The authors studied the effects of temperatures of both processes on the production of syngas; their results showed that maximum production of syngas occurs at a particular temperature. In the pyrolysis stage, the maximum yield of syngas was achieved at 750^{o}C. Whereas, the maximum syngas production during the gasification stage occurred at 850^{o}C after the pyrolysis char from the pyrolysis stage reacted with steam. An attempt to further increase the temperature led to reduction in the gas yield.

Production of syngas by ethanol catalytic decomposition was investigated by Ji et al. [18]. They realized that as the ethanol flow rate increases, it brings about increase in the hydrogen concentration of the syngas, whereas the CO concentration decreases with increase in the ethanol flow rate. This produces syngas with high H_2/CO ratio, improves efficiency of the system, and reduces emissions.

2.3.2 Characteristics of syngas combustion

Syngas has been studied to exhibits various characteristics ranging from its flame speed, extinction limits, and emission characteristics during combustion depending on the ratio of H_2/CO in the fuel, oxidizers in use, amount of diluents, methods of burning and other burning conditions.

Diluents used in combustion experiments are CO_2, water vapour and N_2, but in order to reduce NO_x emission, dilution with CO_2 and water vapour are more effective than that of N_2 [19]. Results reported by Ding et al. [20] showed that dry syngas with CO_2 addition has lower flame extinction temperature than dry syngas with H_2O dilution. Ding et al. [15] also realized syngas with impurity in form of methane has high extinction limit and increase in flame temperature due to rise in the H_2 content which enhances combustion. Addition of CO_2 to the impure syngas results in higher flame extinction limit and temperature than dry syngas [21,22], but the extinction temperature is almost the same with moist syngas. Moist syngas at high pressure diluted with CO_2 or N_2 has been studied to have higher extinction limits and temperature than the ones at atmospheric pressure [20]. This is because rise in pressure increases the burning rate, this, consequently results in higher flame temperature.

CO_2 dilution also affects volumetric heating value of fuels [19], fuels with high CO_2 dilution usually have low volumetric heating value and consequently have high CO emission and vice versa. This is because CO_2 reduces the reaction intensity and therefore results in incomplete

combustion. This, consequently, leads to more CO emissions. However, reduction in the CO emission as a result of CO_2 dilution can be achieved by reducing the equivalence ratio of the fuel. Lieuwen et al. [22] noted that the dilution of synthetic gas with any of the above mentioned diluents lowers the flame speed. Flame speed and temperature with nitrogen is the highest followed by H_2O and then CO_2, at the same dilution percentage and equivalence ratio.

The laminar burning speed of syngas flame is influenced by the amount of H_2 and CO present in the mixture. Di Sarli et al. [21] evaluated the upstretched laminar burning speed of $H_2/CO/O_2/N_2/CO_2$ with the CHEMKIN package coupled with Davis reaction scheme [23]. CO_2 addition was found to reduce the burning velocity to flame extinction [11,22], same with the results of Wang et al. [13], where increase in CO_2 concentration of fuel mixture was also found to be an inhibitor to the reaction process. The chemical effects of CO_2 on methane and hydrogen premixed flames were studied by Liu et al. [24], it was noted that the effects in reducing burning velocity was realized more in the hydrogen flames than in methane flame, and the effect reduces as the equivalence ratio decreases.

Increasing the H_2 composition of the mixture, on the other hand, increases the laminar burning speed and improve the flame structure [13,26,27]. The work of Bouvet et al. [26] showed that there was a rise in the laminar flame speed of syngas when there was an increase in the hydrogen content of the gas mixture. They realized that slight H_2 addition has an increasing effect on the laminar flame speed of CO/air mixture. With 1/99% H_2/CO at equivalence ratio of 0.6, the flame speed was approximately 10 cm/s, while in the case of 10/90% H_2/CO; the flame speed increased to 20 cm/s [26]. Fuels with high hydrogen constituent (like 45% CO, 50% H_2 and 5% CH_4 in [20]) has very high flame temperature and also has low NO concentration, while the fuel with low hydrogen constituent has low flame temperature and high NO concentration.

The influence of the addition of water to fuel mixture on flame speed was studied by Singh et al. [25] for two different syngas fuel mixtures (5% H_2 – 95% CO and 50% H_2 – 50% CO). Results of their investigations showed that for the 5:95 fuel mixtures, the flame speed increases with increase in H_2O content of the fuel up to 20% of H_2O in the mixture, and then reduce with additional H_2O content in the fuel. As for the 50:50 (CO: H_2) fuel mixture, any slight addition of H_2O to the fuel reduces the flame speed.

The effects of equivalence ratio and preheat temperature on syngas combustion were reported in the work of Singh et al. [25]. Their results showed that fuel with low hydrogen component reached their maximum flame speed at higher equivalence ratio than fuel with higher component of hydrogen. They also studied the effects of temperature on the flame speed by conducting experiments using various preheat temperatures. They realized that at every equivalence ratio, as the preheat temperature increases, the flame speed also increases.

The effect of equivalence ratio on the burning characteristics of the fuel depends on the richness of that fuel. The experimental and numerical investigations of Xie et al. [27] showed that laminar burning velocity of the $CH_4/CO_2/O_2$ mixtures for a fuel-rich mixture decreases with increase in equivalent ratio, while that of the fuel-lean mixtures increases with increase in the equivalent ratio.

2.3.3 Emissions of syngas combustion and their reduction

Just like any other fuel, syngas can produce carbon monoxide (CO), NO_x and sulphur dioxide. The emissions generated depend on the syngas properties and compositions, the type as well as the operating conditions of the combustor. Syngas are known to produce very low emissions when compared to conventional fossil fuels. H_2 and CO being the major constituents of syngas, help improve the temperature of the fuel especially in syngas with high H_2/CO ratio. This high

temperature enhances complete combustion and thermal efficiency, and also reduces emissions. Syngas fuels and their power generation are thereby more environmental friendly than fossil fuels. There are three main mechanisms of NO_x formation: thermal formation, fuel NO_x formation as well as prompt NO_x formation. The main NO_x species during syngas combustion is NO [22]. This is mainly due to thermal formation as well as fuels NO formation. Emissions of NO_x can be controlled by methods either within the combustion device called in-furnace control (such as flue gas recirculation) or post combustion control, which is applied after combustion. Control of NO formation during syngas combustion is best done with the first method. CO emissions from syngas combustion are basically due to incomplete combustion.

Alavandi and Agrawal [28] performed experiments on the burning of mixture of $H_2/CO/CH_4$ in a porous burner. Their results showed that increasing the H_2/CO ratio in the mixture decreases the stoichiometric air/fuel ratio, whereas the adiabatic flame temperature increases. Experimental investigations have shown that syngas combustion in a porous burner produces low pollutant emissions and fuel flexibility; fuels with syngas mixtures therefore have lower emissions than pure fuel. Also, addition of syngas in the CH_4 fuel decreases emissions of NO_x and CO. For example, at adiabatic flame temperature T_{ad} = 1600^{o}C, pure CH_4 fuel has CO and NO_x emissions of about 12 and 25ppm respectively. With the addition of 35% H_2 and 35% CO into the fuel, the emission of CO reduced to 5ppm and that of NO_x reduced to 7ppm. Addition of syngas to CH_4 fuel and gasoline brings about reduction in HC and NO_x emissions [18,29].

Emissions of NO_x from syngas combustion was also studied by Zhang et al. [19] and it was realized that micro-mixing technique, that involves miniaturized diffusive combustion, achieved lower NO_x emission but higher wall temperature at the nozzle exit. This, however, can be reduced with

proper addition of diluent. Therefore, CO_2 dilution was introduced into their experiment not only to reduce the NO_x emission, but also to reduce the wall temperature at the nozzle exit.

Ji et al. [18] investigated the effects of addition of syngas generated from the catalytic decomposition of ethanol, on the effectiveness of gasoline engine at lean condition. The emissions in form of HC caused by unburnt hydrocarbon, as well as NO_x reduce with an increase in the syngas volume fraction. Increase in ethanol and decrease in gasoline lead to decrease in the cylinder temperature a little bit, this eventually reduces the NO_x emission.

Syngas oxyfuel with CO_2 mixture has stronger radiation heat loss than the air combustion of CH_4, as well as syngas-air flame [6,13]. This needs to be considered in designing a combustor. There is slight increments in NO_x and CO emissions of gasoline engine at lean conditions when syngas is added to the engine [29]. The work of Dai et al. [29] also showed that syngas addition reduces HC emissions with excess air ratio lower than 1.21, but if the fuel is leaner, the HC emissions tends to increase with the addition of syngas.

The experiments of Dam et al. [30] compared the flame stabilities of Methane-oxyfuel ($CH_4 – O_2$) and syngas oxyfuel (H_2/CO – O_2), with the addition of diluents in the form of CO_2 and steam. The effect of the dilution and H_2 concentration on the flame stability were studied. $CH_4 – O_2$ flames did not stabilize without the addition of the diluent due to higher adiabatic flame temperature. They also realized that increase in the diameter of the burner will make the stability period narrower. Their results also indicated that syngas Oxy-fuel (10% H_2 – 90% CO – O_2) without CO_2 addition will still be stable with burner diameter of 3mm due to reduced flame temperature as compared to $CH_4 – O_2$ flames. Although both flames will require CO_2 for stability at higher burner diameter.

They also realized that a wider period of stability occurred for syngas Oxy-fuel (10% H_2 – 90% CO – O_2) flame than Methane oxyfuel (CH_4 – O_2) flame.

2.4 Mixed Ionic and Electronic Conducting (MIEC) Membranes for Oxygen Separation

Oxycombustion involves combustion of fuel in the presence of purely oxygen. With oxycombustion, the use of pure oxygen increases the CO_2 concentration in the exhaust. This can be achieved in several means. Cryogenic air separation is one of those means, and it is utilized in an industrial scale to achieve oxyfuel combustion. In this approach, separation occurs due to the differing boiling/condensation points of the components of air. This enables separation by distillation at cryogenic temperatures. The major advantage of this approach is that the exhaust gas contains only CO_2 and H_2O. The CO_2 separation can then be achieved after condensation to remove the water vapour. Cryogenics are however operated at very low temperature and elevated pressure, are characterized with high energy consumption and high initial cost of the equipment needed for the process. Another promising technology for achieving oxyfuel combustion is the use of ionic and electronic conducting membrane (MIEC).

Studies and research on MIEC were pioneered by Takahashi et al. [31] by working on Bi_2O_3-BaO. MIEC are very effective means of separating oxygen from air by utilizing the transport of O_2 ions through their crystal structure as a result of O_2 partial pressure differences across the membrane. They are dense, non-porous membrane of high O_2 ionic and electronic conductivity. The transfer of O_2 ion through the membrane is referred to as the Bulk diffusion. They are either perovskites or flourites (non-perovskites) [32]. Example of perovskites is LSCF while an example of non-perovskite is $Ce_{0.8}Pr_{0.2}O_{2-\delta}$.

The membranes are suitable for usage in oxyfuel power station and coal gasification due to the combination of ionic and electronic conductivities in them that allows their usage at high temperature. MIEC exhibits high electronic conductivity at elevated temperatures (700-900ºC). Perovskites membranes are known to have higher O_2 permeation than the non-perovskites [9]. Although, the non-perovskite types require low energy cost to generate oxygen because they can be operated at lower temperature.

2.4.1 Ion Transport Membrane Technology (ITM)

ITM is applicable in various ways including fuel reforming as well as oxyfuel combustion by utilizing its excellent characteristics of high ionic and electronic conductivity [33]. ITM has very high flux and high selectivity, its selectivity for oxygen is 100%, because they allow only oxygen ions to pass through them bringing about very pure oxygen. This has significant advantage when incorporated with power generation cycles. ITM can therefore be used in different reactors due to the very pure oxygen produced which is selectively used at the sweep side of the reactors through transport of its ions Hong et al. [33].

ITMs are used for separating gas using transportation of ionized gas through a non-porous, dense ceramic membrane at elevated temperature. With this, oxygen can be separated from air, which is necessary for oxyfuel combustion of fuels, thereby producing CO_2 and H_2O only. The water produced can be removed by condensation and, therefore, enhance carbon capture. This reduces associated penalties with CO_2 capture, which otherwise would have occurred in other air separation methods like cryogenics, though, cryogenics are good separation techniques for commercial use but are not as pure as ITM [34] and they achieve low second law efficiencies [35].

Many researchers have worked on various membrane materials used for oxygen permeation. Some of these as reported in literature [34] and [36] include: $La_{1-x}SrCo_{1-y}Fe_yO_{3-\delta}$ (LSCF), $SrCo_{0.8}Fe_{0.2}O_{3-\delta}$ (SCF), $La_2NiO_{4+\delta}$ (LNO), $Ba_{0.5}Sr_{0.5}Co_{0.8}Fe_{0.2}O_{3-\delta}$ (BSCF), $La_{0.5}Sr_{0.5}CoO_{3-\delta}$ (LSC), LCFC, $La_{0.4}Ca_{0.6}FeO_{3-\delta}$ (LCF), $BaTi_{0.2}Co_{0.5}Fe_{0.3}O_{3-\delta}$ (BTCF), $BaBi_{0.4}Co_{0.2}Fe_{0.4}O_{3-\delta}$ (BBCF) etc.

2.4.2 Oxygen Transport

Transport of O_2 involves the migration of oxygen through the membrane from region of high partial pressure, air (feed side), to region of lower partial pressure, sweep (permeate side), by utilizing oxygen chemical potential differences and the membrane temperature. The pressures of O_2 on both sides of the ITM determine the values of the O_2 permeation flux. As the oxygen pressure at the sweep end increases, the permeation reduces due to reduction of the driving force of the oxygen permeation and rate of backward reaction is constant whereas the forward reaction's rate on the fuel side increases. This causes rise in the permeate side O_2 partial pressure to reduce the oxygen permeation [37].

The processes involved in the permeation of oxygen from the air to sweep side involves five (5) steps, [9,33,38].

1. Mass transfer of gaseous oxygen from the gas stream to the membrane surface at the feed side, which is the side with the higher pressure side
2. Adsorption of O_2 molecules then the dissociation into ions (surface reaction at feed side)
3. Transport of O_2 ions across the membrane, which is termed the bulk diffusion
4. Association of oxygen ion followed by desorption of oxygen molecules (surface reaction at permeate side)

5. Transfer of oxygen from the membrane surface at the permeate side to the gas stream (low pressure side).

Steps 1 and 2 occur at the higher O_2 partial pressure (feed side), while 4 and 5 occur at the lower O_2 partial pressure (permeate side). The schematic representation of the oxygen transport processes is given in Figure 4.

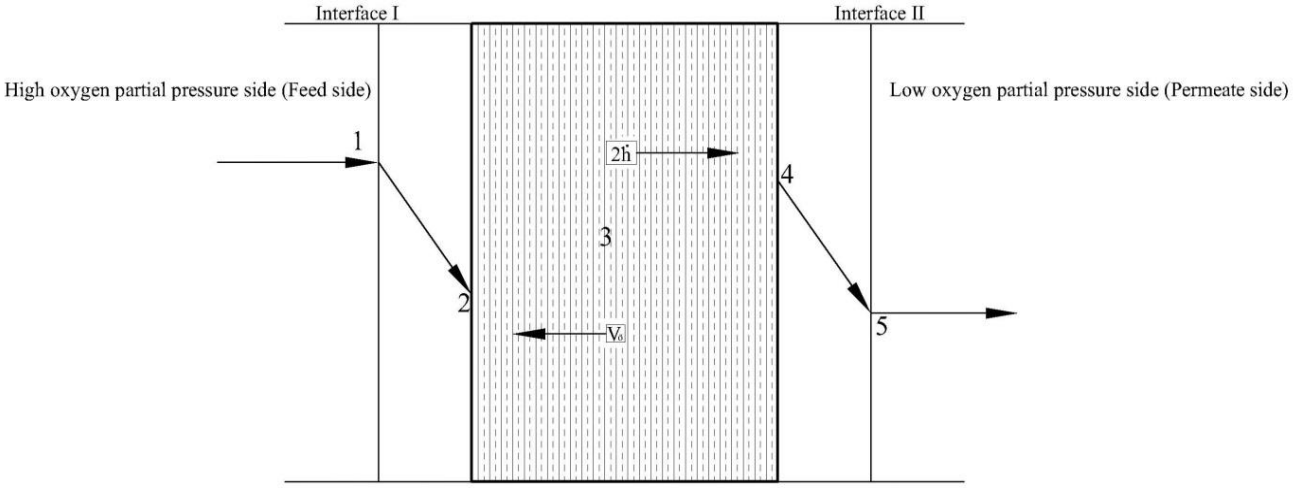

$$\frac{1}{2}O_2 + V_{\ddot{O}} \leftrightarrow O_O^x + 2\dot{h} \qquad\qquad O_O^x + 2\dot{h} \leftrightarrow \frac{1}{2}O_2 + V_{\ddot{O}}$$

Figure 4: Oxygen transport processes across ion transport membrane

2.4.3 Oxygen Vacancy Diffusion

In the cases involving both ionic conductivity as well as electronic conductivity, the oxygen vacancy diffusion coefficients, as well as the forward and backward reaction rates are dependent on temperature. The relationships are best described by Arrhenius equations [37].

$$D_V = D_V^o \exp\left(-\frac{E_D}{RT}\right) \quad (1)$$

$$k_f = k_f^0 \exp\left(-\frac{E_f}{RT}\right) \quad (2)$$

$$k_r = k_r^0 \exp\left(-\frac{E_r}{RT}\right) \quad (3)$$

With the electronic conductivity much more than the ionic, the ionic flux may be given as presented by Dyer et al. [39]:

$$J_{O_2} = \frac{\sigma_i RT}{16LF^2} \ln\left(\frac{P'_{O_2}}{P''_{O_2}}\right) \quad (4)$$

σ_i is the ionic conductivity, which happens to be the only material property in the equation.

The following reactions occur on the membrane:

$$\frac{1}{2}O_2 + V_{\ddot{O}} \overset{\frac{k_f}{k_r}}{\leftrightarrow} O_o^x + 2\dot{h} \quad \text{at the high pressure side (feed side)} \quad (5)$$

$$O_o^x + 2\dot{h} \overset{\frac{k_f}{k_r}}{\leftrightarrow} \frac{1}{2}O_2 + V_{\ddot{O}} \quad \text{at the lower pressure side (permeate side)} \quad (6)$$

Membrane should be highly permeable to oxygen, and structurally stable at elevated temperature. There are some membranes that are highly permeable to oxygen but are not stable at high temperature. The investigation by Qiu et al. [40] was on $SrCo_{0.8}Fe_{0.2}O_{3-\delta}$. In their research, it was realized that the membrane with thickness of 1mm has a high flux of 3.1ml/cm^2-min when operated at 850^{o}C, but the membrane was found to lack chemical and structural stability in reducing conditions. It was also noticed that stability was possible at higher oxygen pressure. In an attempt to improve the stability of the SCF perovskite membrane, Zongping et al. [41] substituted part of Strontium in it with Barium, of higher ionic radius, to form a $Ba_{0.5}Sr_{0.5}Co_{0.8}Fe_{0.2}O_{3-\delta}$ (BSCF) membrane and they realized that apart from the permeability improvement, the membrane's stability also improved greatly as was also the case of Wang et al. [42].

The work by Wang et al. [42] further studied the permeation characteristics of BSCF-5582 by considering temperature ranging from 700-900^{o}C and different pressures. They operated the membrane tube for 150h with permeation of 1.12ml/cm^2-min at 875^{o}C, taking 300ml/min and

60ml/min as the flow rates of the air and permeate gas respectively. Their results showed that increasing the He flow rate in the permeate side results in reduction in the O_2 pressure at the sweep side; this consequently increases the permeation. It was also noted that air flow rate can also have effect on O_2 permeation rate if the flow rate is not more than 150ml/min, but will have no effect at higher flow rates.

Foy and McGovern [36] showed in their research that BSCF has very high oxygen permeation flux when compared to many other membrane types but results of other researchers showed that it lacks stability necessary at high temperature. $La_{1-x}SrCo_{1-y}Fe_yO_{3-\delta}$ (LSCF) membrane, though, with lower oxygen permeation flux but the flux is sufficient in addition to its stability characteristics at elevated temperatures needed for combustion [43].

Kim et al. [44] formulated a model for predicting O_2 permeation flux for tubular membranes $Sm_{0.5}Sr_{0.5}CoO_{3-\delta}$ and $SrCo_{0.8}Fe_{0.2}O_{3-\delta}$. If the transport of O_2 is solely dependent on the O_2 exchange rate of the gas and the membrane surface, then the O_2 permeation flux is given as:

$$J_{O_2} = \frac{2\pi r_1 r_2 L C_i K_{io}}{S(r_1+r_2)}\left(\sqrt{\frac{{P_{O_2}}'}{{P_{O_2}}^0}} - \sqrt{\frac{{P_{O_2}}'}{{P_{O_2}}^0}}\right) \quad (7)$$

But if it is dependent on the diffusion regime, the permeation flux would be given as:

$$J_{O_2} = \frac{\pi L C_i D_a}{2Sln(r_1/r_2)} \ln\left(\frac{{P_{O_2}}'}{{P_{O_2}}''}\right) \quad (8)$$

Xu and Thomson [45] investigated oxygen separation in a membrane with higher electronic conductivity compared to ionic conductivity, they worked on LSCF-6428 membrane by considering variables including temperatures, membrane thickness and O_2 partial pressure. Their results showed that the permeation was affected by surface exchange at the permeate side and the bulk diffusion. Around 1033K, the permeation is determined by the surface exchange at the permeate side but it is mostly controlled by bulk diffusion at more elevated degrees temperatures.

A model for predicting O_2 permeation was developed by Xu and Thomson [45] as presented in Eq. (9), where L in this case is the membrane thickness:

$$J_{O_2} = \frac{\frac{k_r}{k_f}\left(\frac{1}{P''_{O_2}\left(\frac{1}{2}\right)} - \frac{1}{P'_{O_2}\left(\frac{1}{2}\right)}\right)}{\frac{1}{k_f P'_{O_2}\left(\frac{1}{2}\right)} + \frac{2L}{D_V} + \frac{1}{k_f P''_{O_2}\left(\frac{1}{2}\right)}} \tag{9}$$

Asadi et al. [37] studied the oxygen permeation of LSCF-6428. Their research focused on the influence of gas flow rate, temperature, O_2 partial pressure as well as the membrane thickness. Their results showed that rise in temperature increases oxygen permeation, the permeation increases with decrease in membrane thickness owing to the reduction in bulk diffusion resistance. The O_2 permeation increases up to a level called characteristic thickness (L_c) given as:

$$L_c = \frac{D_V}{2k_f}\left(\frac{1}{{P'_{O_2}}^{*n}} + \frac{1}{{P''_{O_2}}^{*n}}\right) \tag{10}$$

Increasing the flow rate of air up to 200cm^3/min has very substantial effect on the permeation, further increment of the flow rate beyond 200cm^3/min only had slight influence on the permeation. The authors also developed a model furthering the research by Xu and Thomson [45] for predicting the permeation flux as:

$$J_{O_2} = \frac{\frac{k_r}{k_f}\left(\frac{1}{{P''_{O_2}}^{*n}} - \frac{1}{{P'_{O_2}}^{*n}}\right)}{\frac{1}{k_f {P'_{O_2}}^{*n}} + \frac{2L}{D_V} + \frac{1}{k_f {P''_{O_2}}^{*n}}} \tag{11}$$

$$P'^{*}_{O_2} = \left(a' + b' Re_f'^{c'}\right)^{-1} P'_{O_2} \tag{12}$$

$$P''^{*}_{O_2} = \left(a'' + b'' Re_f''^{c''}\right)^{-1} P''_{O_2} \tag{13}$$

Where Reynolds number at the feed side is:

$$Re' = \frac{q'}{\pi \nu' \lambda'} \tag{14}$$

And Reynolds number at the permeate side is:

$$Re'' = \frac{q''}{\pi \nu'' \lambda''} \tag{15}$$

Where a, b, c and n are constants used for correction terms

Tan and Li [38] investigated LSCF-6428 membrane for both concurrent and countercurrent flow pattern. It was realized that the concurrent flow pattern is better than the countercurrent. Their results further showed that increment in membrane area brought about increment in oxygen productivity for a particular feed flow rate. Notwithstanding, the membrane area will have no affect again once the maximum oxygen productivity is reached.

It is worth noting that conventional work in literature relating to ion transport membrane whether experimental or numerical utilizes non-reacting/inert gases as their sweep gas. However, in recent times, few researchers have been able to predict oxygen permeation numerically by utilizing reactive gas [46 – 52]. The use of reactive gas, methane as the sweep gas has been utilized in the work of Ben-Mansour et al. [46]**.** The effects of the fuel on the permeation were studied. BSCF membrane with thermal conductivity of $20 Wm^{-1}K^{-1}$ was used. In all cases, it was realized that the use of the reactive gas as the sweep gas raises the permeation flux. This is as a result of reaction of the gas with the permeated oxygen thereby increasing the chemical potential gradient. The permeation flux for the reaction mode was noticed to be higher than the separation only mode owing to increased O_2 partial pressure difference between the feed and the sweep side. CO_2 served as diluent to replace nitrogen in the permeate side. It was also noticed that high maximum temperature can be achieved if the flow rate increases with less CO_2.

Hong et al. [33] also performed numerical simulation of ITM using LSCF membrane with methane as the reactive gas. Their results showed that unlike in the case of using rare gas as the permeate gas, when the reactive gas (methane) is used, the membrane absorbs heat from the sweep side and transfer it to the air side; this increases the temperature and further raises the O_2 permeation. Furthermore, the authors emphasized the influence of high O_2 pressure at the air side; influence of partial pressure difference on permeation was reported by the authors to be more than that due to flow rate but not up to that of increasing the inlet temperature.

Increasing the feed side flow rate raises the O_2 permeation flux up to an extent (between 100-150 ml/min in most cases) beyond which the permeation flux will be constant irrespective of the amount of air flow rate. On the other hand, the oxygen permeation flux rises with increase in permeate gas flow rate [37,38,42,53].

In addition to oxygen separation, ion transport membranes can also be used in partial oxidation of methane to syngas [39,54–58]. The separated oxygen is consumed in the permeate side of the membrane in fuel conversion process. In order to enhance the fuel conversion process for syngas production in the membrane sweep side, certain catalyst coatings should be used in both sides of the membrane. In the feed side of the membrane, catalyst are required in order to promote oxygen separation form the feed gas, air cathodes similar to those used in solid oxide fuel cells can be used. In order to enhance fuel oxidation process toward more syngas production, noble metals or nickel can be used as a catalyst in the sweep side of the membrane [56]. However, the process of syngas production using ITM reactors is highly expensive due to high temperature requirement and cost of syngas separation at the exit section of the reactor.

In recent studies, ITMs like BCFZ, LSTF, LSCF, SCF and the likes have been utilized in the generation of hydrogen via water splitting [59 – 66]. At elevated temperature, water splits into

hydrogen and oxygen. If a perovskite membrane (MIEC) is utilized, with some amount of steam as the feed gas, otherwise called the hydrogen generation side, the oxygen can be transported to the sweep side, also known as oxygen permeation side and then hydrogen will be generated from the steam dissociation. It has been proven that according to the steam dissociation reaction and oxygen permeation process, hydrogen generation rate doubles the oxygen permeation rate. $J_{H_2} = 2J_{O_2}$. It is worth noting at this point that as the rate of hydrogen generation depends on oxygen permeation, factors that enhance more oxygen permeation will consequently improve the amount of hydrogen generation.

CHAPTER 3

MODEL DEVELOPMENT AND SOLUTION METHODOLOGY

Numerical simulation of the present work is achieved using FLUENT software. The membrane type LSCF-6428 is considered in the modelling as they are reported to have high oxygen partial pressure [36] and are chemically stable at elevated temperature [43]. The membrane is dense and non-porous ceramic membrane with mixed ionic and electronic conductivities at elevated temperature. The mechanism of oxygen transport through this membrane involves the five steps discussed earlier. Figure 5 illustrates the mechanism involved in oxygen transport.

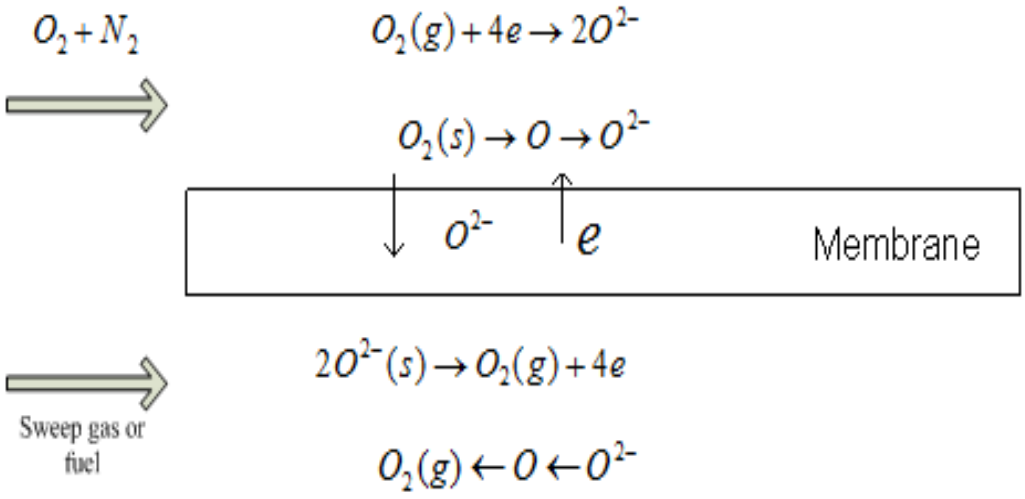

Figure 5: Oxygen transport mechanism across the membrane

Oxygen separation through the dense non-porous LSCF membrane is achieved by the use of oxygen permeation flux equation as presented by Xu and Thomson [45].

$$J_{O_2} = \frac{D_V K_r\left(P_{O_2}^{\prime\left(\frac{1}{2}\right)} - P_{O_2}^{\prime\prime\left(\frac{1}{2}\right)}\right)}{2LK_f\left(P'_{O_2}P''_{O_2}\right)^{\frac{1}{2}} + D_V\left(P_{O_2}^{\prime\left(\frac{1}{2}\right)} + P_{O_2}^{\prime\prime\left(\frac{1}{2}\right)}\right)} \quad (16)$$

The permeation flux model can also be expressed in terms of the three resistances to oxygen permeation as shown in Eq. (17). These resistances are resistance to surface exchange at feed side R'_{ex}, resistance to bulk diffusion R_{diff}, and resistance to surface exchange at sweep side R''_{ex}. Expressions to quantify them are presented in Eqns. (18-21).

$$J_{O_2} = \frac{\frac{K_r}{K_f}\left(P_{O_2}^{\prime\prime-\left(\frac{1}{2}\right)} - P_{O_2}^{\prime-\left(\frac{1}{2}\right)}\right)}{R_t} \quad (17)$$

$$R_t = R'_{ex} + R_{diff} + R''_{ex} \quad (18)$$

$$R'_{ex} = \frac{1}{K_f P_{O_2}^{\prime\left(\frac{1}{2}\right)}} \quad (19)$$

$$R_{diff} = \frac{2L}{D_v} \quad (20)$$

$$R''_{ex} = \frac{1}{K_f P_{O_2}^{\prime\prime\left(\frac{1}{2}\right)}} \quad (21)$$

Results reported by previous investigators [37,45] have shown that at lower temperatures, permeation is more dependent on surface exchange at the permeate side of the membrane, whereas, it is more controlled by bulk diffusion at elevated temperatures. The partial pressures of oxygen at the feed and sweep side P'_{O_2} and P''_{O_2} respectively are the driving forces of permeation. D_v, k_f and k_r represent the coefficient of bulk diffusion through the membrane, and the forward and reverse reaction rate constants. At the feed side, the partial pressure of oxygen can be varied by varying

the concentration of oxygen in air. As for O_2 partial pressure at the sweep side, it can be computed from the relation presented in Eq. (22).

$$P''_{O_2} = P_{o_2} Y_{o_2} \quad (22)$$

Where P_{O_2} is 1atm of oxygen pressure and Y_{o_2} is the concentration of oxygen in the sweep side. Computational Fluid Dynamics (CFD) is utilized to simulate the present problem. Few researchers have been able to apply CFD method for gas separation from a mixture [67 – 70]. Their works showed promising results by considering simulations under different operating conditions and various parametric studies were made. CFD and experimental results are in agreement. Therefore, modelling and simulation involving gas separation in membrane can be performed with CFD.

3.1 Governing Equations

The models of interest are solved using the finite volume approach of CFD. The continuity, momentum and energy equations are solved to obtain the pressure and velocity field of the mixture. The considered cases are under laminar and steady state conditions considering Newtonian working fluids. The conservation equations of species are solved by the FLUENT software by predicting the local mass fraction of each species, Y_i, and utilizing the convection-diffusion equation for the i^{th} species [71]. The conservation and species equations are shown in Eqns. (23-26).

$$\nabla(\rho U) = S_i \quad (23)$$

$$(\rho UU) + \nabla p = \mu \nabla^2 U \quad (24)$$

$$(\rho C_p) U . \nabla T = \nabla . (\mathrm{k} \nabla \mathrm{T}) \quad (25)$$

$$\nabla.(\rho U Y_i) - \nabla.\left(\rho D_{i,m} \nabla Y_i\right) = S_i \quad (26)$$

Where p is pressure, μ is the viscosity, U is the velocity vector, ρ is the density, k is thermal conductivity and S_i is a term that represents the oxygen source/sink. The source term allows the permeation of only O_2 through the membrane, and the flow of the specie is accounted for by the source/sink term. Species leave the membrane at one side and appear at the other side through the sink and source terms, respectively. The oxygen permeation J_{O_2} is positive at the sweep side (source term) and negative at the feed side (sink term).

S_i is given as shown in Eq. (27):

$$S_i = \begin{cases} \frac{+J_{O_2} A_{cell} MW_{O_2}}{V_{cell}} & at\ the\ permeate\ side \\ \frac{-J_{O_2} A_{cell} MW_{O_2}}{V_{cell}} & at\ the\ feed\ side \end{cases} \quad (27)$$

The value of S_i is modeled in such a way that its value is always equal to zero except when i = O_2. The binary mass diffusion coefficient $D_{i,j}$ of the component i in the component j determines the diffusion coefficient. Computation of the diffusion in the case of a mixture $D_{i,m}$ can be achieved using Eq. (28) [43].

$$D_{i,m} = \frac{1 - X_i}{\sum_{j, j \neq 1} \left(\frac{X_i}{D_{i,j}} \right)} \quad (28)$$

The binary mass diffusion coefficient, $D_{i,j}$, can be calculated by utilizing Chapman-Enskog formula using the kinetic theory [72].

3.2 Radiation Model

Radiation model is included in the computational work in order to avoid over-prediction of the reactor temperature. The model used in the present work is the Discrete Ordinate (DO) due to its

very good prediction ability of oxyfuel combustion characteristics in micro-channels [73]. DO solves radiative transfer equation (RTE) for emitting, scattering and absorbing medium. The RTE equation in the direction $\vec{S}$ is given as Eq. (29) [74].

$$\frac{dI(\vec{r},\vec{s})}{ds} + (a + \sigma_s)I(\vec{r},\vec{s}) = \frac{an^2(\sigma T^4)}{\pi} + \frac{\sigma_s}{4\pi}\int_0^{4\pi} I\,(\vec{r},\vec{s}')\phi(\vec{s}.\vec{s}')d\Omega' \qquad (29)$$

Where a is the absorption coefficient m^{-1}, n is refractive index, I is the intensity of radiation and s is the path length. The DO model converts Eq. (29) into equation for radiation intensity in the spatial coordinates (x,y,z) [74]. The absorption coefficient used is variable absorption, which is good for simulation of radiation in combustion problems. In an attempt to consider the influence of radiation on gas mixtures, weighted-sum-of-grey-gases-model (WSGGM) of domain based is used in this research. In this model, the total emissivity is evaluated using Eq. (30) [75].

$$\epsilon = \sum_{i=0}^{i=I} a_{\epsilon_i}(T)[1 - e^{-k_i PL}] \qquad (30)$$

In this case, a_{ϵ_i} is the emissivity weighting factors for the grey gas i. These factors depend on temperature T. k_i is the absorption coefficient and L is the gas layer thickness. The internal emissivity used for all the walls in the present computational work as well as membrane and its shadow is 0.8 [43].

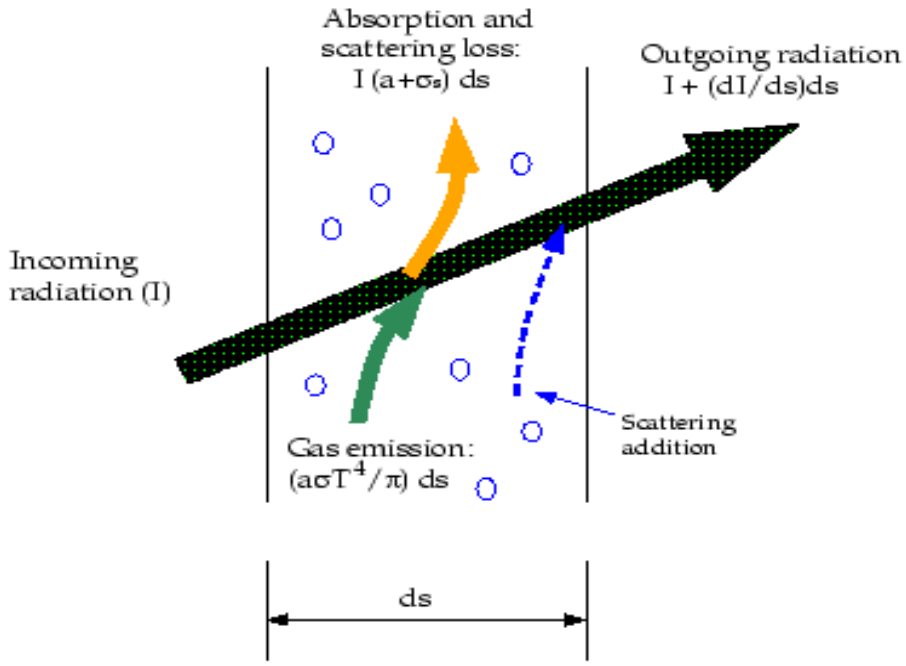

Figure 6: Radiation heat transfer [74]

3.3 Reactor specifications and boundary conditions

The reactor in the present work has a tubular shape. It is 100 mm length, 10 mm radius shared by two tubes, one for the air side and the other for the fuel side. Syngas is supplied as fuel through the inner tube and it is surrounded by air in an annulus. The inner tube has a radius of 2 mm and the outer tube has a radius of 10 mm as shown in Figures 7 and 8. The computational geometry is built with structural mesh in order to reduce numerical errors. The geometry is divided into two flow zones, one for the feed (air side) and the other for the sweep side (fuel side). The two zones are separated by a wall serving as the membrane. Each of the zones has mass flow inlets for introducing the air (79% and 21% by moles of nitrogen and oxygen respectively) in the feed zone and syngas (CO/H_2) with CO_2, together serving as the sweep gas in the permeate zone. They also have pressure outlets for the outflows. The two walls (top and bottom) are treated as adiabatic

condition. Buoyancy effects are neglected in the present work. There are 25000 quadrilateral cells in all, 30 mass flow inlets cells for the air side and 20 mass flow inlet cells for the syngas side. The geometry was modelled as two dimensional and axisymmetric. The syngas reaction mechanism, thermochemical and transport data files were imported into the FLUENT software using the CHEMKIN mechanism import. The fuel composition, temperature, flow rate, amount of diluents and air composition were imposed at the inlet of the feed and sweep zone. In order to ensure isothermal conditions, both the feed and sweep gases are introduced at the membrane temperature. In order to ensure higher accuracy, second order upwind discretization is utilized in this work. The PRESTO scheme is used for pressure to avoid interpolation errors and pressure gradient assumption on boundaries, while the SIMPLE algorithm is used for the pressure-velocity coupling [76]. Under-relaxation of the scalars and variables was considered to avoid divergence. In order to further aid convergence of the computational work, the Aggressive Advanced Multi-grid (AMG) scheme is utilized. The scheme is set to 'F-cycle' for the pressure, conservation and species equations, and the Bi-Conjugate Gradient Stabilized Method (BCGSTAB) is employed to avoid irregular convergence. The problem utilized a segregated algorithm by solving the individual governing equations sequentially [74]. In order to achieve fully converged solution, the residual values for all the species, continuity, momentum and energy equations were set to 10^{-9} and the mass fraction of the species as well as static temperature were monitored at the outlet of the sweep zone.

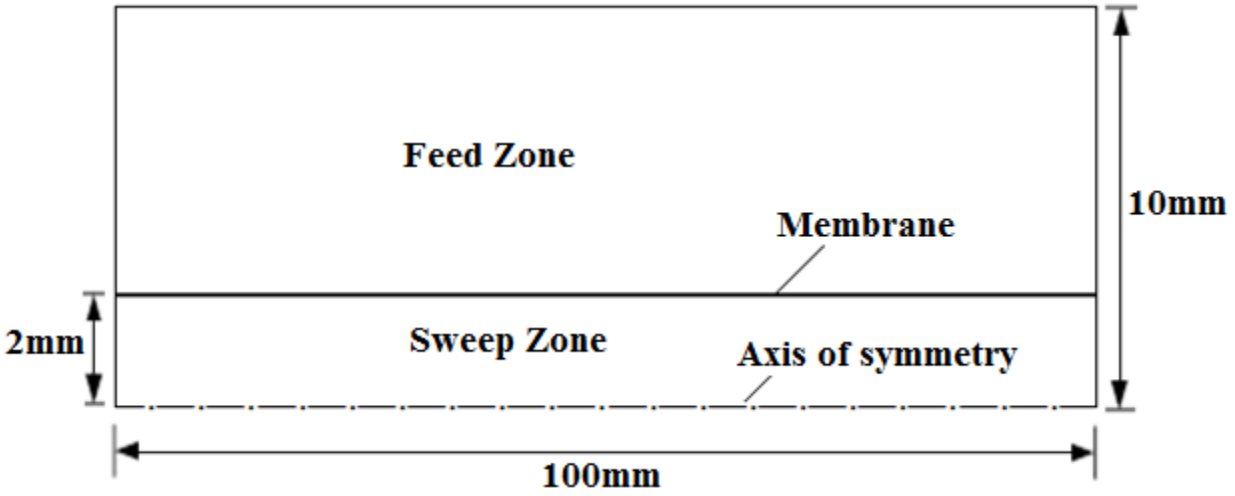

Figure 7: The flow zones considered in the current work

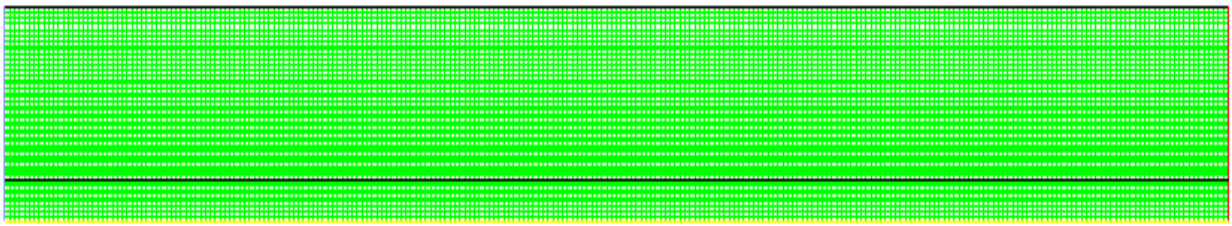

Figure 8: Computational grid for the present work

3.4 Chemical Kinetics (CHEMKIN) Solver

In order to include combustion cases in the present work, the volumetric reaction option was activated in the FLUENT solver. Detailed reaction kinetics are frequently required to represent combustion, utilizing CHEMKIN solver will enhance accuracy, speed and stability to the calculations using finite-rate multi-step reaction kinetics [77]. CHEMKIN is a program that allows the integration of complex chemical kinetics into simulations of reacting flow. It is used in many applications like combustion and chemical processing. The CHEMKIN file involving five (5) species for reduced kinetic reaction of synthetic gas involving 3 steps reaction was imported into the FLUENT software. The reactions involved were gotten from the global mechanism of

Westbrook and Dryer [78], with kinetic parameters optimized by Cuoci et al. [79] to improve the simplified mechanism for CFD applications.

3.5 User Defined Function (UDF)

The oxygen permeation through the ITM is achieved numerically with the aid of UDF written in C++. This, is then compiled and hooked into FLUENT 14.0 software. There are three macros considered in the UDF: The 'Define Initialize', 'Define Adjust' and 'Define Source'. They enable the adding and subtracting of the source term in continuity and species transport equation. Hydraulic jump problem was resolved with the aid of patching in the two computational zones with the values of species mass fraction. The species mass fractions determine the initial partial pressures of the species. The UDF updates the solution after iterations.

3.6 Numerical Modeling

Two numerical models are developed and utilized in the present work. One of them is the ITM user defined function (UDF) written and hooked to FLUENT to cater for the permeation of oxygen from the air in the feed zone to the sweep zone of the membrane. The second model is for synthetic gas reaction kinetics. This is applied at the sweep side of the membrane. The oxygen permeation model for LSCF-6428 reported by Xu and Thomson [45] was utilized with the experimental data of Li et. al [80]. Xu and Thomson developed a model for oxygen permeation having the effects of both surface exchange on the feed and sweep side of the membrane as well as bulk diffusion in terms of oxygen partial pressures at steady state as shown in Eq. (9).

The pre-exponential coefficients as well as the activation energy are presented in Eqns. (31-33).

$$K_f = 3.5 * 10^7 \exp\left(-\frac{27289.8}{T}\right) \ (m/atm^{0.5}s) \quad (31)$$

$$K_r = 1.232 * 10^{10} \exp\left(-\frac{29021.7}{T}\right) \ (mol/m^2 s) \quad (32)$$

$$D_v = 1.58 * 10^{-4} \exp\left(-\frac{8851.7}{T}\right) \ (m^2/s) \quad (33)$$

On the other hand, the syngas model in the present work was reported by Cuoci et al. [79], after carrying out optimizations for the kinetic parameters of global mechanism reported by Westbrook and Dryer [78]. Non-linear regression approach was utilized in optimizing the Dryer-Westbrook mechanism presented in Eqns. (34-36).

$$CO + 0.5O_2 \rightarrow CO_2 \qquad r_1 = 2.24 * 10^{12} \exp\left(-\frac{40700}{RT}\right)[CO][H_2O] \quad (34)$$

$$CO_2 \rightarrow CO + 0.5O_2 \qquad r_2 = 5 * 10^{8} exp\left(-\frac{40700}{RT}\right)[CO_2] \quad (35)$$

$$H_2 + 0.5O_2 \rightarrow H_2O \qquad r_3 = 9.87 * 10^{8} \exp\left(-\frac{7400}{RT}\right)[H_2][O_2] \quad (36)$$

The reactions with optimized parameters are shown in Eqns. (37-39):

$$CO + 0.5O_2 \rightarrow CO_2 \qquad r_1 = 2.30 * 10^{11} \exp\left(-\frac{31700}{RT}\right)[CO][H_2O] \quad (37)$$

$$CO_2 \rightarrow CO + 0.5O_2 \qquad r_2 = 4.45 * 10^{9} exp\left(-\frac{41300}{RT}\right)[CO_2] \quad (38)$$

$$H_2 + 0.5O_2 \rightarrow H_2O \qquad r_3 = 1.35 * 10^{8} \exp\left(-\frac{6900}{RT}\right)[H_2]^{0.87}[O_2]^{1.1} \quad (39)$$

The units are in calorie, mole, liter and second.

The first two reactions (Eqns. 37 and 38), are meant for the CO in the syngas, while the third reaction (Eq. 39), caters for the hydrogen content in the fuel.

3.7 Validation

The present work involves two numerical models, one caters for the permeation of oxygen with the aid of UDF written in C++ and hooked to FLUENT, while the other is utilized for the syngas reaction mechanism. The validation for each model is done by comparison with experimental results available in literature.

3.7.1 Validation for Oxygen Permeation Model (ITM-UDF)

The validation of the present model for oxygen permeation was carried out. Thus, the present numerical results using the model reported by Xu and Thomson [45] as presented in Eq. (9) were compared with experimental data from Li et al. [80] after fitting values for the forward and reversed rate constants (k_f and k_r), as well as the diffusion coefficient (D_v) of Eq. (9). The approach involves fitting a value for one of the paramenters while others are kept constant, until all the parameters have been fitted to arrive at expressions presented in Eqns. (31-33). In the experimental work, the effects of the sweep gas (Ar in this case) on the oxygen permeation flux were investigated with the air flow rate kept constant. The model parameters from the experiment and their values are summarized in Table 3, while the schematic of the geometry is shown in Figure 9.

Table 3: Model parameters and values for ITM (UDF) model validation

Parameters	**Values**
Air flow rate	24.1cm^3 (STP)/min
Argon flow rate	varies
Temperature	800 – 900^oC

In the numerical simulation, another geometry was developed in GAMBIT to represent the experimental set up and incorporated in the FLUENT software with mass flow inlet for air and argon, and one pressure outlet for each. The geometry was modelled as axisymetric.

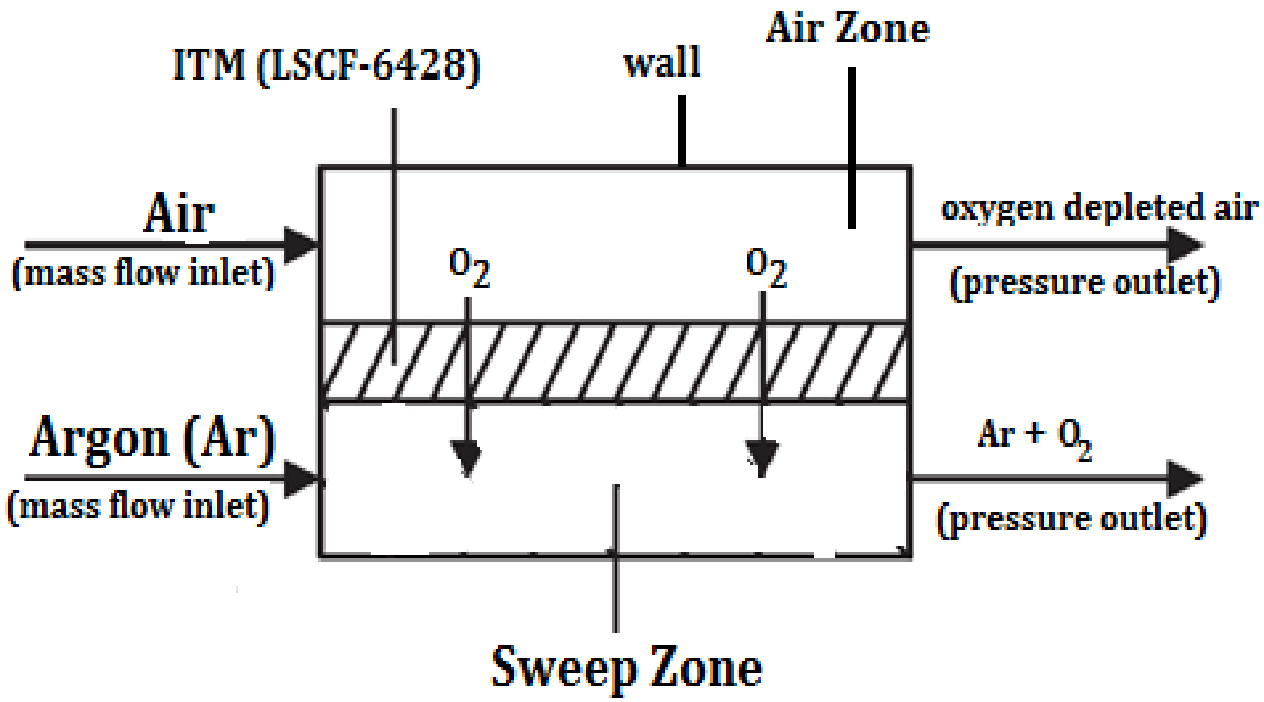

Figure 9: Schematic of reactor for oxygen permeation with Argon as sweep gas

As expected in both experimental and numerical solutions, as the temperature rises, the permeation flux increases. This is because as temperature increases, the diffusion coefficient, D_v and the forward and reversed rate constants (k_f and k_r) increases. The forward is more sensitive to temperature differences and defines oxygen adsorption on the membrane surface, while the reverse defines the desorption. Hence, increase in temperature increases the permeation of oxygen as shown in Figure 10. Also, this may be attributed to the reduction in membrane resistance to oxygen permeation while increasing the temperature as presented in Eq. (9). Increasing the sweep gas flow rates causes reduction in the partial pressure of oxygen at the sweep side. This increases O_2 partial pressure differences (ΔP) and thereby enhances more oxygen permeation.

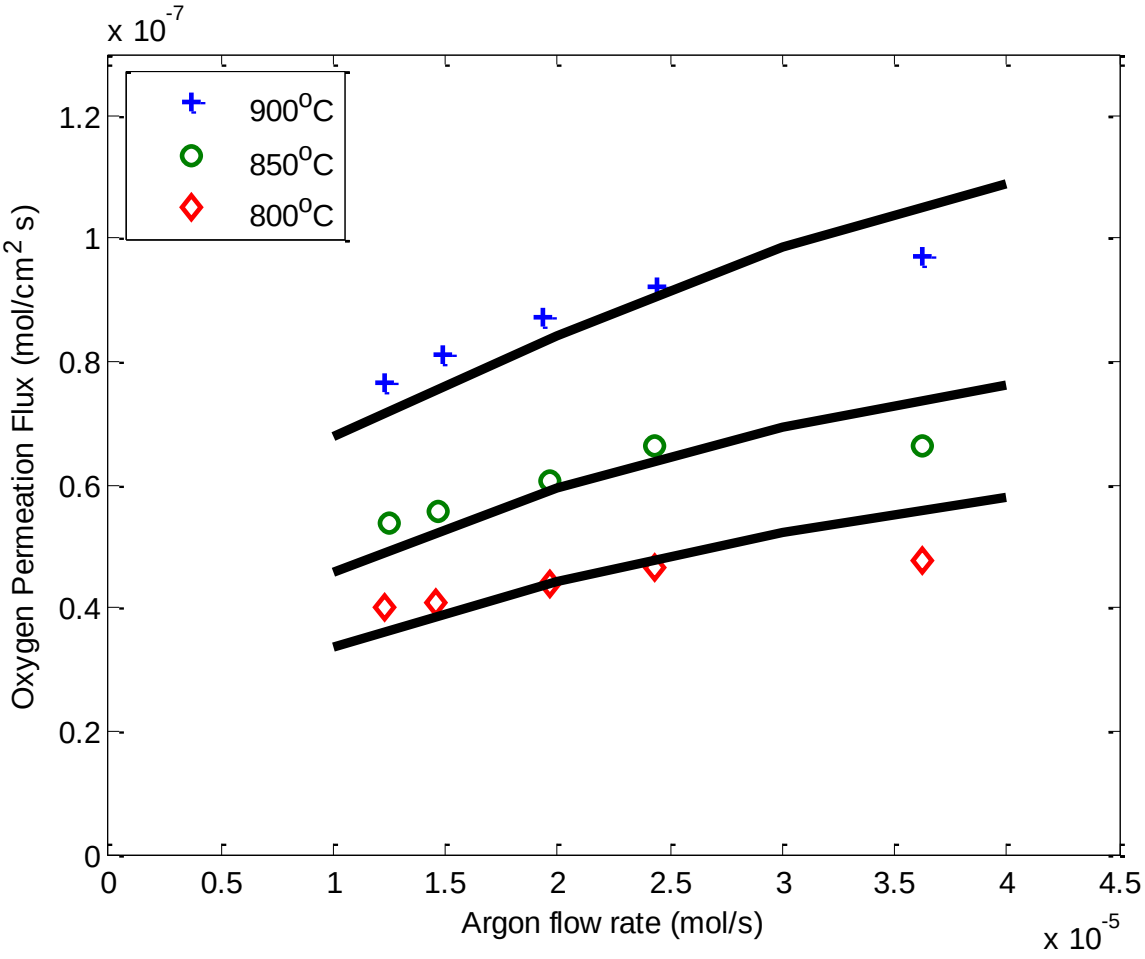

Figure 10: Influence of sweep flow rates on oxygen permeation flux at different inlet temperatures (symbols for experimental Li et al. [80] and lines for present numerical results)

As can be seen in the Figure, both the experimental and numerical modelling results follow similar trend. It is however noticed that the numerical results are in agreement with the experimental data more at lower flow rates of Argon. The numerical model is therefore more reliable at lower flow rates when Argon is used as the sweep gas. The difference in the permeation values of the numerical results from the experimental data especially at high flow rates may be attributed to experimental uncertainties, and may also be due to the differences in the surface structure of the membrane used for the experimental data and the one used for developing the numerical model.

3.7.2 Synthetic gas model validation

The synthetic gas model in the presented work was presented earlier in Eqns. (37-39). The model is validated with experimental results reported by Barlow et. al [81]. Their experiment was on turbulent jet flame of syngas dilluted with nitrogen (40% CO, 30% H_2 and 30% N_2). The experimental parameters and values are summarized in Table 4. The jet with a diameter of 4.58 mm is concentrated at the center line of the tubular reactor with a diameter of 196 mm, and the coflow around the jet consists of air provided at a temperature of 290K and a velocity of 0.75 m/s. The geometry is shown in Figure 11.

Table 4: Model parameters and values for syngas model validation

Parameters	**Values**
Velocity and inlet temperure of air	**0.75m/s, 290K**
Velocity and inlet temperature of jet	**76m/s, 292K**
Inner and outer diameters of the jet	**D_i = 4.58mm, D_o = 6.34mm**
Temperature of Top wall	**300K**
Reynolds number	**16710**
Model	**Eddy-Dissipation Concept (EDC)**
$Y_{O2,coflow}$, $Y_{N2,coflow}$, $Y_{H2O,coflow}$	**0.22884, 0.76363, 0.00753**
$Y_{CO,jet}$, $Y_{H2,jet}$, $Y_{N2,jet}$	**0.55446, 0.0297, 0.41584**

A new mesh was developed and refined to correctly represent the experimental set up in the numerical model, and simulations were performed using eddy dissipation concept (EDC). The modelled geometry for the turbulent simulation is shown in Figure 11. The problem is solved assuming symmetry about the centerline. The computational domain extends for 400mm after the burner nozzle and 196mm from the centerline. The boundary conditions are: two velocity inlets

for both air and fuel, a pressure outlet for the exit. The top surface was treated as a wall with temperature condition. After the simulations, the numerical results for the calculated mass fractions of CO, H_2 and O_2 were analysed and compared with the recorded experimental data. Plots for both experimental and numerical results are presented along the centre line of the reactor from the inlet to the exit sections.

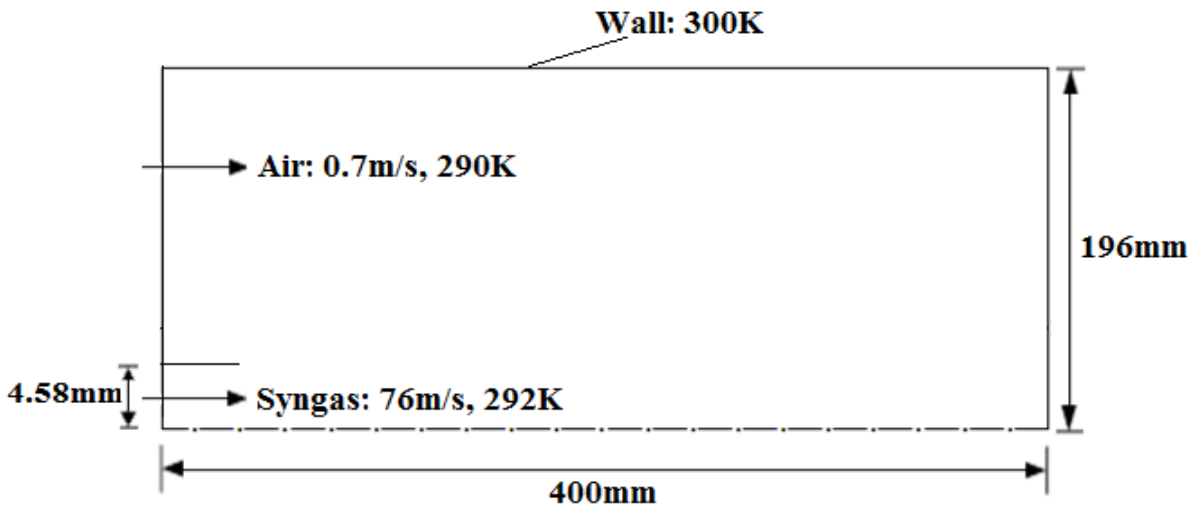

Figure 11: Schematic of the modelled geometry for syngas validation

Figure 12 shows the mass fraction of hydrogen along the center line. It would be seen from the plot that the model was able to predict the fraction of H_2 very well when compared with the experimental data. It is seen that its concentration in the axial direction reduces. This is due to combustion leading to consumption of hydrogen. It is also noticed that the amount of hydrogen in the fuel is completely burned at axial location of about 0.2m. There is a very good agreement between the numerical simulation results and the recorded experimental data as shown in the Figure. Figure 13 shows the mass fraction of CO, It is seen that its concentration in the axial direction is reduced. This is due to combustion and it is completely burned at axial location of

about 0.16m. There is a very good agreement in terms of values and trends between the numerical results and the recorded experimental data as shown in the Figure.

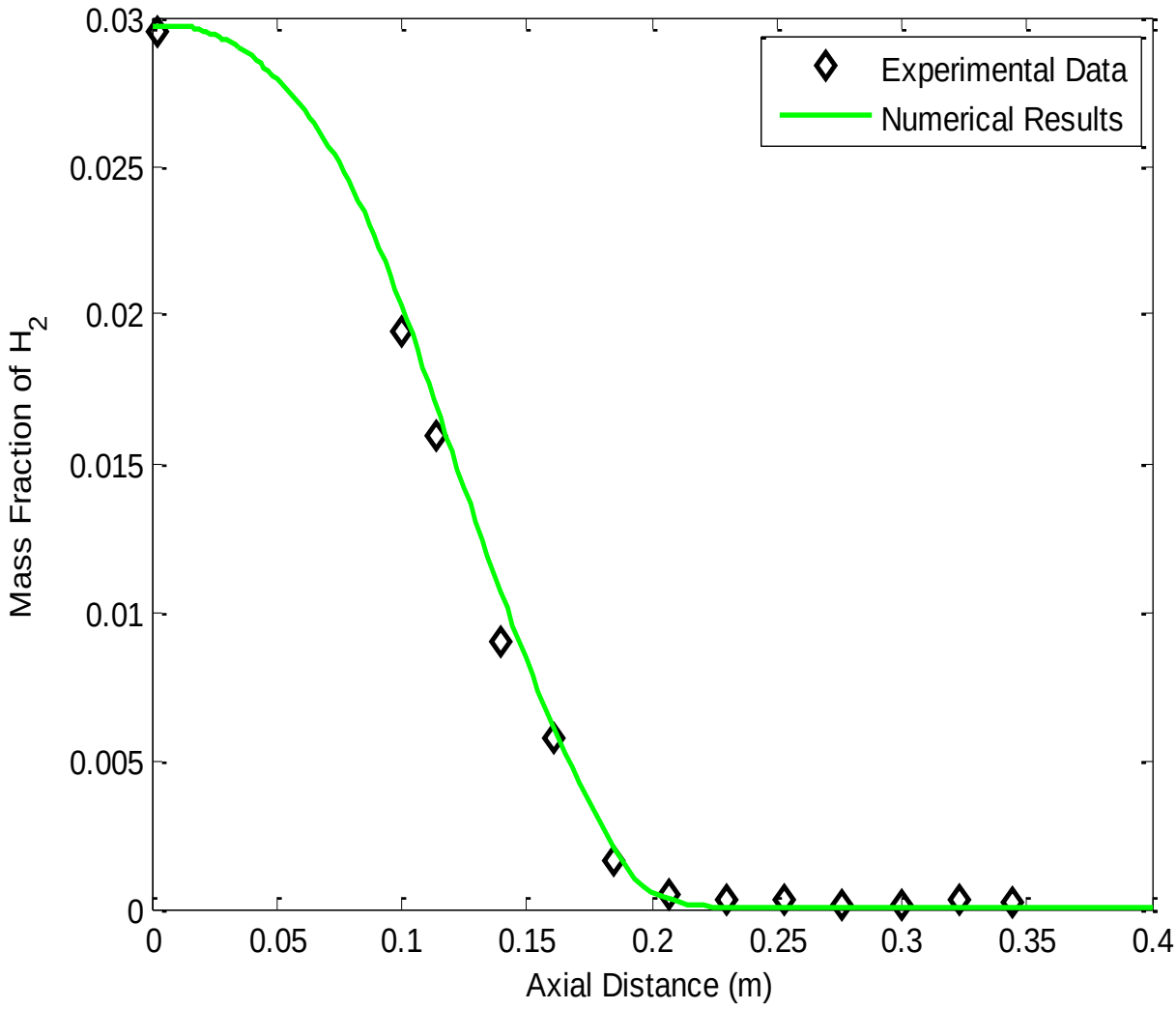

Figure 12: Mass Fraction of hydrogen along the center line for syngas validation (symbols for experimental Barlow *et. al* [81] and lines for present numerical results)

Figure 14 depicts the mass fraction of O_2, it is noticed that at the vicinity of the jet inlet, the concentration of O_2 is small, this is due to the jet flow. Away from the jet flow, and along the length of the reactor, there was rise in the concentration of oxygen. This is due to diffusion of oxygen. Comparison of the numerical model results were also in agreement with the experimental

data, though there were slight deviations at some points. All in all, there are very good agreements between the computational results and the recorded experimental data for the two models in the present work. These comparisons reflect the reliability of the permeation (UDF) and synthetic gas reaction kinetics model to be applied in the present numerical investigations in an oxygen transport reactor.

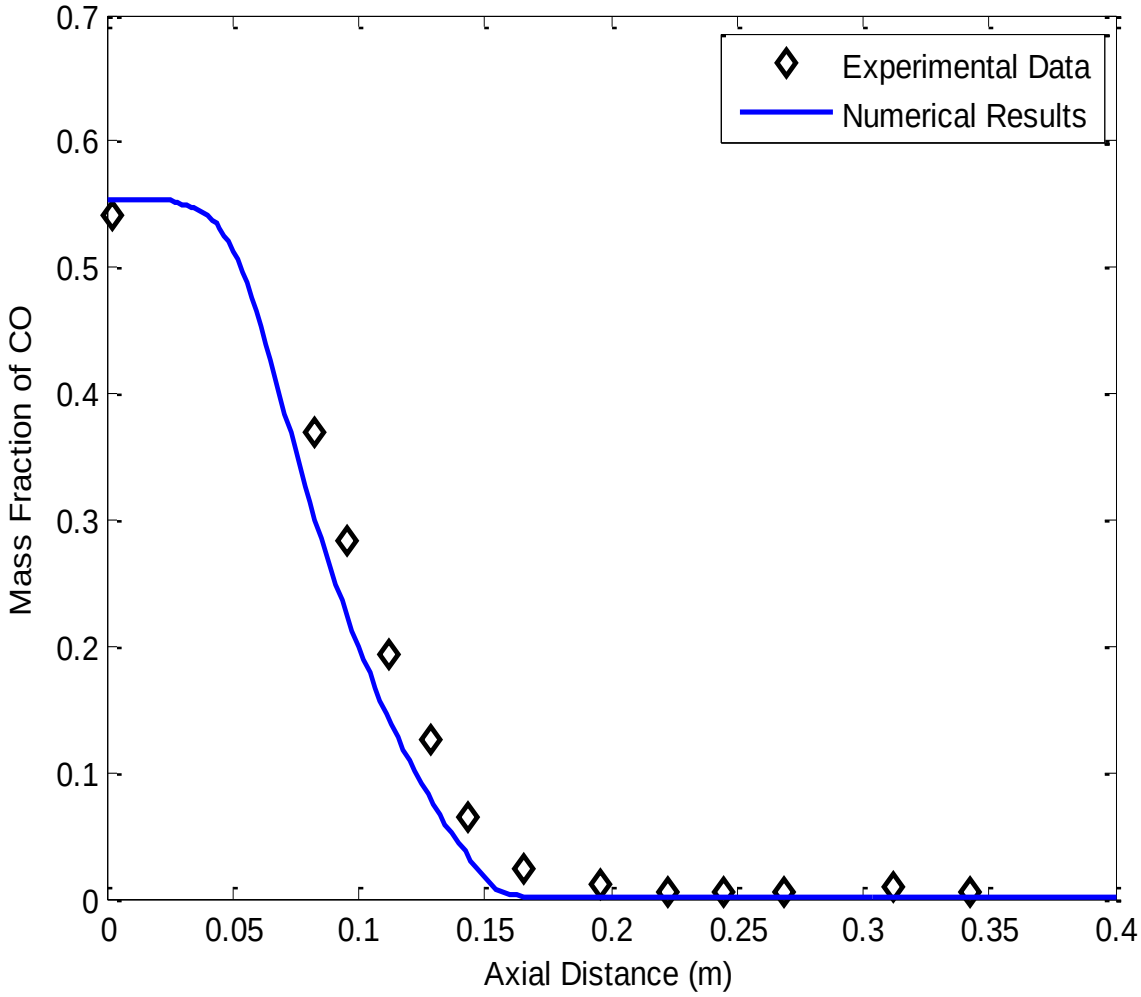

Figure 13: Mass Fraction of CO along the center line for syngas validation (symbols for experimental Barlow et. al [81] and lines for present numerical results)

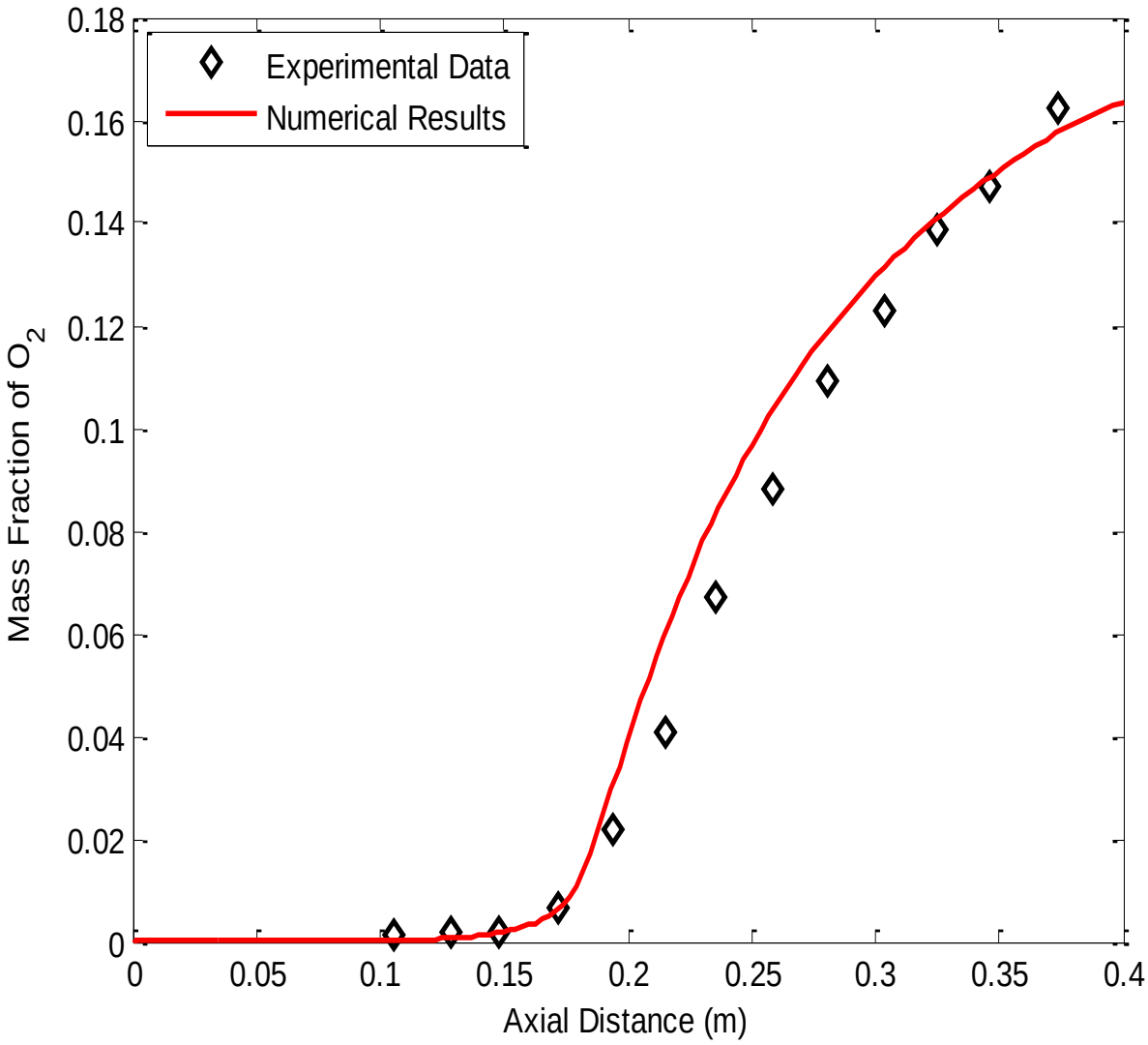

Figure 14: Mass fraction of oxygen along the center line for syngas validation (symbols for experimental Barlow et. al [81] and lines for present numerical results)

CHAPTER 4

RESULTS AND DISCUSSION

4.1 Grid Independence Test

In order to ensure that the solution of the present work is grid independent, and that the numerical solution is free of false diffusion, a grid independence test was carried out, the grid was generated using GAMBIT software and it is made finer very close to the membrane wall at both sides. The test was carried out considering different grids ranging from 1000 grid points to 36000 grid points. The results are shown in Figure 15 where the influence of grid refinement on the O_2 permeation rate is displayed. The difference between the permeation rates of 1000 to 4000 grids is more than 30%, with grid refinement to 16000 grids, the difference reduces to around 25%, further refinement to 25000 lead to difference of 8%. Finally, when the grid was refined to 36000, the difference was less than 1%. Further refinement was noticed to have no advantage, and can lead to additional computational efforts and time.

4.2 Non-reactive (separation) case

The first case considered involved the separation of oxygen from air using the membrane without reaction taking place at the sweep zone, this is to show the potential of the ITM for oxygen separation from air. Figure 16 depicts the amount of O_2 permeation in mol/m^2s with the parameters and their corresponding values shown in Table 5. All the analysis in this section is based on the non-reactive case.

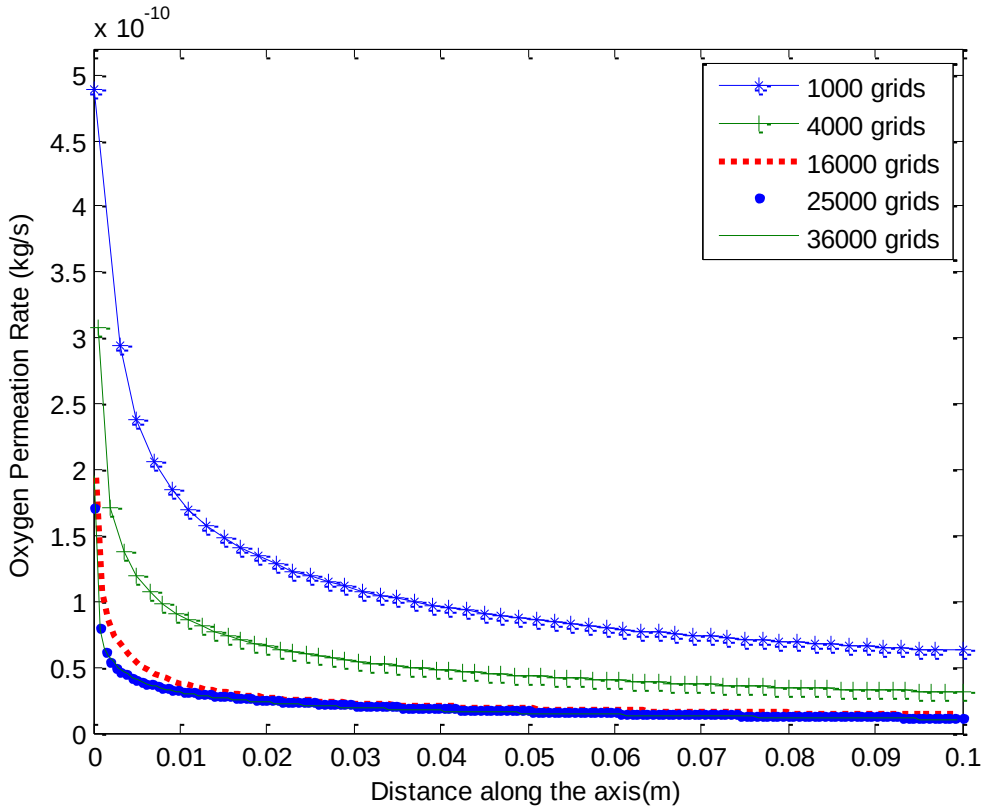

Figure 15: Grid independence test

Table 5: List of parameters and their corresponding values for the base case

Parameters	**Values**
Feed gas flow rate	5.43E-6 kg/s
Sweep gas flow rate	5.43E-7 kg/s
Fuel and CO_2 composition	$CO/H_2/CO_2$: 0.05/0.05/0.9
Feed side inlet temperature	1173k
Sweep side inlet temperature	1173K
Feed gas composition	N_2/O_2 : 0.78/0.21
Density of membrane	6000kg/m^3
Thermal conductivity of membrane	4 W/m-K [43]

At the inlet of the sweep side, the partial pressure of oxygen equals zero, this implies that maximum partial pressure differences (ΔP) are achieved at the inlet, therefore there is maximum driving force at the inlet. This eventually leads to maximum permeation. It could be seen that the permeation flux along the axis of the reactor reduces due to absence of reaction, which could have increased the reactor temperature and increase the oxygen partial pressure differences that would lead to more permeation of oxygen. As a result of oxygen ions desorption taking place at the sweep side along the length of the reactor, the partial pressure of oxygen increases at that side leading to reduced partial pressure differences and consequently reducing the permeation of oxygen along the length of the reactor. The partial pressure differences become almost constant towards the end of the reactor. This is the reason while the permeation flux also appears to have constant value towards the sweep outlet.

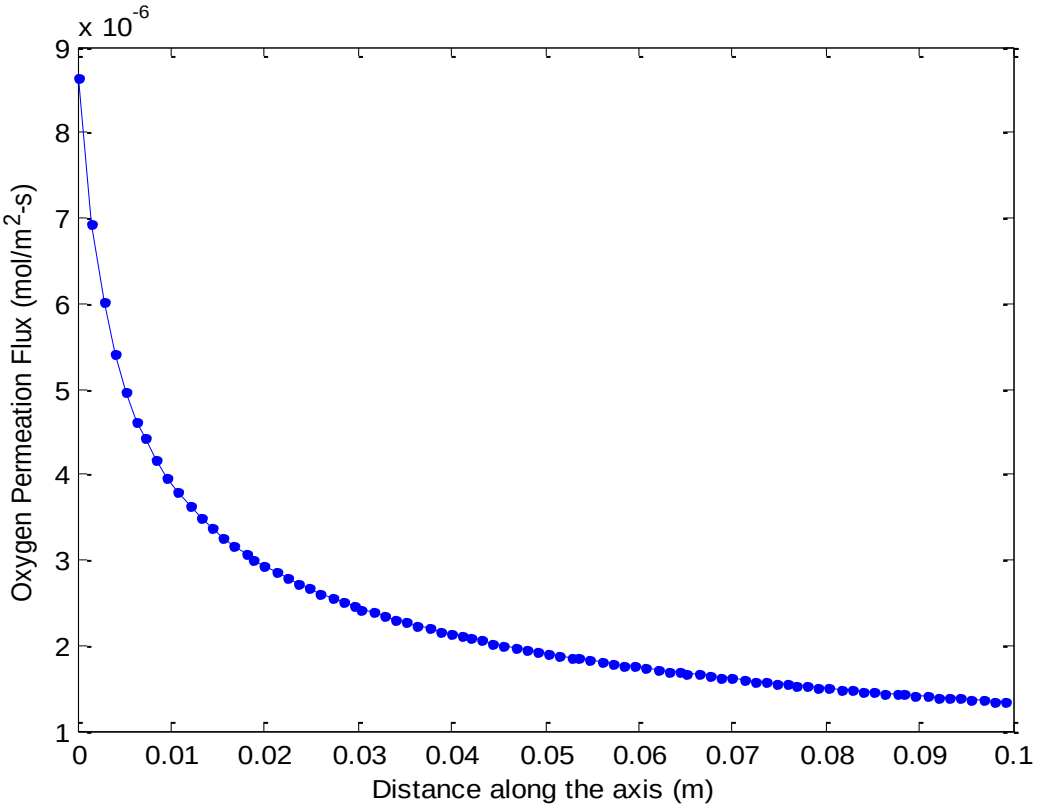

Figure 16: Oxygen permeation flux for non-reacting case

4.2.1 Effects of inlet temperature on permeation for non-reactive case

The effects of inlet temperature on the permeation flux for a non-reactive case have been investigated. The inlet temperature range from 700^0C to 900^0C while keeping other parameters constant at their base values. Figure 17 shows the influence of inlet temperature on the oxygen permeation flux. It is obvious from the Figure that as the inlet temperature increases, the amount of oxygen permeated increases leading to more permeation flux. This is as a result of bulk diffusion, which is the driving force of oxygen permeation at high temperature. The result of this section is in agreement with previous investigations in literature [37, 38, 42].

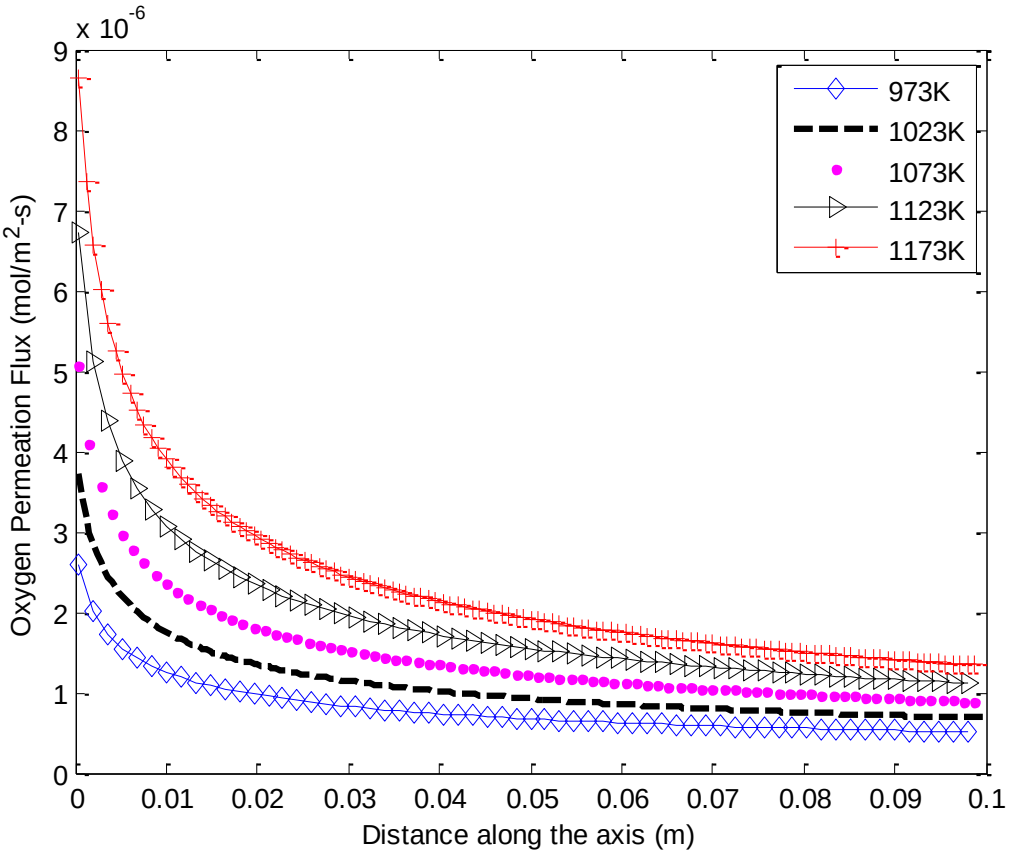

Figure 17: Effects of inlet temperature on oxygen permeation for non-reactive case

4.2.2 Effects of Sweep gas flow rates on permeation for non-reactive case

An attempt to study the influence of the sweep gas flow rates is made in this section. The flow rate of the sweep gas which comprises syngas with CO_2 has significant influence on the amount of oxygen permeated to the sweep side of the membrane. The flow rate was varied from 2.43E-7 kg/s to 3.43E-6 kg/s, while the flow rate of the feed gas was kept at constant value of 5.43E-7 kg/s. Also, other parameters were kept unchanged. As expected, there was rise in the amount of oxygen permeated as the sweep gas flow rate increases as shown in Figure 18a. This is due to the reduction in the partial pressure of oxygen at the downstream as presented in Figure 18b bringing about increased partial pressure differences and therefore more driving force for oxygen permeation. It is also noticed that for all cases, the permeation flux is reduced along the length of the reactor because reaction, which could have increased the driving force for more permeation was not in consideration in these cases.

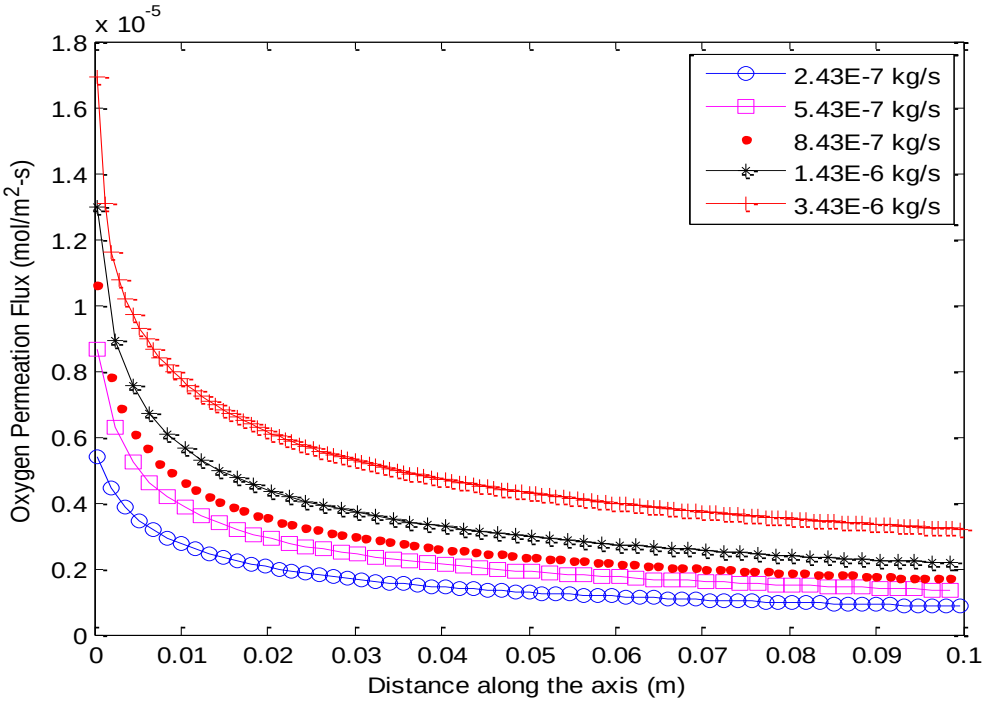

(a) Effects of sweep flow rates on oxygen permeation for non-reactive case

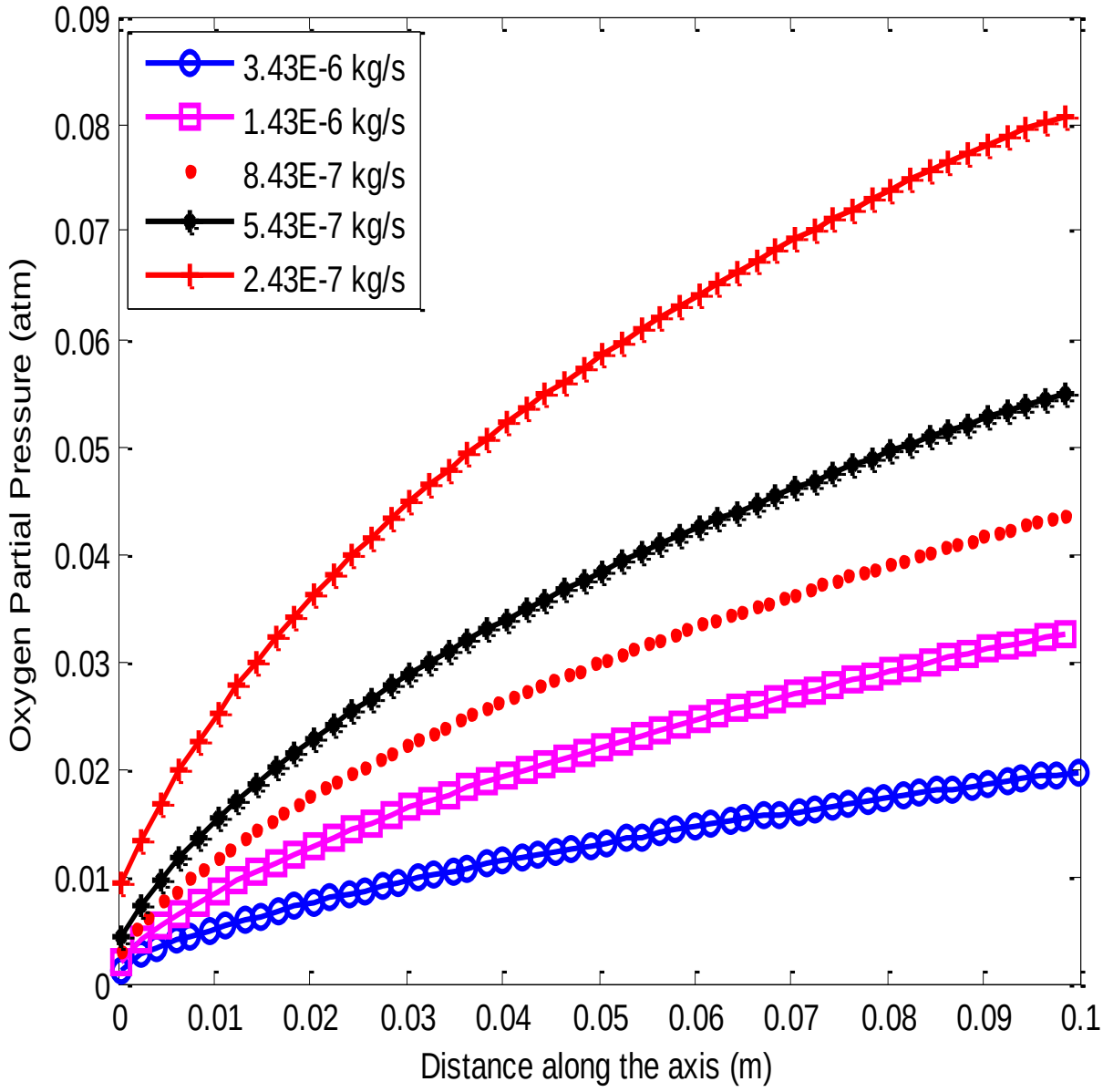

(b) Effects of sweep flow rates on oxygen partial pressure at permeate zone

Figure 18: Effects of sweep flow rates on (a) oxygen permeation flux and (b) oxygen partial pressure at permeate zone

4.3 Combustion (reactive case)

The results presented in this section involve reaction between the permeated oxygen and the syngas fuel. The combustion characteristics of synthetic gas in an OTR are analyzed in this section. The reactive (combustion) case was carried out using the three reactions presented in Eqns. (37-39). The syngas fuel with compositions being imposed at the inlet section of the sweep side reacts with the permeated oxygen after separation from air in the feed side of the membrane. It is noticed that the reaction improves the amount of permeated oxygen. As the oxygen is consumed in the reaction, more and more oxygen is permeated to react with the fuel supplied in the reactor.

4.3.1 Influence of reaction on oxygen permeation

In order to show the influence of reaction on the permeation flux, Figure 19 depicts comparison for the O_2 permeation flux for the reactive and non-reactive cases using the same conditions as presented in Table 5. It is clearly seen that the permeation flux in the case of the reactive case is far higher than the non-reactive case. The values in the reactive case range from 2.54E-6 mol/m^2s to 3.4E-5 mol/m^2s, while that of the non-reactive case range from 1.34E-6 to 8.64E-6 mol/m^2s. This shows that the reactive case has more oxygen permeation potential than the non-reactive case, with flux in the reactive case about four times that of the non-reactive case.

The result is in agreement with previous investigations in the literature like Ben Mansour et al. [46]. This is attributed to the fact that the oxygen permeated in the reactive case is consumed and this increases the difference in oxygen partial pressure between the two sides of the membrane and thereby leads to more permeation. Also, there is rise in temperature as a result of the reaction, this further increases the rate constants and with K_f being more sensitive to temperature than K_r, the movement of oxygen from the feed to the sweep side increases.

4.3.2 Kinetic Rate of Reactions and Temperature Profile

The plots of the kinetic rates for the three reactions presented in Eqns. (37-39) are shown in Figure 20. In the kinetic rates plots for the first two reactions (Eqns. 37 and 38), it is noticed that the two reactions have almost the same rate values, this makes the two plots overlap. The reason for this is because the first reaction involves formation of CO_2 from the oxidation of CO while the second involves the dissociation of CO_2 into CO and O_2. At first, there is reduction of CO_2 to CO due to the present of hydrogen. After a while, there is oxidation of CO to CO_2 with the permeated oxygen from the feed side. The third reaction rate shown in the Figure is for the hydrogen in the reaction leading to the formation of H_2O. It is noticed that the kinetic rate for the third reaction becomes very close to zero (around 0.0067kgmol/m^3s) at around 0.025m of the reactor length. This result from the hydrogen consumed due to combustion. This reaction appears to be exothermic and contribute more to the reactor temperature. It is clearly seen from the Figure that as soon the amount of hydrogen is consumed, the reactor temperature begins to reduce.

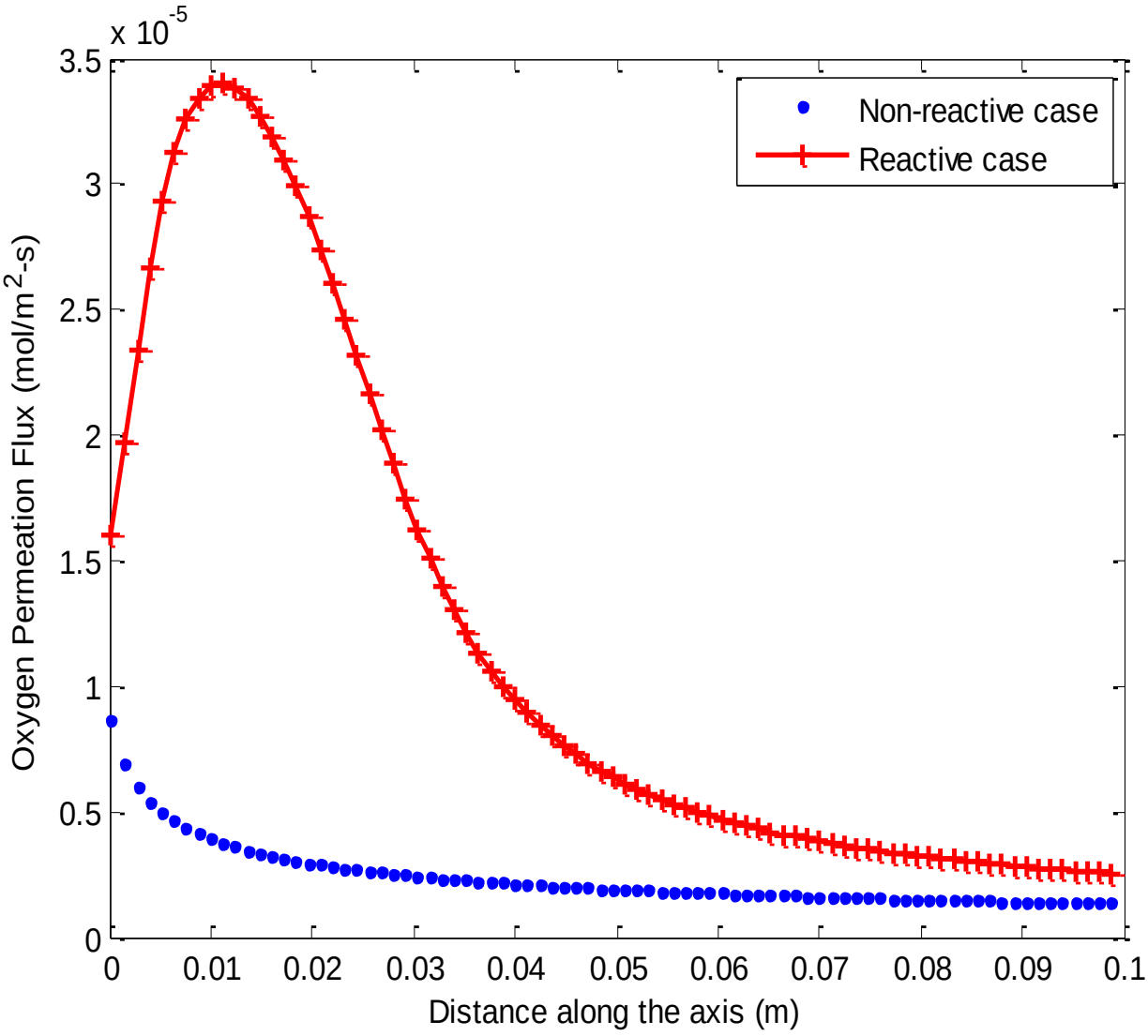

Figure 19: Reactive and non-reactive cases comparison

The profile of the temperature along the length of the reactor is shown in Figure 21a. It is noted that just like the kinetic rate of reactions, the temperature profile also increases from 1173K to 1242K. This rise in temperature can be attributed to the combustion taking place in the reactor.

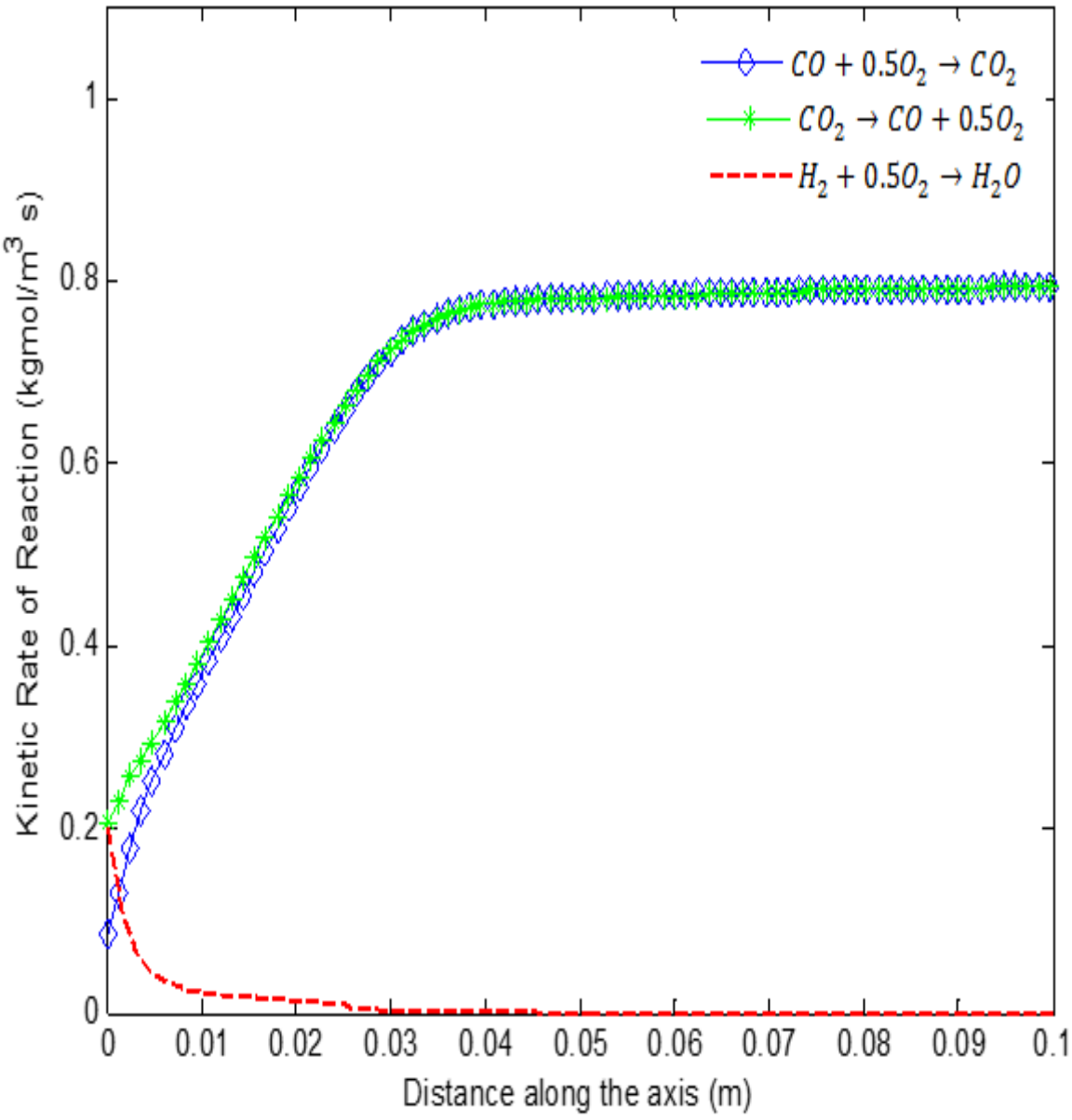

Figure 20: Kinetic rates for reactions

In order to investigate the temperature distribution in the two computational zones, the radial profile of the temperature is plotted at four different sections along the length of the reactor which are X/L = 0.1, X/L = 0.2, X/L = 0.5 and X/L = 1 corresponding to X = 0.01m, 0.02m, 0.05m, and 0.1mm respectively. The plot is shown in Figure 21b. As expected, the combustion is taking place at the sweep side of the membrane after the permeation. This leads to higher temperature at the

permeate side. It is also realized that the highest temperature occurs at around 0.02m length of the reactor where X/L = 0.2. This is in agreement with kinetic rate of reactions presented in Figure 20. In all the cases, the peak temperature occurs close to the membrane surface because the membrane absorbs heat from the sweep to the feed sides. The heat transferred to the membrane raises its temperature and this further leads to more oxygen permeation. Slightly above the membrane towards the feed side, reduction of temperature occurs in all the cases considered as shown in the Figure. The highest rise in the reactor temperature was realized at the point X/L = 0.1, where there was around 26K increment in temperature. This shows that the combustion of the fuel was early enough and the consumption of the synthetic gas was reasonable, giving its composition in the sweep gas. A contour plot is also made for the temperature distribution after the simulations as shown in Figure 21c. The contour plot also shows similar trends with the axial and radial temperature profiles, where the maximum temperature was noticed very close to the membrane wall separating the feed and sweep zone.

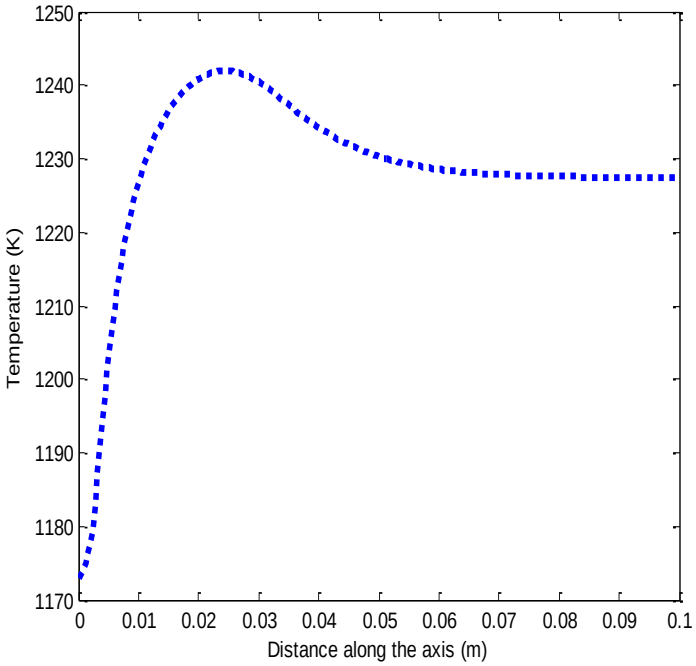

(a) Axial Temperature Profile

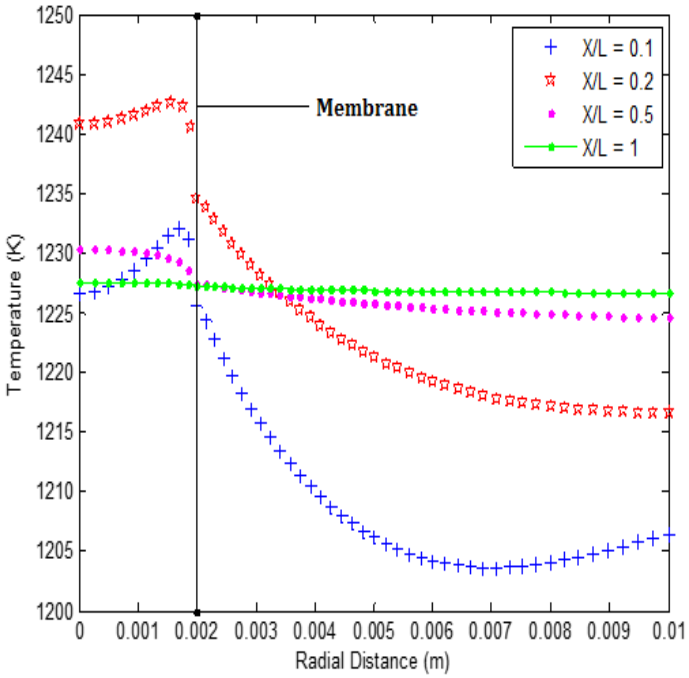

(b) Radial Temperature Profile

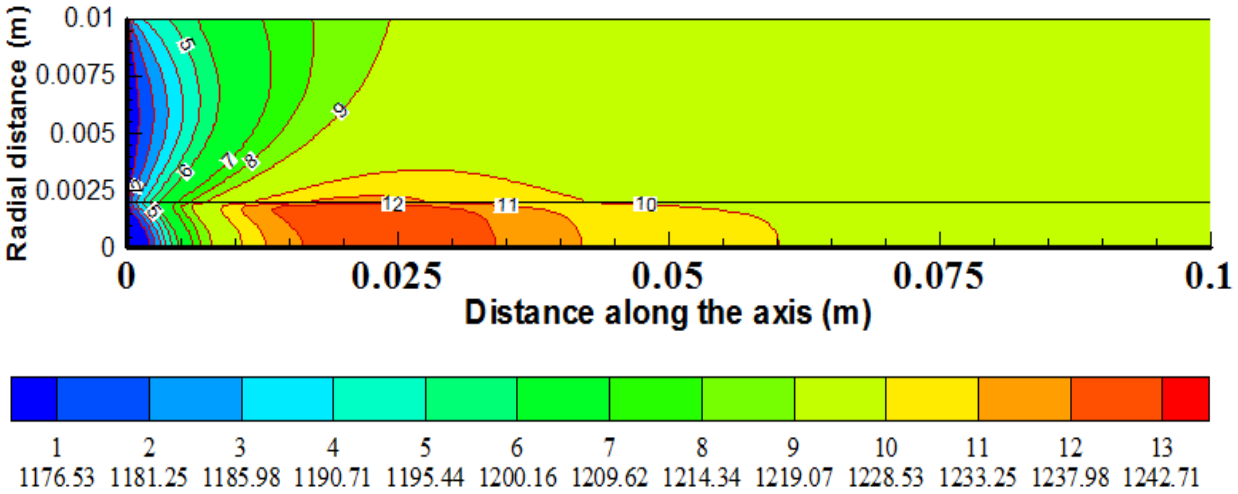

(c) Temperature contour for the base case

Figure 21: Plots of temperature (a) axial profile (b) radial profile and (c) contour plot

4.3.3 Mass Fraction of Species

The combustion characteristics of syngas in terms of species concentration are analyzed in this section. Figure 22 shows the concentration of various species in terms of mass fraction along the center line of the reactor. Concentration of each of the species is calculated as a fraction of total species concentration. The amount of H_2 in the fuel is being consumed for the formation of H_2O. This leads to reduction in the values of H_2 and consequent rise in the values of H_2O. The mass fraction of oxygen is noticed to be increasing through the length of the reactor, this is an indication of permeation of more oxygen due to combustion. The combustion leads to more oxygen partial pressure potential and, accordingly, more oxygen permeation. It is noticed that concentration of oxygen increases till the end of the reactor. This is because concentrations of other major species (CO and H_2) have reduced due to their consumption during the combustion process. Mass fractions of CO and CO_2 appear not to follow similar trend with H_2 and H_2O. This may be attributed to the fact that there are two reactions involving CO and CO_2 as shown in Eqns. (37 and 38) At the entrance region, there was rise in the concentration of CO at the expense of CO_2, which means the reaction leading to CO formation ($CO_2 \rightarrow CO$), Eq. (38), was predominant at that stage when compared to CO_2 formation. After a while, in the downstream regions, the reverse situation occurs, which shows the predominancy of the other reaction leading to the formation of CO_2 ($CO \rightarrow CO_2$). Then, stability was achieved through the length of the reactor. The trend of this result is similar to the results presented in the results reported by Fogler [82].

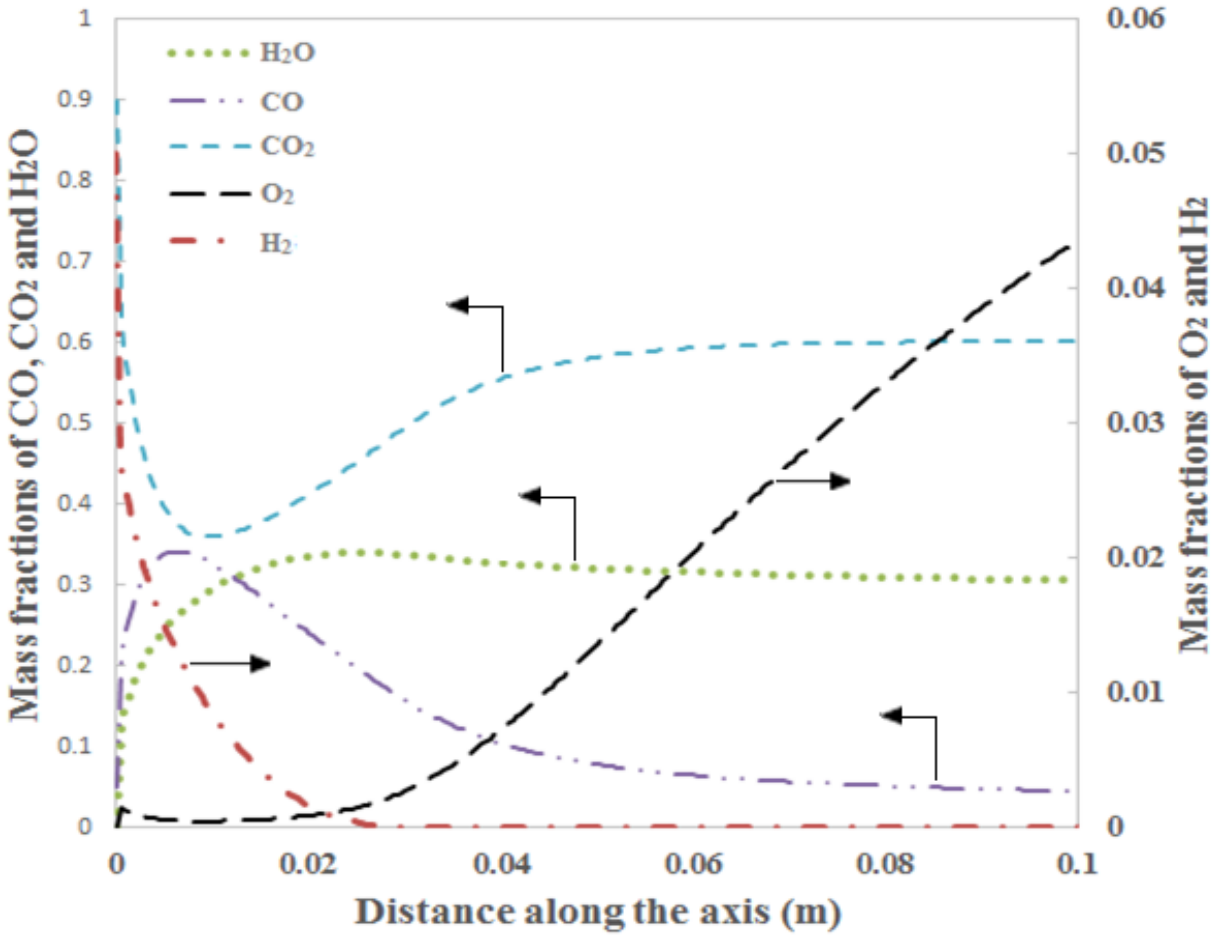

Figure 22: Mass fraction of species (CO, CO_2 and H_2O are on the left y-axis, while H_2 and O_2 are on the right y-axis)

4.3.4 Factors affecting reactor temperature and oxygen permeation in an OTR

Some parameters of interest are known to have influence on combustion characteristics in an OTR, they include: fuel composition, sweep gas flow rate, inlet temperature, CO_2 circulation and the likes. Fuel composition levels involves changing CO/H_2 ratio in the sweep gas, CO_2 circulation involves the fraction of CO_2 in the sweep gas at the expense of the fuel. All these parameters are imposed at the sweep inlet section of the reactor. In order to fully understand the effects of these parameters, parametric studies were carried out to investigate the parameters and their effects. At this stage, it is worth noting that temperature rise and/or increase in partial pressure difference will

enhance more permeation. Hence, any parameter that raises the reactor temperature, the feed side oxygen partial pressure, or reduces the sweep side oxygen partial pressure will have favourable effects on oxygen permeation and will enhance combustion of the reactive gas.

In this section, therefore, four different influential parameters having five levels each, are studied in order to fully understand the effects of each of them on the oxycombustion characteristics. Table 6 shows the parameters, their levels and their corresponding values. The approach involves changing the levels of a single parameter and keeping all others at their base values. This will enable one to study that single changing parameter and will prevent others from influencing the results.

4.3.4.1 Effects of inlet temperature

The effects of inlet temperature was studied by varying the temperature from 973K to 1173K, which are ideal for permeation of the needed oxygen for combustion, while all other parameters are kept constant. Results in the literature show that, at lower temperatures, the oxygen permeation is as a result of surface exchange while the determining factor at higher temperature is the bulk diffusion [45,79]. Figures 23a and 23b exhibit the influence of inlet temperature on oxygen permeation and the reactor temperature profile respectively. It is noticed that as the inlet temperture increases, the overall reactor temperature also increases due to combustion and also more permeation occurs. This is because a rise in the inlet temperature improves the combustion process due to increase in the rate constants (K_f and K_r), which have effects on the permeation flux as shown in Eq. (9). The forward rate K_f, which determines adsorption of oxygen, is more sensitive to temperature than the reversed rate constant K_r, which determines desorption. This leads to more permeation from the feed to sweep side and then the permeation flux increases with temperature. It was also noticed that with increase in the inlet temperature, combustion was quicker and

therefore the maximum reactor temperature was achieved earlier than the cases with lower inlet temperature. This combustion characteristics of syngas is in agreement with the work of Singh et al. [25]**,** where it is shown that as the preheat temperature in syngas combustion increases, the flame speed increases. This has overall increasing effect on the reactor temperature. The location of the peak of oxygen permeation coincides with the location of the peak in combustion temperature as shown in the Figures because more oxygen permeation improves the combustion process as explained above. The peak location is moved toward the reactor inlet section as the inlet temperature is increased. This can be attributed to the increase in oxygen permeation flux at high temperature which results in faster formation of a flammable mixture of fuel and oxygen.

Table 6: Different cases used in the present work for parametric study

Parameters	Sweep flow rates (kg/s)	Temperature (K)	CO_2 Circulation syngas/CO_2 (%)	Fuel Composition CO/H_2 by %
Cases	2.43E-7	973	25/75	90/10
	5.43E-7	1023	20/80	70/30
	8.43E-7	1073	15/85	50/50
	1.43E-6	1123	10/90	30/70
	3.43E-6	1173	5/95	10/90

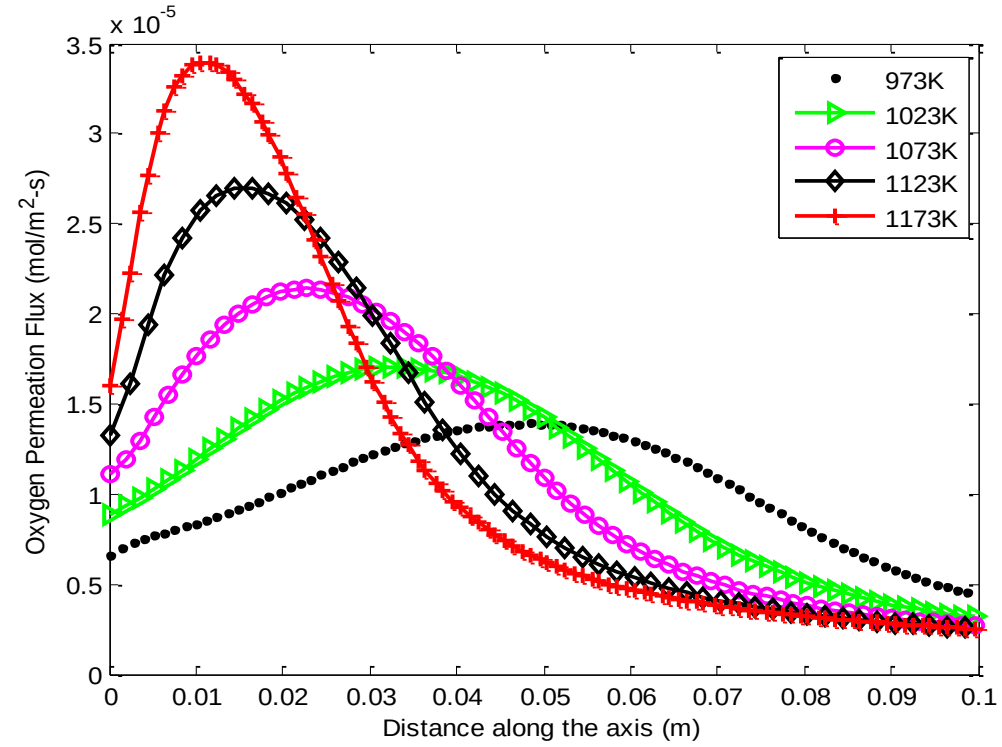

(a) Effects of inlet temperatuere on oxygen permeation flux

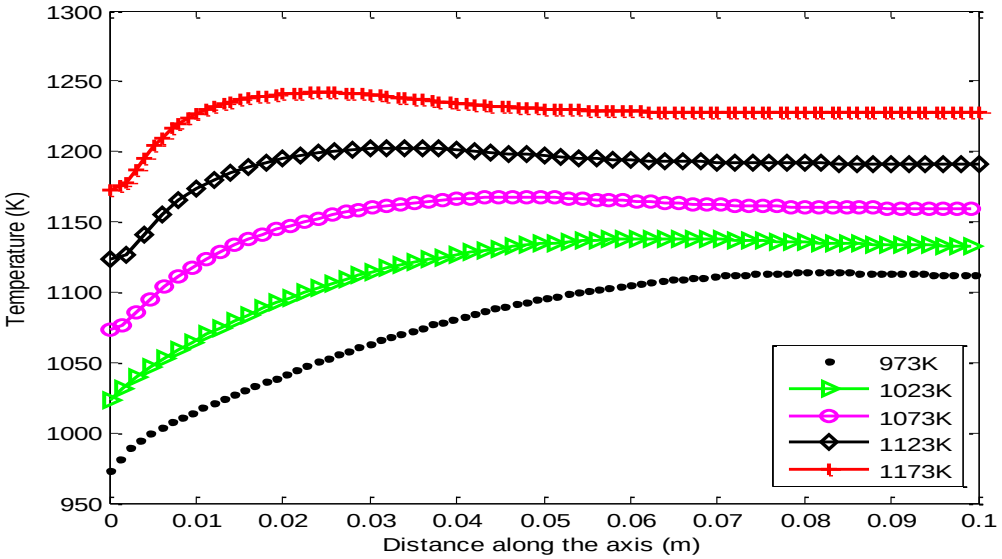

(b) Effects of inlet temperature on the reactor axial temperature distribution

Figure 23: Effects of inlet temperature on (a) oxygen permeation flux (b) reactor axial temperature distribution.

4.3.4.2 Effects of sweep gas flow rate

Another influential parameter affecting the performance of an ITM as well as the combustion characteristics in the OTR is the sweep gas flow rate. The value of the flow rate is imposed at the inlet section of the sweep gas. In order to investigate its effects, the sweep flow rate is varied from 2.43E-7 kg/s to 3.43E-6 kg/s while keeping all other parameters at their base values. The effects of sweep gas flow rates on reactor temperature and permeation flux are presented in Figures 24a and 24c respectively. Increasing the sweep gas flow rates improves the amount of oxygen permeated. This can be attributed to the fact that more sweep gas flow rates raises the amount of fuel in the sweep side and dilutes the permeated oxygen. With this, the extra fuel is expected to consume the permeated oxygen and reduces the oxygen partial pressure at the sweep side as shown in Figure 24b. With the oxygen partial pressure at the feed side being kept at constant value of 0.21atm, there is more partial pressure differences between the feed and sweep side of the membrane and thereby increasing oxygen driving force, which will eventually lead to more permeation. The trends of the results are in agreement with results in literature [42,79,82]**.** It is also noticed that there are delays in combustion when the flow rate increases. This can be attributed to the rise in the amount of the fuel as a result of flow rate increment; this will require more oxygen for combustion. Therefore, there is a delay in combustion unlike sweep gas with low fuel as a result of low mass flow rate. The effects of flow rate on permeation is felt more at high flow rates, this is also the case in terms of oxygen partial pressure differences as shown in Figure 24b. The reactor temperature also increases with increase in flow rate as shown in Figure 24a. This is because there are more fuels due to high flow rate and more oxygen is permeated, therefore enhancing combustion, which eventually leads to higher temperatures.

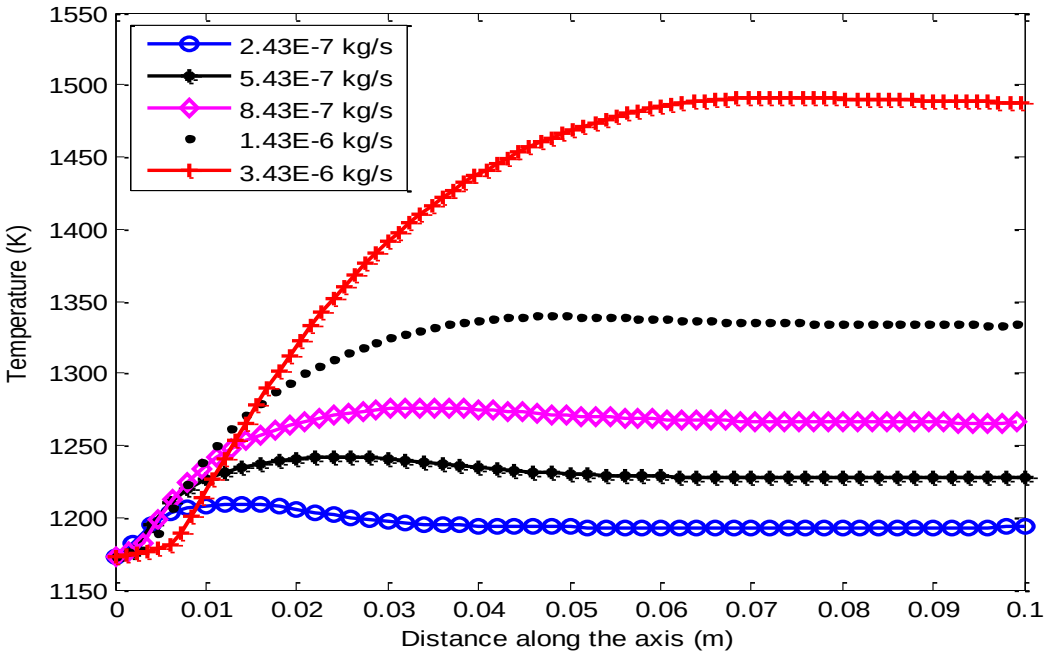

(a) Effects of sweep flow rate on reactor temperature

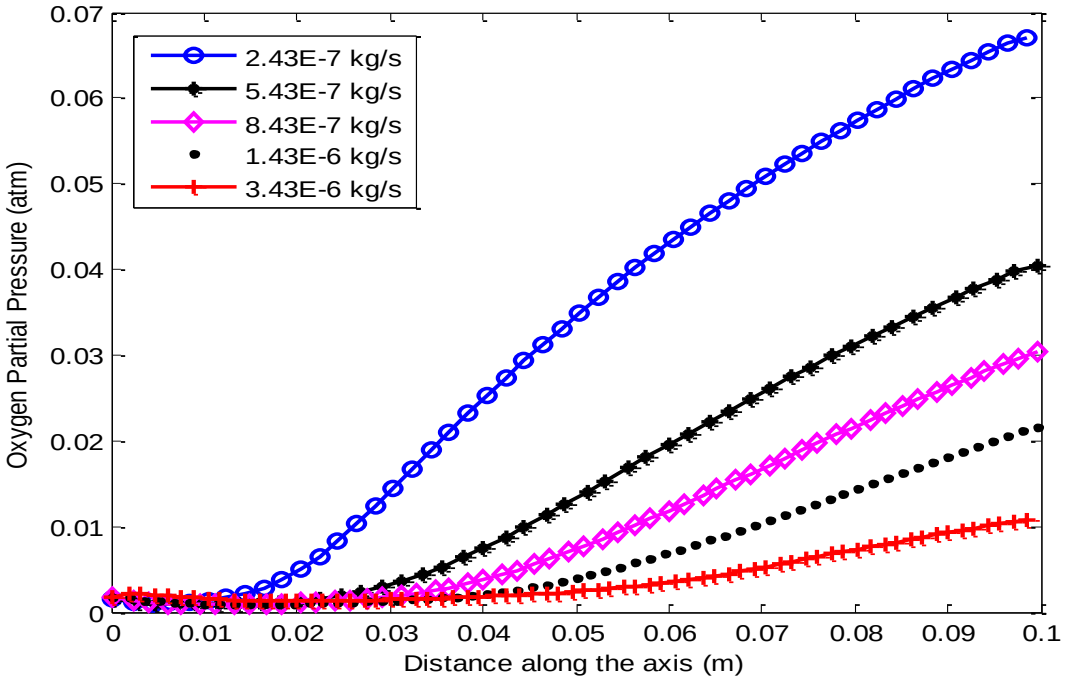

(b) Effects of sweep flow rate on partial pressure

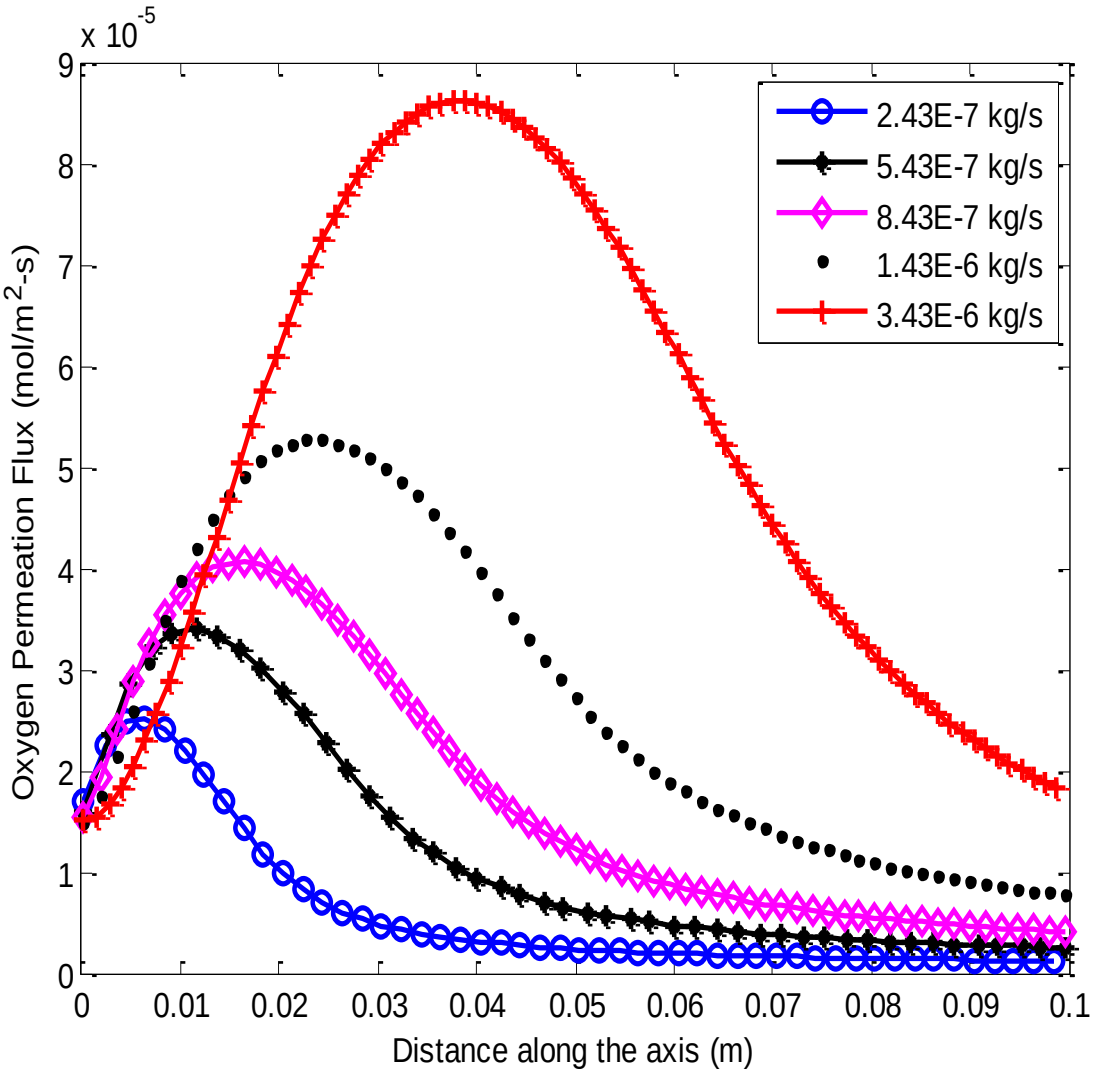

Figure 24: Effects of sweep flow rate on (a) reactor temperature (b) partial pressure (c) oxygen permeation flux

4.3.4.3 Effects of fuel composition

Fuel composition (CO and H_2 fraction) also have significant influence on the characteristics of syngas combustion in an OTR, O_2 permeation rate through the membrane, as well as the reactor temperature. Synthetic gas considered in the present work comprises CO and H_2. The addition of CO_2 is not serving as fuel; it merely serves as a replacement for the depleted N_2 as a diluent and to moderate the reactor temperature. In order to show the influence of the fuel composition, the

CO/H_2 ratio is varied by increasing the amount of hydrogen in the fuel at the expense of CO. The ratio varies from CO/H_2 = 1:9 to CO/H_2 = 9:1. The simulations are carried out with fuel/diluent ratio (syngas/CO_2) of 1:9. The amount of CO_2 in the sweep gas and all other parameters other than CO/H_2 ratio are kept constant at their base values in order to focus on the effects of fuel composition only. It is noticed that increasing the amount of hydrogen in the syngas composition increases the reactor temperature as shown in Figure 25a. This may be attributed to the better ignition characteristics and high flame speed of hydrogen, and the fact that increasing the amount of hydrogen increases the thermal and mass diffusivity of the fuel, which consequently increases the flame speed and the reactor temperature. It is also noticed, as presented in Figure 25b that higher amount of hydrogen in the fuel results in more oxygen permeation. This can be attributed to the increase in combustion temperature while increasing inlet hydrogen concentration in the syngas mixture. This may also be due to the fact that increasing hydrogen (which has a small molecular weight) composition in the fuel results in overall reduction of the molecular weight of the fuel. This leads to increase in the volumetric flow rates and enables the sweep gas to sweep more oxygen, and accordingly, more permeation. Hence, increasing the hydrogen composition in the fuel enhances permeation of oxygen as well as the reactor temperature. The reverse is the case when the amount of CO in the fuel is increased. Increasing hydrogen concentration resulted in a delay in formation of a flammable mixture due to the increased amount of required oxygen for combustion in such cases. This may justify the movement of the peak locations of temperature and oxygen flux toward the reactor exit as hydrogen concentration is increased in the inlet syngas mixture. The details of the effects of the fuel composition on reactor axial temperature distribution are also shown with the aid of contour plots in Figure 27, where the temperatures are in Kelvin.

These results are in agreement with that of Ding et al. [20], Natarajan et al. [84], and Lapalme and Seers [85]

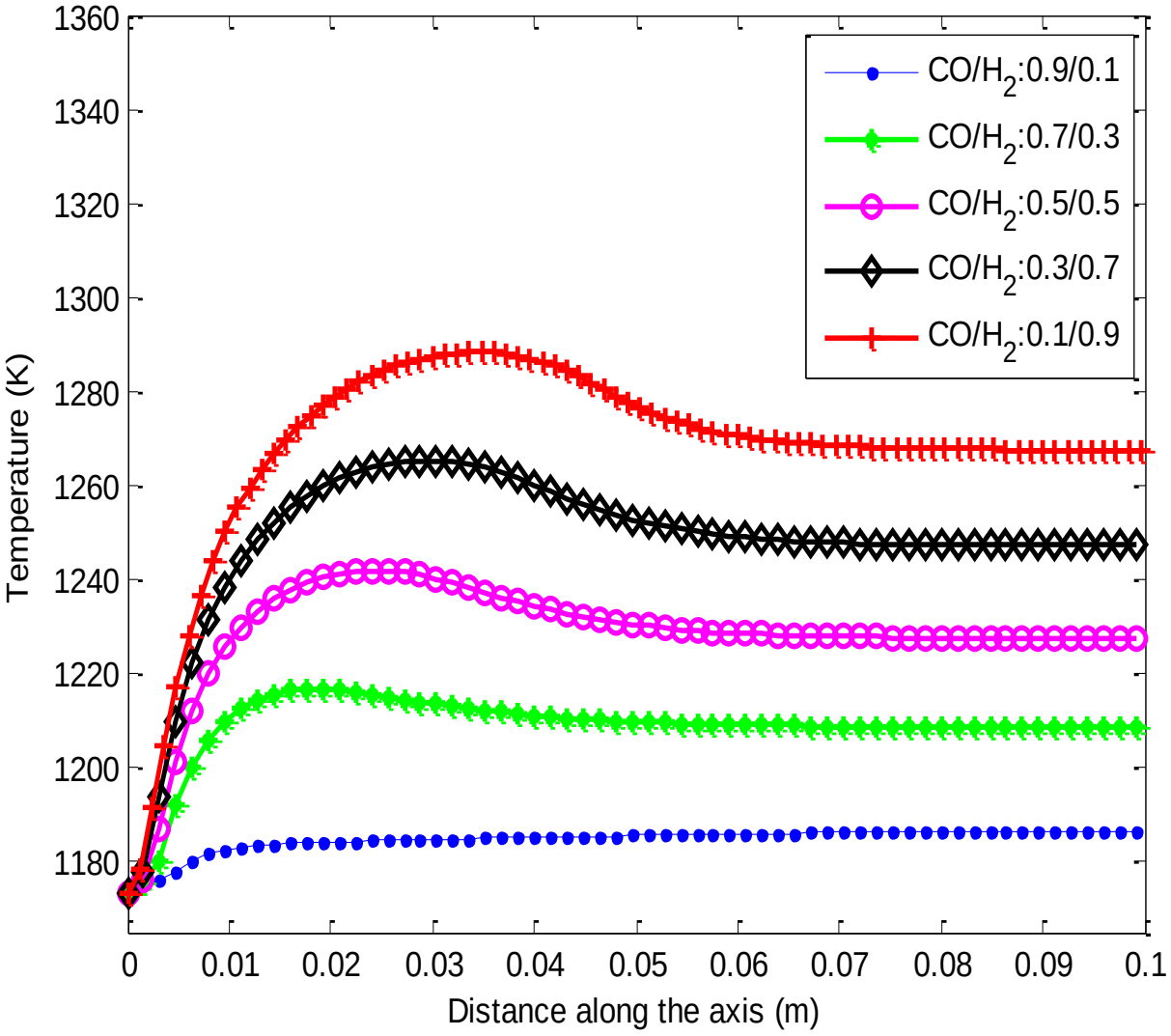

(a) Effects of fuel composition (CO/H_2 ratio) on reactor axial temperature distribution

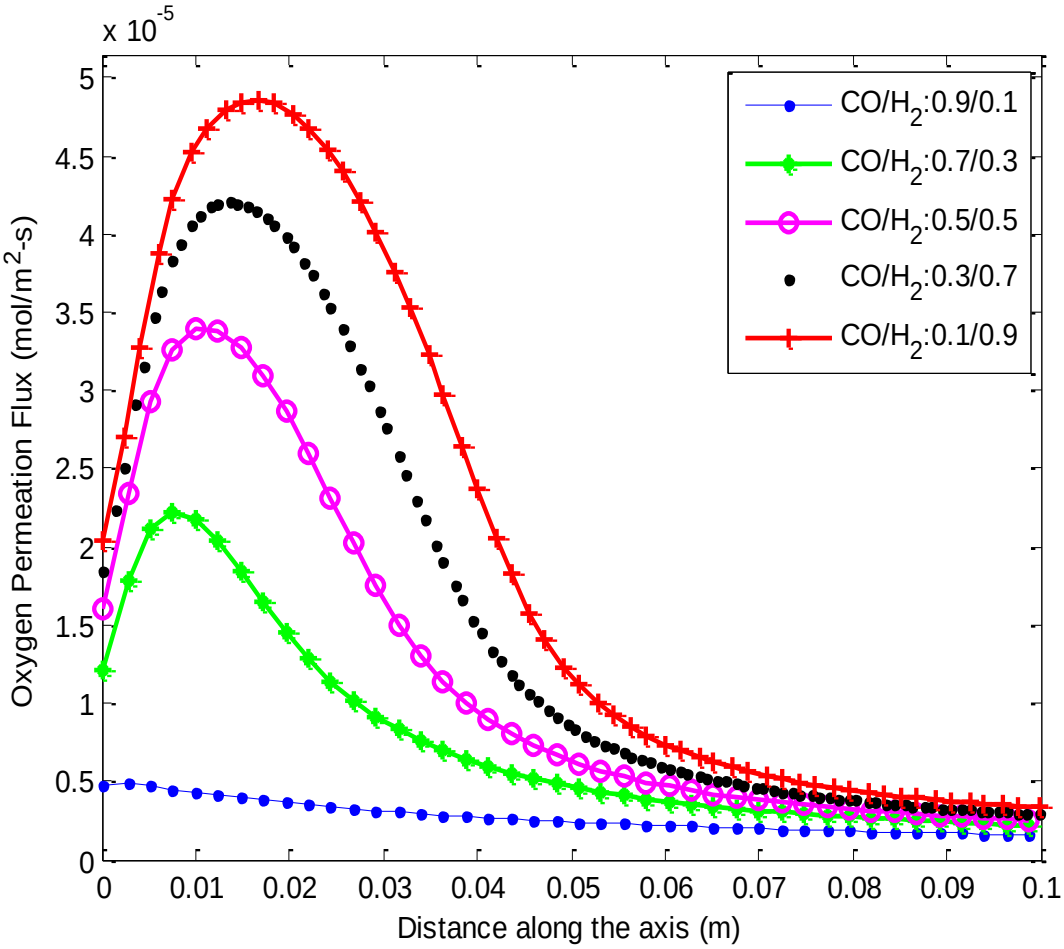

(b) Effects of fuel composition (CO/H_2 ratio) on oxygen permeation flux

Figure 25: Influence of syngas fuel composition on (a) reactor temperature (b) oxygen permeation

4.3.4.4 Effects of CO_2 circulation

The addition of CO_2 in the reactor compensates for the depleted nitrogen and serves as diluent in the reaction. Thereby, moderating the reactor temperature. The influence of CO_2 circulation on the reactor temperature and oxygen permeation through the LSCF-6428 membrane has also been investigated in the present work. Five different cases were considered by varying the mass fraction of CO_2 in the sweep gas. The considered cases were with 75-95% of CO_2 as shown in Table 6. It

is seen that the reactor temperature reduces with increase in CO_2 as shown in Figure 26a. This may be due to high heat capacity of CO_2 and the reduction in flame speed, as a result, the reactions intensity is reduced which results in reduction in the combustion temperature inside the reactor. Also, increasing the concentration of CO_2 while reducing fuel concentration results in reduction in the reacting species and, as a result, the reactions rates are reduced. The reaction rates have direct effect on the combustion temperature as shown in Figures 21 and 22. The trends of these results are in agreement with that of Azharuddin et al.[68], Natarajan et al. [84], and Lapalme and Seers [85]. It is also realized that as the amount of CO_2 circulated in the reactor increases, the amount of oxygen permeation flux reduces. This can be attributed to the high molecular weight of CO_2. Increasing the amount of CO_2 circulation raises the overall molecular weight of the sweep gas thereby increasing the density. With the mass flow rate kept constant, the volumetric flow rate which is inversely proportional to density reduces as density increases. This reduces the ability of the permeate gas to sweep the permeated oxygen, and thereby reduces the permeation. Therefore, increasing the amount of CO_2 in the sweep gas reduces the oxygen permeation flux as shown in Figure 26b. It should be noted that while reducing the fuel concentration (increasing CO_2 concentration), the amount of fuel is reduced and, accordingly, the required amount of oxygen to form a flammable mixture is reduced. This may justify the movement of the peak locations of both temperature and oxygen flux toward the reactor inlet as the fuel concentration is reduced at reactor inlet. The effects of the CO_2 circulation on the overall reactor temperature are further presented in form of contour plots as shown in Figure 28, where the temperatures are in Kelvin.

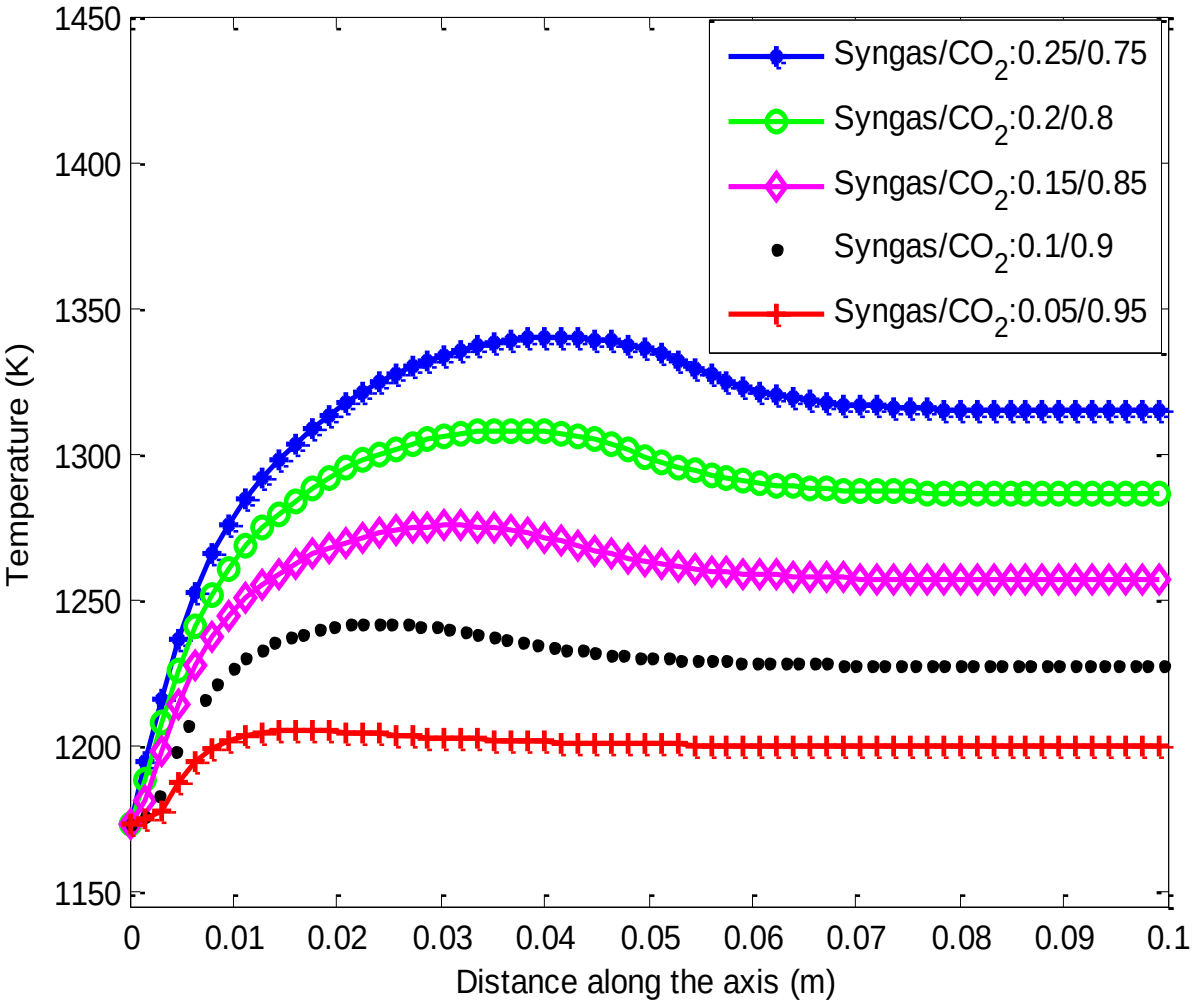

(a) Effects of CO_2 circulation on the reactor axial temperature distribution

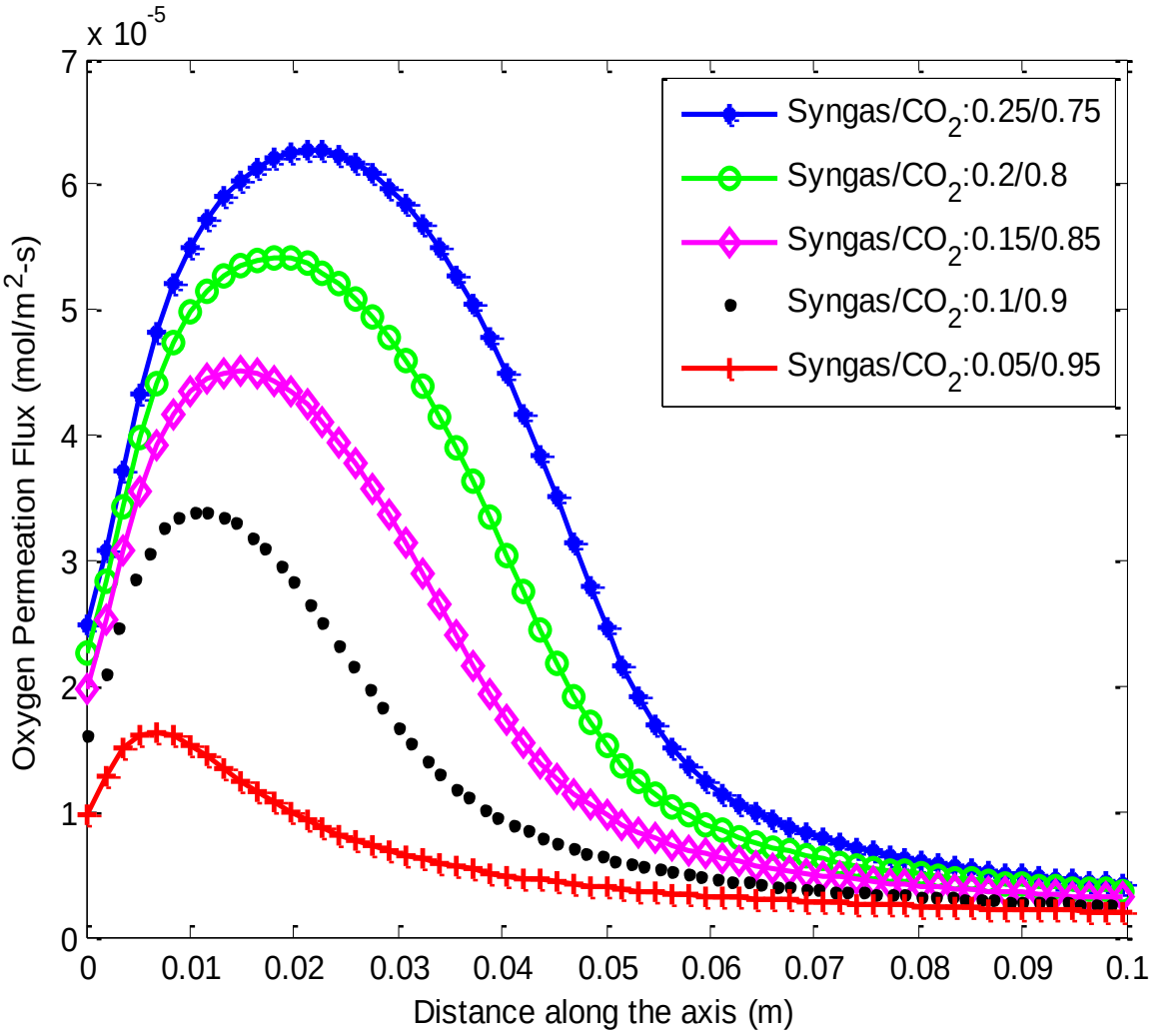

(b) Effects of CO_2 circulation on oxygen permeation flux

Figure 26: Effects of CO_2 circulation on (a) reactor temperature (b) oxygen permeation flux

CO/H_2 : 0.9/0.1

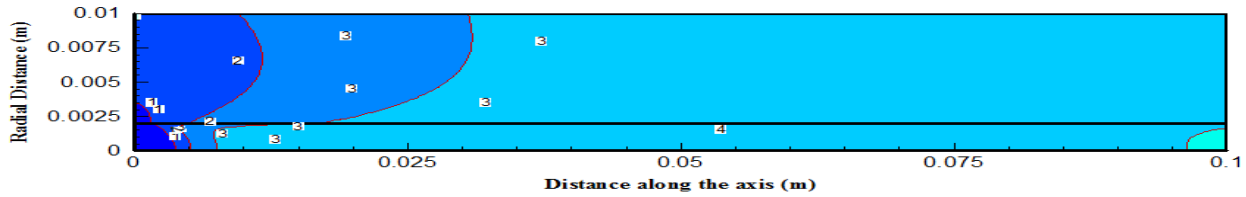

CO/H_2 : 0.7/0.3

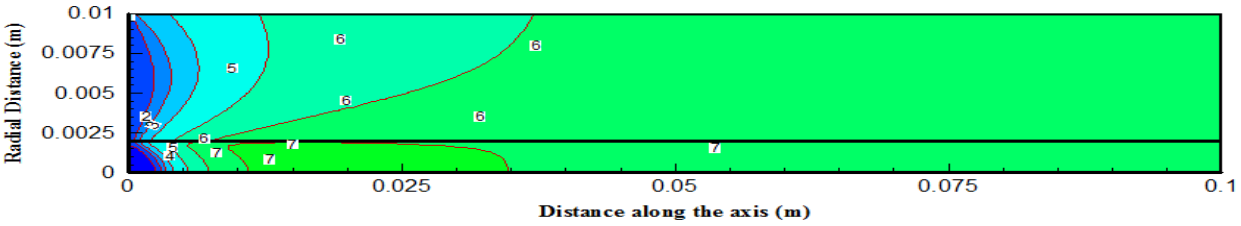

CO/H_2 : 0.5/0.5

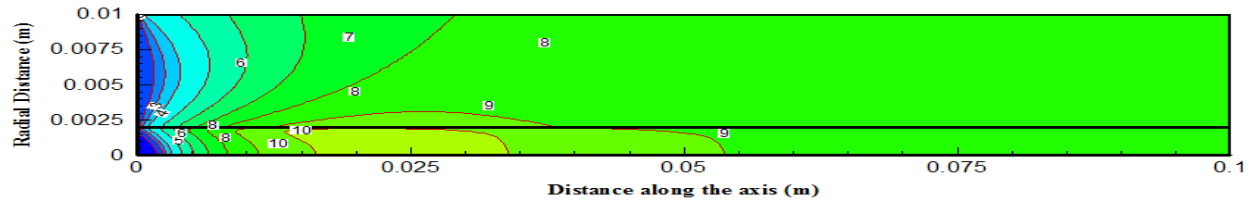

CO/H_2 : 0.3/0.7

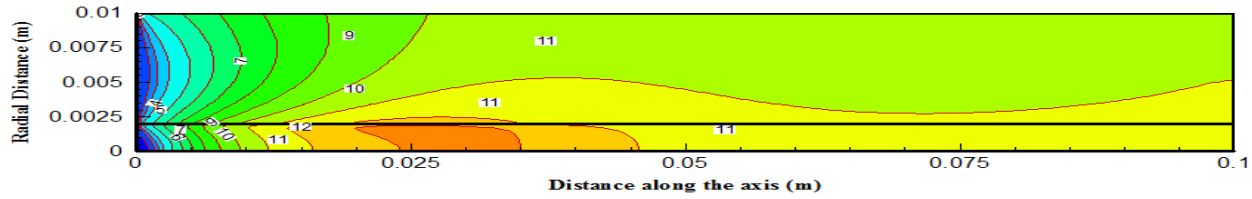

CO/H_2 : 0.1/0.9

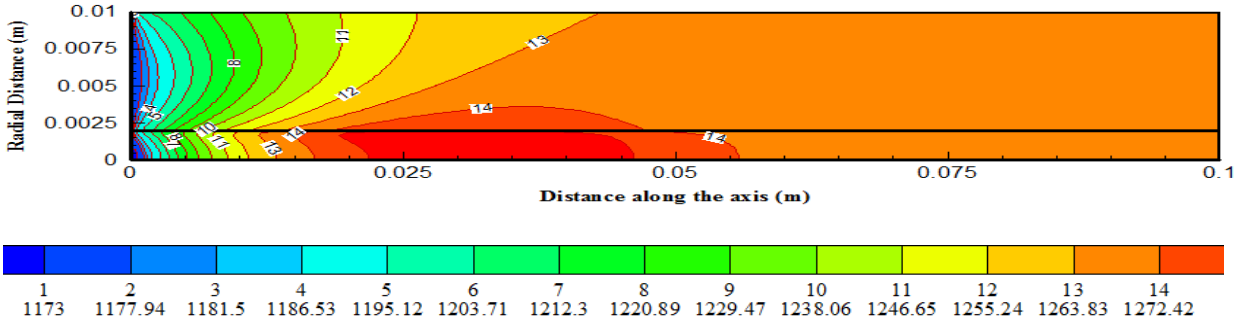

Figure 27: Temperature contours for different fuel compositions

Syngas/CO_2 : 0.05/0.95

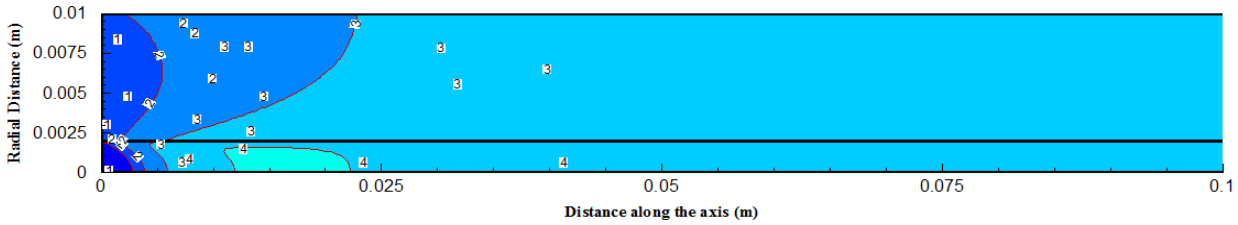

Syngas/CO_2 : 0.1/0.9

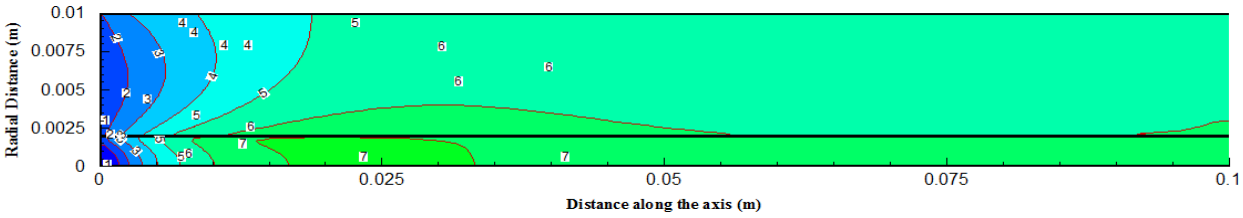

Syngas/CO_2 : 0.15/0.85

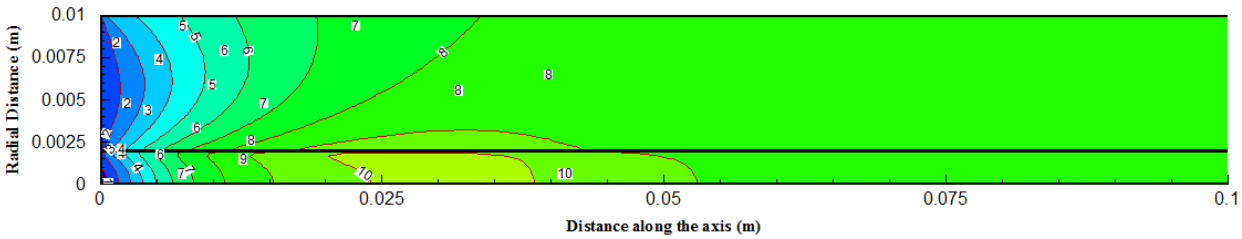

Syngas/CO_2 : 0.2/0.8

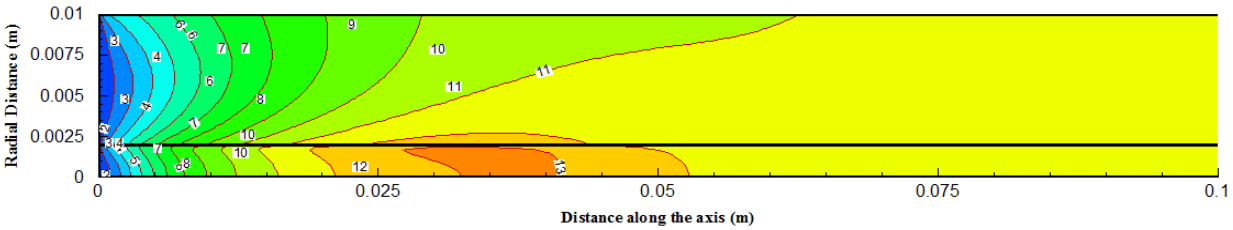

Syngas/CO_2 : 0.25/0.75

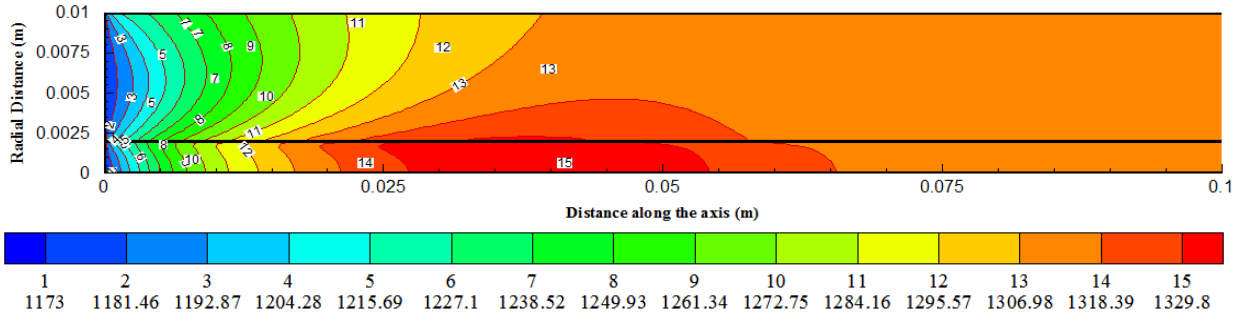

Figure 28: Temperature contours for different CO_2 circulation

4.4 Results of syngas including CH_4 among species

Simulations for a case involving syngas with the inclusion of CH_4 were performed for both reactive and non-reactive cases. As discussed earlier, the case was carried out with small amount of fuel to make the combustion more realistic. The fraction of the fuel considered in this case is 1:1:1 for the $CH_4/CO/H_2/CO_2$. The values of the parameters used are same with the case without CH_4 as sumarized in Table 5 earlier, but now with the inclusion of methane, making the sweep gas composition of $CH_4/CO/H_2/CO_2$:0.5/0.5/0.5/0.85. Additional reaction (Eq. 40) involving CH_4 presented by Andersen et al. [86] was added to the three steps syngas reaction mechanism presented by Cuoci et al. [79], which was previously used. This makes it a 4-step reaction.

$$CH_4 + 1.5O_2 \rightarrow CO + 2H_2O \qquad r_1 = 1.59 * 10^{13} \exp\left(-\frac{47800}{RT}\right)[CH_4]^{0.7}[O_2]^{0.8} \tag{40}$$

The results of the simulations from this case are shown in Figures 29-31. Figure 29 compares the oxygen permeation flux for syngas case involving CH_4 in the the reactive and non-reactive conditions. As expected, the reactive case has higher temperature. This may be attributed to the consumption of the permeated oxygen in the reacting case and this increases the difference in oxygen partial pressure between the two sides of the membrane, and thereby leads to more oxygen permeation.

Comparison is also made for the temperature profiles and oxygen permeation flux between cases with and without CH_4 as shown in Figures 30 and 31. It is seen that the reactor temperature and oxygen permeation flux in the case with CH_4 is lower than the case without CH_4. This is because inclusion of CH_4 to syngas composition and keeping the amount of CO_2 in the sweep side constant reduces the reactivity of the fuel because CH_4 is less reactive as compared to H_2. This reduces

performance and the flame temperature, and eventually leads to lower reactor temperature as well as oxygen permeation flux.

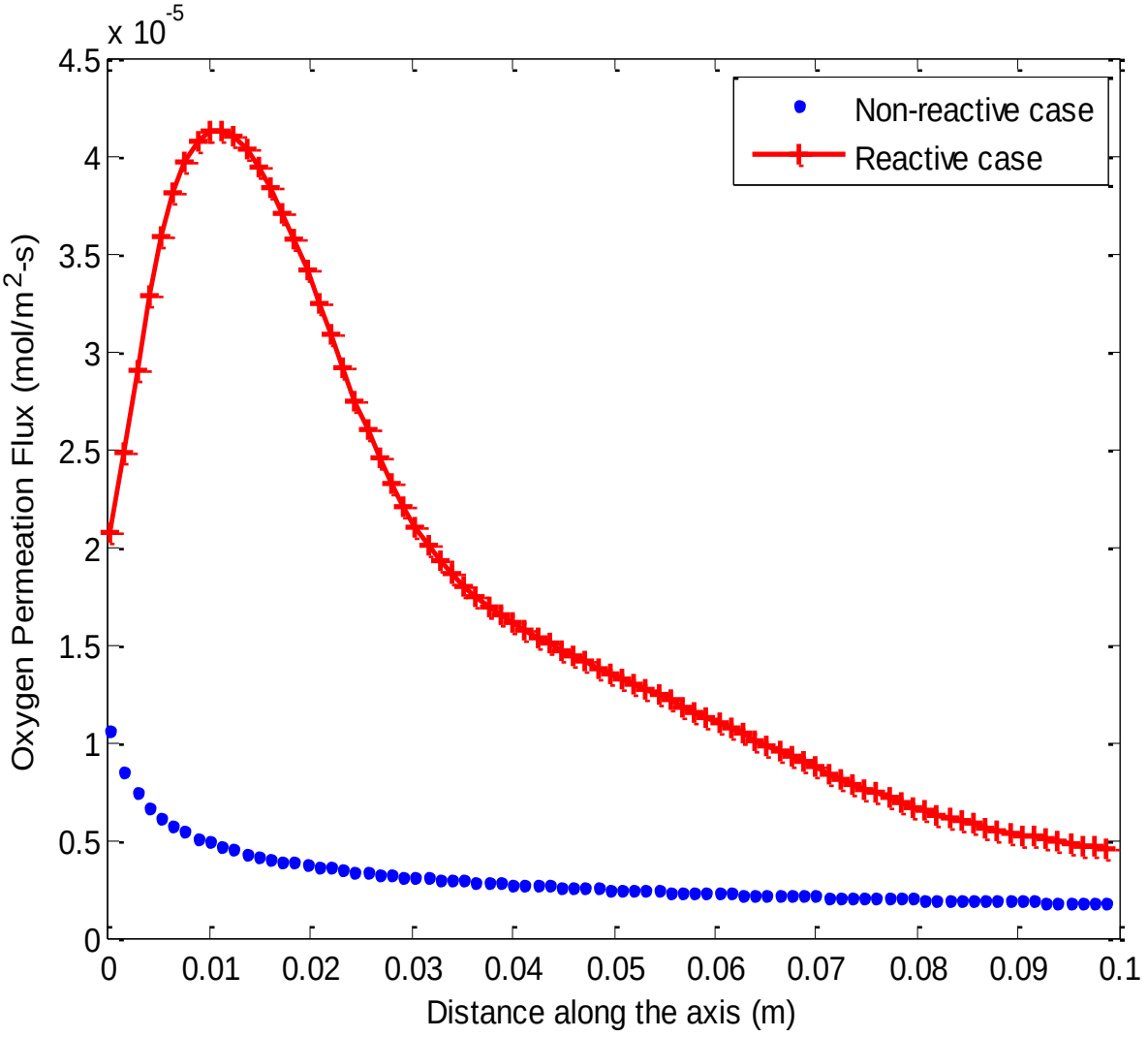

Figure 29: Reactive and non-reactive cases comparison for syngas with CH_4

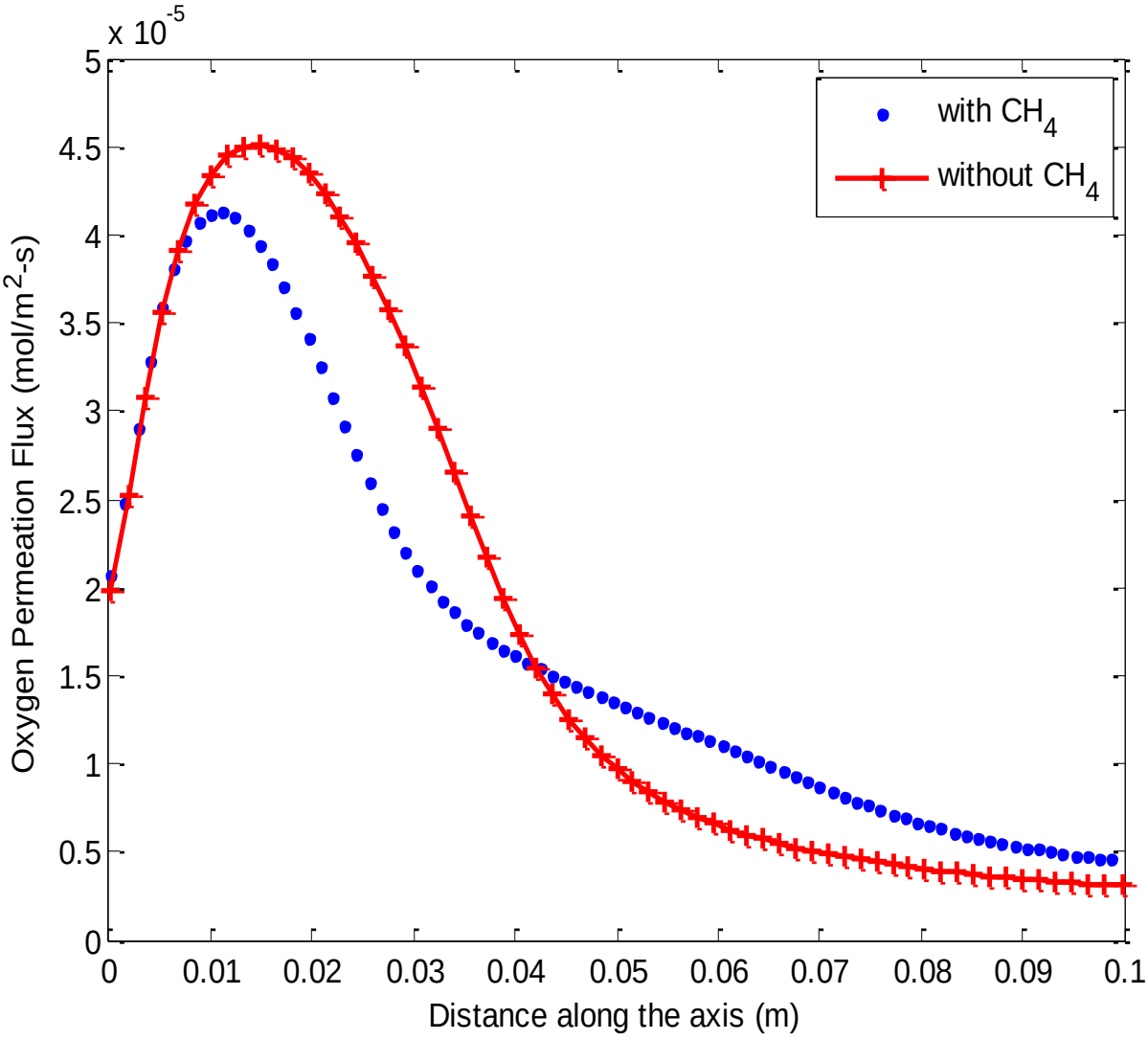

Figure 30: Comparison between oxygen permeation flux for cases with and without CH_4

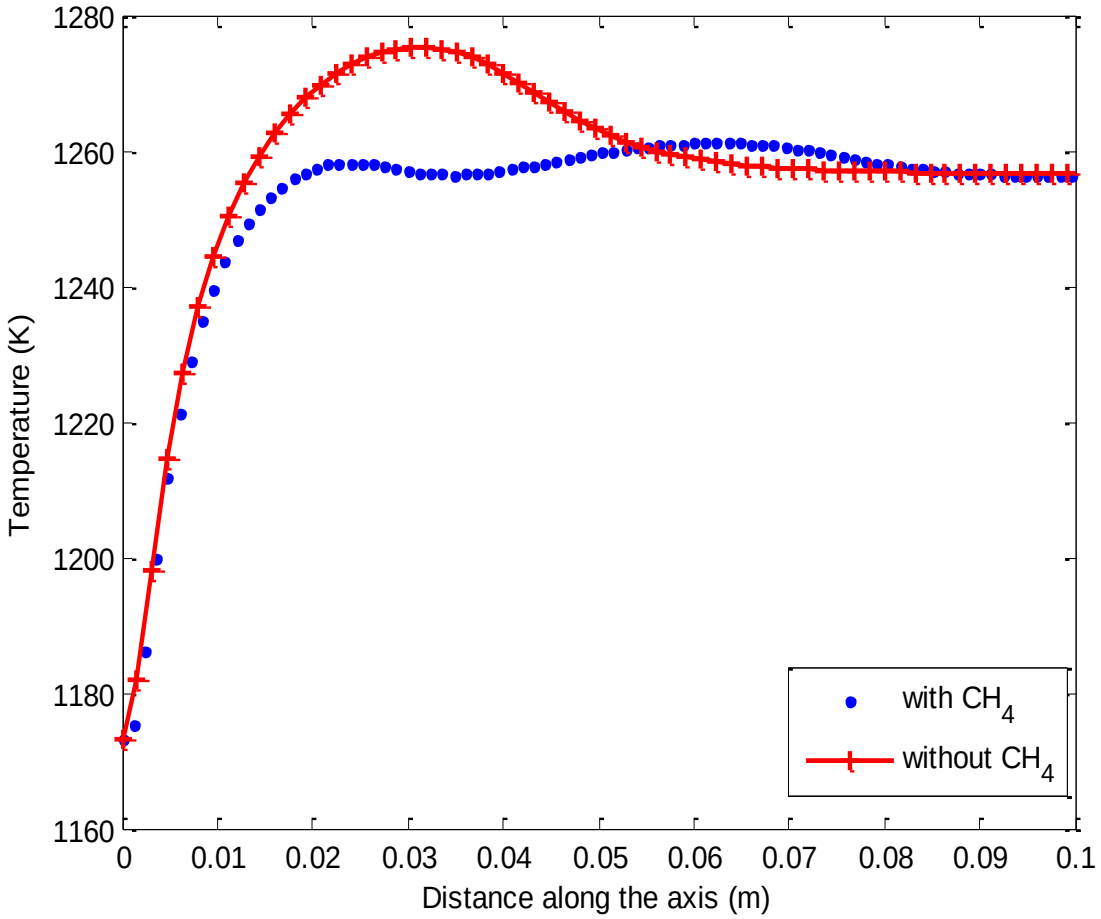

Figure 31: Temperature profile comparison for case with and without CH_4

4.5 Energy balance in the oxygen transport reactor

In order to perform thermodynamic analysis of the combustion process, energy balance is carried out for the base case with list of parameters shown in Table 5. A block diagram for the OTR is shown in Figure 32. The energy balance relations are presented in Eqns. (41-45). The thermodynamic analysis is performed by considering all the masses entering and leaving the feed side as well as the permeate side of the membrane. The total heat transfer rate across the membrane is also taking into consideration in the analysis.

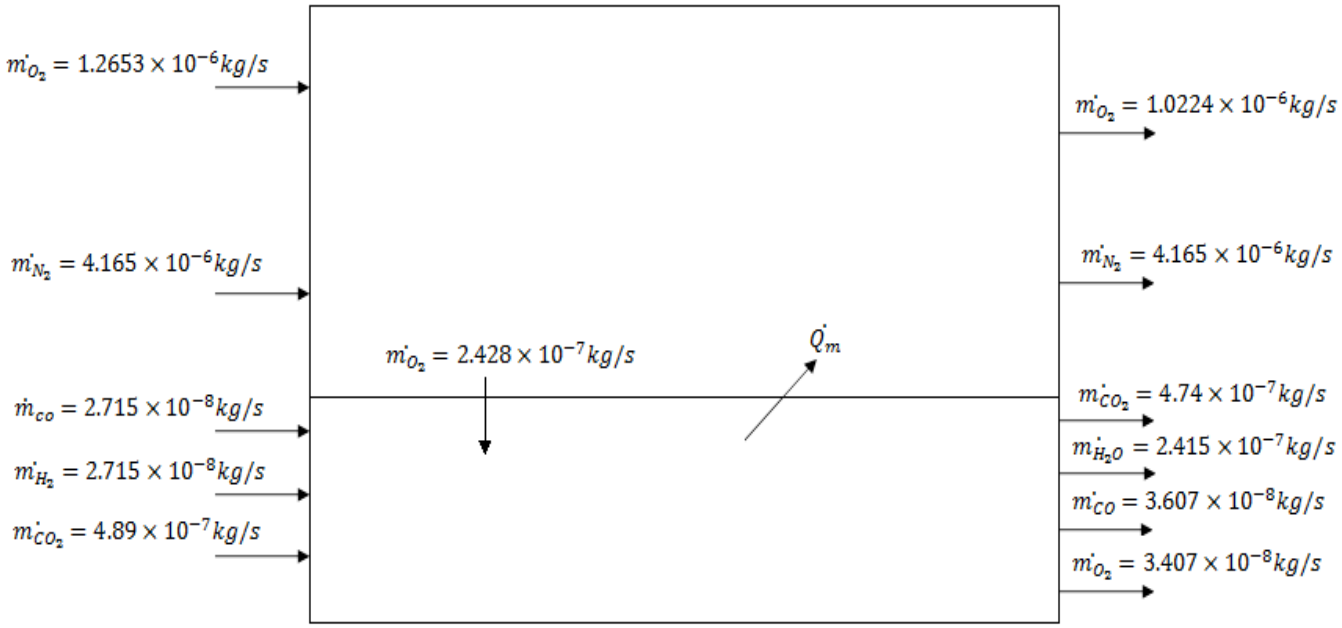

Figure 32: Block diagram of the OTR with mass balance for all species

4.5.1 Energy equations in the feed side

Feed inlet:

$$Q_{feed_{inlet}} = m_{O_2} C_{p_{O_2}} \left(T_{air_{inlet}} - T_r\right) + m_{N_2} C_{p_{N_2}} (T_{air_{inlet}} - T_r) \quad (41)$$

Feed outlet:

$$Q_{feed_{outlet}} = m_{O_2} C_{p_{O_2}} \left(T_{air_{outlet}} - T_r\right) + m_{N_2} C_{p_{N_2}} (T_{air_{outlet}} - T_r) \quad (42)$$

4.5.2 Energy equations in the permeate side

Sweep inlet:

$$Q_{sweep_{inlet}} = m_{CO}(LCV_{CO} + C_{p_{CO}}\left(T_{fuel_{inlet}} - T_r\right)) + m_{H_2}(LCV_{H_2} + C_{p_{H_2}}(T_{fuel_{inlet}} - T_r)) +$$

$$m_{CO_2} C_{p_{CO_2}} \left(T_{fuel_{inlet}} - T_r\right) \quad (43)$$

Sweep outlet:

$$Q_{sweep_{outlet}} = m_{CO}\left(LCV_{CO} + C_{p_{CO}}\left(T_{fuel_{outlet}} - T_r\right)\right) + m_{H_2O}C_{p_{H_2}}\left(T_{fuel_{outlet}} - T_r\right) +$$

$$m_{CO_2}C_{p_{CO_2}}\left(T_{fuel_{outlet}} - T_r\right) + Q_m \quad (44)$$

In order to achieve energy balance in the system, the total energy entering the control volume should be equal to the total energy leaving the control volume. This implies that:

$$Q_{feed_{inlet}} + Q_{sweep_{inlet}} = Q_{feed_{outlet}} + Q_{sweep_{outlet}} \quad (45)$$

4.5.3 Energy entering the control volume

$\boldsymbol{m_{O_2}C_{p_{O_2}}\left(T_{air_{inlet}} - T_r\right)}$ = 1.2652 x 10^{-6} x 1.11 x (1173 – 298.15)

= 1.229W

$\boldsymbol{m_{N_2}C_{p_{N_2}}(T_{air_{inlet}} - T_r)}$ = 4.1648 x 10^{-6} x 1.198 x (1173 – 298.15)

= 4.365W

$m_{CO}(LCV_{CO} + C_{p_{CO}}\left(T_{fuel_{inlet}} - T_r\right))$ = 2.715 x 10^{-8} (10160.4 + 1.211 x (1173 – 298.15))

= 0.305W

$m_{H_2}(LCV_{H_2} + C_{p_{H_2}}(T_{fuel_{inlet}} - T_r))$ = 2.715 x 10^{-8} (120094 + 15.4 x (1173 -298.15))

= 3.626W

$m_{CO_2}C_{p_{CO_2}}\left(T_{fuel_{inlet}} - T_r\right)$ = 4.89 x 10^{-7} x 1.272 x (1173-298.15)

= 0.544W

Total energy entering the C.V = $Q_{feed_{inlet}} + Q_{sweep_{inlet}}$

= 1.229 + 4.365 + 0.305 + 3.626 + 0.544 = **10.07W**

4.5.4 Energy leaving the control volume

$m_{O_2} C_{p_{O_2}} \left(T_{air_{outlet}} - T_r\right)$ = 1.0224 x 10^{-6} x 1.112 x (1226.843 – 298.15)

= 1.055W

$m_{O_2} C_{p_{O_2}} \left(T_{fuel_{outlet}} - T_r\right)$ = 3.4073 x 10^{-8} x 1.112 x (1227.503 – 298.15)

= 0.0352W

$m_{N_2} C_{p_{N_2}} \left(T_{air_{outlet}} - T_r\right)$ = 4.1648 x 10^{-6} x 1.2 x (1226.843 – 298.15)

= 4.641W

$m_{CO} \left(LCV_{CO} + C_{p_{CO}} \left(T_{fuel_{outlet}} - T_r\right)\right)$ = 3.6067 x 10^{-8} x (10160.4 + 1.22 x (1227.503 – 298.15))

= 0.4073W

$\boldsymbol{m_{H_2O} C_{p_{H_2O}} \left(T_{fuel_{outlet}} - T_r\right)}$ = 2.415 x 10^{-7} x 2.455 x (1227.503 – 298.15)

= 0.5509W

$m_{CO_2} C_{p_{CO_2}} \left(T_{fuel_{outlet}} - T_r\right)$ = 4.74 x 10^{-7} x 1.283 x (1227.503 – 298.15)

= 0.565W

Total heat transfer rate across the Membrane (from result reports of FLUENT), Q_m = 2.8804W

Total energy leaving the C.V = $Q_{feed_{outlet}} + Q_{sweep_{outlet}}$

= 1.055 + 0.0352 + 4.641 + 0.4073 + 0.5509 + 0.565 + 2.8804

= **10.13W**

The calculations above show that energy is balanced, and the numerical results are right in thermodynamic point of view.

CHAPTER 5

CONCLUSIONS AND RECOMMENDATIONS

This chapter comprises of two sections. The first section summarizes the results of the presemt work while the second section makes some recommendations that could further enhance future research.

5.1 Conclusions

In this thesis work, a two dimensional geometry was modeled to investigate the oxycombustion characteristics of synthetic gas in an OTR with the aid of computational fluid dynamics. The present work was able to study the permeation potential of LSCF-6428 membrane with a reactive gas, syngas, which comprises CO and H_2. A selective wall that served as the dense and non-porous membrane (ITM) separates the feed and sweep sides considered in this work. The membrane allows the permeation of only oxygen due to presence of oxygen vacancies in its crystal lattice. The permeation is modelled with the aid of UDF that is compiled and hooked to the FLUENT software. Air, which comprises nitrogen and oxygen served as the feed gas, while synthetic gas/CO_2 serves as the reactive/sweep gas. Two numerical models were considered in the work, one for the permeation (UDF) and the other for syngas reaction kinetics, which was imported via the CHEMKIN import with the transport and thermochemical data files. Validations of the two numerical models were performed by comparing the computational results with available experimental data, and there were reasonable agreements between the numerical results and recorded experimental data for both models.

5.1.1 Non-reactive case (separation only)

The essence of this section of the work is to study the permeation potential of the membrane in a cold combustion without activating the volumetric reaction of the FLUENT. From the results, the following conclusions can be inferred:

- The highest permeation occurs at the inlet section of the sweep zone because the oxygen partial pressure at that section is the lowest, and therefore highest partial pressure difference (ΔP), which is the driving force for permeation,
- Increasing the inlet temperature leads to increment in the amount of oxygen permeated as a result of bulk diffusion of oxygen at higher temperature,
- Increasing the sweep flow rate reduces the partial pressure of oxygen at the fuel side. This leads to more O_2 partial pressure differences and then more oxygen permeation.

5.1.2 Reactive case (combustion case)

The reactive case involves combustion due to the reaction between the permeated oxygen and the fuel. This is achieved by activating the volumetric reaction option of the FLUENT software. After the computational works were performed and analyzed, it was noticed that temperature rise and/or increase in partial pressure difference enhance more permeation. Hence, any parameter that raises the reactor temperature, the feed side oxygen partial pressure or reduces the sweep side oxygen partial pressure, will have favourable effects on oxygen permeation, and will enhance combustion of the reactive gas. In addition, certain conclusions can be arrived at from this work, which includes the following:

- Comparison between the reactive and non-reactive case showed that the reactive has more oxygen permeation potential than the non-reactive, with flux of about 4 times the non-reactive case,

- Increase in the inlet temperature increases the permeation potential and the reactor temperature. This can be attributed to the improvement in the combustion process due to the increase in the reaction rates, which affects the permeation flux,
- The location of the peak of oxygen permeation flux coincides with the location of the peak in combustion temperature of the reactor,
- Increasing the sweep (syngas and CO_2) flow rate raises the amount of fuel. This leads to more consumption of oxygen and more permeation as well as rise in the reactor temperature,
- Reducing the CO/H_2 ratio of synthetic gas increases the reactor temperature due to high ignition characteristics and flame speed of hydrogen, this further leads to more permeation. Although, this also results in delay in formation of flammable mixture due to increased amount oxygen required for combustion,
- CO_2 moderates the reactor temperature by reducing the reaction intensity and increasing the radiation losses, therefore, syngas with more CO_2 composition have lower temperature and consequently, lower permeation flux. CO_2 also behaves as an inhibitor in oxycombustion of synthetic gas,
- Comparison between syngas comprising CO and H_2 with the one comprising CO, H_2 and CH_4 shows that due to lower reactivity of CH_4, the case with CH_4 has lower reactor temperature and lower oxygen permeation flux.

5.2 Recommendations

The present work has been able to show the potential of ITM for oxycombustion with a stable and flexible reactive gas, syngas. In the present work, a simplified three-step reaction kinetics mechanism comprising CO, H_2 and CO_2 is used in the present work for oxidation of the fuel into

CO_2 and H_2O, but in reality, there will be other species like OH, H_2O_2, CH_4, N_2 and so on, depending on the method of gasification for syngas production. Hence, detailed reaction mechanism of syngas could be used to further investigate the effects and stability of those other species in the OTR. Furthermore, the utilized model for the permeation of oxygen in this work is based on oxygen partial pressure at bulk stream measured at the feed inlet and permeate outlet. Further works can still be made to quantify the oxygen concentration based on the local values at the vicinity of the membrane to cater for possible oxidation reaction at the membrane surface. Investigations on the optimization of ion transport membrane reactor for industrial applications could also be carried out. Further research on ITM can still be done by material scientists to improve oxygen permeation potential of ion transport membrane. It would also be interesting to investigate the use of ITM for oxygen selection from sources other than air. For example, from water after splitting into hydrogen and oxygen.

Nomenclature

Symbol	Definition	unit
A_{cell}	Area of cell	m^2
C_i	Density of oxygen ions	mol/m^3
C_p	Specific heat at constant pressure	kJ/kg-K
D_a	Ambipolar oxygen ion-electron hole diffusion coefficient	cm^2/sec
$D_{i,j}$	Diffusion coefficient of the component *i* in the component *j*	m^2/s
$D_{i,m}$	Diffusion coefficient in the mixture	m^2/s
D_v	Diffusion coefficient of oxygen vacancy	cm^2/sec
E	Activation energy	kJ/mol
ϵ	Emissivity	-
F	Faraday's constant	C/mol
$\dot{h}$	Electron hole	-
J_{O_2}	Oxygen permeation flux	mol/m^2-sec
k_f	Forward reaction rate	cm $atm^{-0.5}sec^{-1}$
k_{io}	Surface exchange coefficient	cm/sec
k_r	Reverse reaction rate	mol/cm^2-sec
L	Length of the tube	m

L_c	Characteristic membrane thickness	mm
LCV	Lower calorific value	kJ/kg
P	Total pressure	atm
PRESTO	Pressure Staggering Option	-
$P_{O_2}^0$	Atmospheric pressure	atm
$P_{O_2}^{'}$	Partial pressure of oxygen at the shell side or feed side	atm
$P_{O_2}^{''}$	Partial pressure of oxygen in the tube or permeate side	atm
$Q_{feedinlet}$	Total heat transfer rate entering the feed side of the membrane	W
$Q_{feedoutlet}$	Total heat transfer rate leaving the feed side of the membrane	W
Q_m	Total heat transfer rate across the membrane	W
$Q_{sweepinlet}$	Total heat transfer rate entering the sweep side of the membrane	W
$Q_{sweepoutlet}$	Total heat transfer rate leaving the sweep side of the membrane	W
q'	Volumetric flow rate of feed gas	cm^3/min
q''	Volumetric flow rate of sweep gas	cm^3/min
r_1	Inner radius of the tubular membrane	m
r_2	Outer radius of the tubular membrane	m
R	Ideal gas constant	J/mol K
$\vec{r}$	Position vector	-
S	Effective surface area of the tubular membrane	m^2

$\vec{s}$	Direction vector	-
$\vec{s}'$	Scattering direction vector	-
S_i	Source/ Sink term	Kg/m^3-s
T	Temperature	K
U	Velocity vector	m/s
V_{cell}	Volume of cell	m^3
$V_{\ddot{O}}$	Oxygen vacancy	-
X_i	Mole fraction	-
Y_i	Mass fraction	-
σ	Stefan-Boltzmann constant	W/m^2-K^4
σ_i	Ionic conductivity	Sm^{-1}
σ_e	Electronic conductivity	Sm^{-1}
σ_s	Scattering coefficient	m^{-1}
μ	Dynamic viscosity	kg/m-s
ρ	Fluid density	Kg/m^3

References

[1] "United Nations Climate Change Conference, 7-18 December, 2009," in *Copenhagen Summit*.

[2] "Fifth Annual Conference on Carbon Capture & Sequestration, Alexandria, U.S.A," 2006.

[3] B. Dawoud, E. Amer, and D. Gross, "Experimental investigation of an adsorptive thermal energy storage," *Int. J. energy Res.*, vol. 31, no. December 2010, pp. 135–147, 2007.

[4] J. Gibbins and H. Chalmers, "Carbon capture and storage," *Energy Policy*, vol. 36, no. 12, pp. 4317–4322, Dec. 2008.

[5] T. Fujimori and T. Yamada, "Realization of oxyfuel combustion for near zero emission power generation," *Proc. Combust. Inst.*, vol. 34, no. 2, pp. 2111–2130, Jan. 2013.

[6] M. B. Toftegaard, J. Brix, P. A. Jensen, P. Glarborg, and A. D. Jensen, "Oxy-fuel combustion of solid fuels," *Prog. Energy Combust. Sci.*, vol. 36, no. 5, pp. 581–625, Oct. 2010.

[7] K.Cobb,"http://www.resilience.org/stories/2007-02-01/best-method-carbon-sequestration." 2007.

[8] J. D. Figueroa, T. Fout, S. Plasynski, H. McIlvried, and R. D. Srivastava, "Advances in CO_2 capture technology—The U.S. Department of Energy's Carbon Sequestration Program," *Int. J. Greenh. Gas Control*, vol. 2, no. 1, pp. 9–20, Jan. 2008.

[9] A. Leo, S. Liu, and J. C. D. Da Costa, "Development of mixed conducting membranes for clean coal energy delivery," *Int. J. Greenh. Gas Control*, vol. 3, no. 4, pp. 357–367, Jul. 2009.

[10] P. Kutne, B. K. Kapadia, W. Meier, and M. Aigner, "Experimental analysis of the combustion behaviour of oxyfuel flames in a gas turbine model combustor," *Proc. Combust. Inst.*, vol. 33, no. 2, pp. 3383–3390, Jan. 2011.

[11] M. A. Nemitallah and M. A. Habib, "Experimental and numerical investigations of an atmospheric diffusion oxy-combustion flame in a gas turbine model combustor," *Appl. Energy*, vol. 111, pp. 401–415, Nov. 2013.

[12] C. Y. Liu, G. Chen, N. Sipöcz, M. Assadi, and X. S. Bai, "Characteristics of oxy-fuel combustion in gas turbines," *Appl. Energy*, vol. 89, no. 1, pp. 387–394, Jan. 2012.

[13] J. Wang, Z. Huang, H. Kobayashi, and Y. Ogami, "Laminar burning velocities and flame characteristics of CO–H_2–CO_2–O_2 mixtures," *Int. J. Hydrogen Energy*, vol. 37, no. 24, pp. 19158–19167, Dec. 2012.

[14] J. Rostrup-Nielsen, J. Sehested, and J. Norskov, "Hydrogen and Synthesis Gas by Steam- and CO_2 Reforming," *Adv. Catal.*, vol. 47, pp. 65–139, 2002.

[15] Q. Xie, S. Kong, Y. Liu, and H. Zeng, "Syngas production by two-stage method of biomass catalytic pyrolysis and gasification.," *Bioresour. Technol.*, vol. 110, pp. 603–9, Apr. 2012.

[16] A. S. Bodke, S. Bharadwaj, and L. Schmidt, "The effect of ceramic supports on partial oxidation of hydrocarbons over noble metal coated monoliths," *J. Catal.*, vol. 179, no. 1, pp. 138–149, 1998.

[17] P. Lv, Z. Yuan, C. Wu, L. Ma, Y. Chen, and N. Tsubaki, "Bio-syngas production from biomass catalytic gasification," *Energy Convers. Manag.*, vol. 48, no. 4, pp. 1132–1139, Apr. 2007.

[18] C. Ji, X. Dai, S. Wang, C. Liang, B. Ju, and X. Liu, "Experimental study on combustion and

emissions performance of a hybrid syngas–gasoline engine," *Int. J. Hydrogen Energy*, vol. 38, no. 25, pp. 11169–11173, Aug. 2013.

[19] Y. Zhang, T. Yang, X. Liu, L. Tian, Z. Fu, and K. Zhang, "Reduction of Emissions from a Syngas Flame Using Micromixing and Dilution with CO_2," *Energy & Fuels*, vol. 26, pp. 6595–6601, 2012.

[20] N. Ding, R. Arora, M. Norconk, and S.Y. Lee, "Numerical investigation of diluent influence on flame extinction limits and emission characteristic of lean-premixed H_2–CO (syngas) flames," *Int. J. Hydrogen Energy*, vol. 36, no. 4, pp. 3222–3231, Feb. 2011.

[21] V. Di Sarli, A. Basco, F. Cammarota, A. Di Benedetto, E. Salzano, V. Diocleziano, I. Chimica, and N. Federico, "FLAMMABILITY OF SYNGAS/CO_2 MIXTURES IN OXYGEN-ENRICHED AIR," in *XXXV Meeting of the Italian Section of the Combustion Institute*, 2012, pp. 1–6.

[22] T. C. Lieuwen, V. Yang, and R. Yetter, *SYNTHESIS GAS COMBUSTION: Fundamentals and Applications*. Boca Raton: CRC Press, Taylor & Francis Group, 2010.

[23] S. G. Davis, A. V. Joshi, H. Wang, and F. Egolfopoulos, "An optimized kinetic model of H_2/CO combustion," *Proc. Combust. Inst.*, vol. 30, no. 1, pp. 1283–1292, Jan. 2005.

[24] F. Liu, H. Guo, and G. J. Smallwood, "The chemical effect of CO_2 replacement of N_2 in air on the burning velocity of CH_4 and H_2 premixed flames," *Combust. Flame*, vol. 133, no. 4, pp. 495–497, Jun. 2003.

[25] D. Singh, T. Nishiie, S. Tanvir, and L. Qiao, "An experimental and kinetic study of syngas/air combustion at elevated temperatures and the effect of water addition," *Fuel*, vol. 94, pp. 448–456, Apr. 2012.

[26] N. Bouvet, S. Lee, I. Gökalp, and R. J. Santoro, "Flame Speed Characteristics of Syngas (H_2-CO) with Straight Burners for Laminar Premixed Flames," in *Proceedings of the European Combustion Meeting*, 2007, pp. 1–6.

[27] Y. Xie, J. Wang, M. Zhang, J. Gong, W. Jin, and Z. Huang, "Experimental and Numerical Study on Laminar Flame Characteristics of Methane Oxy-fuel Mixtures Highly Diluted with CO_2," *Energy & Fuels*, vol. 27, no. 10, pp. 6231–6237, Oct. 2013.

[28] S. K. Alavandi and A. K. Agrawal, "Experimental study of combustion of hydrogen–syngas/methane fuel mixtures in a porous burner," *Int. J. Hydrogen Energy*, vol. 33, no. 4, pp. 1407–1415, Feb. 2008.

[29] X. Dai, C. Ji, S. Wang, C. Liang, X. Liu, and B. Ju, "Effect of syngas addition on performance of a spark-ignited gasoline engine at lean conditions," *Int. J. Hydrogen Energy*, vol. 37, no. 19, pp. 14624–14631, Oct. 2012.

[30] B. K. Dam, N. D. Love, and A. R. Choudhuri, "Flame Stability of Methane and Syngas Oxy-fuel Steam Flames," *Energy & Fuels*, vol. 27, pp. 523–529, 2012.

[31] T. Takahashi, T. Esaka, and H. Iwahara, "Electrical conduction in the sintered oxides of the system Bi_2O_3-BaO," *J. Solid State Chem.*, vol. 16, no. 3–4, pp. 317–323, Jan. 1976.

[32] J. Sunarso, S. Baumann, J. M. Serra, W. A. Meulenberg, S. Liu, Y. S. Lin, and J. C. Diniz da Costa, "Mixed ionic–electronic conducting (MIEC) ceramic-based membranes for oxygen separation," *J. Memb. Sci.*, vol. 320, no. 1–2, pp. 13–41, Jul. 2008.

[33] J. Hong, P. Kirchen, and A. F. Ghoniem, "Numerical simulation of ion transport membrane reactors: Oxygen permeation and transport and fuel conversion," *J. Memb. Sci.*, vol. 407–408, pp. 71–85, Jul. 2012.

[34] N. D. Mancini and A. Mitsos, "Ion transport membrane reactors for oxy-combustion – Part I: intermediate-fidelity modeling," *Energy*, vol. 36, no. 8, pp. 4701–4720, Aug. 2011.

[35] A. P. Simpson and A. J. Simon, "Second law comparison of oxy-fuel combustion and post-combustion carbon dioxide separation," *Energy Convers. Manag.*, vol. 48, no. 11, pp. 3034–3045, Nov. 2007.

[36] K. Foy and J. McGovern, "Comparison of Ion Transport Membranes," in *Fourth Annual Conference on Carbon Capture and Sequestration*, 2005, pp. 1–11.

[37] A. A. Asadi, A. Behrouzifar, M. Iravaninia, T. Mohammadi, and A. Pak, "Preparation and Oxygen Permeation of $La_{0.6}Sr_{0.4}Co_{0.2}Fe_{0.8}O_{3-\delta}$ (LSCF) Perovskite-Type Membranes : Experimental Study and Mathematical Modeling," *Ind. Eng. Chem. Res.*, vol. 51, pp. 3069–3080, 2012.

[38] X. Tan and K. Li, "Modeling of Air Separation in a LSCF Hollow-Fiber Membrane Module," *Am. Inst. Chem. Eng.*, vol. 48, no. 7, pp. 1469–1477, 2002.

[39] P. N. Dyer, R. E. Richards, S. L. Russek, and D. M. Taylor, "Ion transport membrane technology for oxygen separation and syngas production," *Solid State Ionics*, vol. 134, pp. 21–33, 2000.

[40] L. Qiu, T. H. Lee, L. Liu, Y. L. Yang, and A. J. Jacobson, "Oxygen permeation studies of $SrCo_{0.8}Fe_{0.2}O_{3-\delta}$," *Solid State Ionics*, vol. 76, pp. 321–329, 1995.

[41] S. Zongping, W. Yang, Y. Cong, D. Hui, T. Jianhua, and X. Guoxing, "Investigation of the permeation behavior and stability of a $Ba_{0.5}Sr_{0.5}Co_{0.8}Fe_{0.2}O_{3-\delta}$ oxygen membrane," *J. Memb. Sci.*, vol. 172, pp. 177–188, 2000.

[42] H. Wang, Y. Cong, and W. Yang, "oxygen permeation study in a tubular

$Ba_{0.5}Sr_{0.5}Co_{0.8}Fe_{0.2}O_{3-\delta}$ oxygen permeable membrane," *J. Memb. Sci.*, vol. 210, pp. 259–271, 2002.

[43] M. A. Habib, P. Ahmed, R. Ben-Mansour, H. M. Badr, P. Kirchen, and A. F. Ghoniem, "Modeling of a combined ion transport and porous membrane reactor for oxy-combustion," *J. Memb. Sci.*, vol. 446, pp. 230–243, Nov. 2013.

[44] S. Kim, Y. L. Yang, A. J. Jacobson, and B. Abeles, "Oxygen surface exchange in mixed ionic electronic conductor membranes," *Solid State Ionics*, vol. 121, pp. 31–36, 1999.

[45] S. J. Xu and W. J. Thomson, "Oxygen permeation rates through ion-conducting perovskite membranes," *Chem. Eng. Sci.*, vol. 54, pp. 3839–3850, 1999.

[46] R. Ben Mansour, M. A. Habib, H. M. Badr, Azharuddin E, and M. Nemitallah, "Characteristics of Oxy-fuel Combustion in an Oxygen Transport Reactor," *Energy & Fuels*, vol. 26, pp. 4599–4606, 2012.

[47] N. D. Mancini and A. Mitsos, "Ion transport membrane reactors for oxy-combustion-Part II: Analysis and comparison of alternatives," *Energy*, vol. 36, no. 8, pp. 4721–4739, 2011.

[48] M. A. Habib, M. A. Nemitallah, and R. Ben-Mansour, "Recent development in oxy-combustion technology and its applications to gas turbine combustors and ITM reactors," *Energy and Fuels*, vol. 27, no. 1, pp. 2–19, 2013.

[49] M. A. Nemitallah, M. A. Habib, and R. Ben-mansour, "Design of an ion transport membrane reactor for application in fire tube boilers," *Energy*, vol. 81, pp. 787–801, 2015.

[50] M. A. Nemitallah, M. A. Habib, R. Ben-mansour, and A. F. Ghoniem, "Design of an ion transport membrane reactor for gas turbine combustion application," *J. Memb. Sci.*, vol. 450, pp. 60–71, 2014.

[51] M. A. Nemitallah, M. A. Habib, and R. Ben Mansour, "Investigations of oxy-fuel combustion and oxygen permeation in an ITM reactor using a two-step oxy-combustion reaction kinetics model," *J. Memb. Sci.*, vol. 432, pp. 1–12, 2013.

[52] R. Ben Mansour, M. A. Nemitallah, and M. A. Habib, "Numerical investigation of oxygen permeation and methane oxy-combustion in a stagnation flow ion transport membrane reactor," *Energy*, vol. 54, pp. 322–332, 2013.

[53] A. Behrouzifar, A. A. Asadi, T. Mohammadi, and A. Pak, "Experimental investigation and mathematical modeling of oxygen permeation through dense $Ba_{0.5}Sr_{0.5}Co_{0.8}Fe_{0.2}O_{3-\delta}$ (BSCF) perovskite-type ceramic membranes," *Ceram. Int.*, vol. 38, no. 6, pp. 4797–4811, Aug. 2012.

[54] J. Abrardo, D. Bennett, M. Carolan, C. Chen, W. Schinski, J. Steppan, and W. Waldron, "Development of the ITM Syngas ceramic membrane technology," in *2004 AIChE Spring National Meeting*, 2004, pp. 1406–1411.

[55] M. F. Carolan, C. M. Chen, J. Chen, C. F. Miller, E. Minford, and W. E. Waldron, "ITM Ceramic Membrane Technology to Product Synthesis Gas," in *ECS Transactions*, 2008, vol. 13, no. 26, pp. 319–325.

[56] C. M. Chen, D. L. Bennett, M. F. Carolan, E. P. Foster, W. L. Schinski, and D. M. Taylor, "ITM Syngas ceramic membrane technology for synthesis gas production," *Stud. Surf. Sci. Catal.*, vol. 147, pp. 55–60, 2004.

[57] X. Zhu, Q. Li, Y. He, Y. Cong, and W. Yang, "Oxygen permeation and partial oxidation of methane in dual-phase membrane reactors," *J. Memb. Sci.*, vol. 360, no. 1–2, pp. 454–460, 2010.

[58] C. F. Miller, J. Chen, M. F. Carolan, and E. P. Foster, "Advances in ion transport membrane technology for Syngas production," *Catal. Today*, vol. 228, pp. 152–157, 2014.

[59] U. Balachandran, T. H. Lee, S. Wang, and S. E. Dorris, "Use of mixed conducting membranes to produce hydrogen by water dissociation," *Int. J. Hydrogen Energy*, vol. 29, no. 3, pp. 291–296, 2004.

[60] K. Lee, Y. Choe, J. Lee, and H. Hwang, "Fabrication of a Microtubular $La_{0.6}Sr_{0.4}Ti_{0.2}Fe_{0.8}O_{3-\delta}$ by Electrophoretic Deposition for Hydrogen Production," *Adv. Mater. Sci. Eng.*, pp. 1–7, 2015.

[61] H. Wang, S. Gopalan, and U. B. Pal, "Hydrogen generation and separation using $Gd_{0.2}Ce_{0.8}O_{1.9-\delta}$ -$Gd_{0.08}Sr_{0.88}Ti_{0.95}Al_{0.05}O_{3\pm\delta}$," *Electrochimica Acta*, vol. 56, no. 20. pp. 6989–6996, 2011.

[62] H. Jiang, F. Liang, O. Czuprat, K. Efimov, A. Feldhoff, S. Schirrmeister, T. Schiestel, H. Wang, and J. Caro, "Hydrogen production by water dissociation in surface-modified $BaCo_xFe_yZr_{1-x-y}O_{3-\delta}$ hollow-fiber membrane reactor with improved oxygen permeation," *Chem. - A Eur. J.*, vol. 16, no. 26, pp. 7898–7903, 2010.

[63] U. Balachandran, T. Lee, and S. Dorris, "Hydrogen production by water dissociation using mixed conducting dense ceramic membranes," *Int. J. Hydrogen Energy*, vol. 32, no. 4, pp. 451–456, 2007.

[64] C. Y. Park, T. H. Lee, S. E. Dorris, and U. Balachandran, "Hydrogen production from fossil and renewable sources using an oxygen transport membrane," *Int. J. Hydrogen Energy*, vol. 35, no. 9, pp. 4103–4110, 2010.

[65] W. Li, X. Zhu, Z. Cao, W. Wang, and W. Yang, "Mixed ionic-electronic conducting

(MIEC) membranes for hydrogen production from water splitting," *Int. J. Hydrogen Energy*, vol. 40, no. 8, pp. 3452–3461, 2015.

[66] C. Y. Park, T. H. Lee, S. E. Dorris, Y. Lu, and U. Balachandran, "Oxygen permeation and coal-gas-assisted hydrogen production using oxygen transport membranes," *Int. J. Hydrogen Energy*, vol. 36, no. 15, pp. 9345–9354, 2011.

[67] A. E. Farooqui, M. A. Habib, H. M. Badr, and R. Ben-mansour, "Modeling of ion transport reactor for oxy-fuel combustion," *Int. J. Engine Res.*, vol. 37, pp. 1265–1279, 2013.

[68] A. E. Farooqui, H. M. Badr, M. A. Habib, and R. Ben-mansour, "Numerical investigation of combustion characteristics in an oxygen transport reactor," *Int. J. Engine Res.*, 2013.

[69] M. A. Habib, R. Ben Mansour, and M. A. Nemitallah, "Modeling of oxygen permeation through a LSCF ion transport membrane," *Comput. Fluids*, vol. 76, pp. 1–10, May 2013.

[70] M. Coroneo, G. Montante, M. Giacinti Baschetti, and a. Paglianti, "CFD modelling of inorganic membrane modules for gas mixture separation," *Chem. Eng. Sci.*, vol. 64, no. 5, pp. 1085–1094, Mar. 2009.

[71] L. Anetor, E. Osakue, and C. Odetunde, "Reduced Mechanism Approach of Modeling Premixed Propane-Air Mixture Using ANSYS Fluent," *Eng. J.*, vol. 16, 2012.

[72] A. von Hippel, *Molecular Engineering.*, vol. 123, no. 3191. Boston (Mass.) : McGraw-Hill, 1956.

[73] R. Ben-Mansour, M. A. Habib, and P. Ahmed, "The effect of radiation on oxy-fuel combustion characteristics in microchannels," *Appl. Mech. Mater.*, vol. 302, pp. 49–54, 2013.

[74] Fluent Inc., "Fluent 6.3 User's guide,." Fluent Inc., Lebanon. NH, 2006.

[75] M. A. Rajhi, R. Ben-Mansour, M. A. Habib, M. A. Nemitallah, and K. Andersson, "Evaluation of gas radiation models in CFD modeling of oxy-combustion," *Energy Convers. Manag.*, vol. 81, pp. 83–97, 2014.

[76] S. V. Patankar, *Numerical Heat Transfer and Fluid Flow*. Hemisphere Publishing Corporation, 1980.

[77] "http://www.reactiondesign.com/products/chemkin-cfd/." .

[78] C. K. Westbrook and F. L. Dryer, "Chemical kinetic modeling of hydrocarbon combustion," *Prog. Energy Combust. Sci.*, vol. 10, no. 1, pp. 1–57, Jan. 1984.

[79] A. Cuoci, A. Frassoldati, T. Faravelli, and E. Ranzi, "Accuracy and Flexibility of Simplified Kinetic Models for CFD applications," *Ital. Sect. Combust. Inst. Combust. Colloquai*, pp. 1–6, 2009.

[80] K. Li, X. Tan, and Y. Liu, "Single-step fabrication of ceramic hollow fibers for oxygen permeation," *J. Memb. Sci.*, vol. 272, pp. 1–5, 2006.

[81] R. S. Barlow, G. J. Fiechtner, C. D. Carter, and J. Y. Chen, "Experiments on the scalar structure of turbulent $CO/H_2/N_2$ jet flames," *Combust. Flame*, vol. 120, no. 4, pp. 549–569, Mar. 2000.

[82] H. S. Fogler, *Elements of Chemical Reaction Engineering*, Fourth. Prentice Hall PTR International Series, 2006.

[83] Y. Wei, J. Tang, L. Zhou, J. Xue, Z. Li, and H. Wang, "Oxygen Separation through U-Shaped Hollow Fiber Membrane Using Pure CO_2 as Sweep Gas," *Am. Inst. Chem. Eng.*, vol. 58, no. 9, pp. 2856–2864, 2012.

[84] J. Natarajan, T. Lieuwen, and J. Seitzman, "Laminar flame speeds of H_2/CO mixtures:

Effect of CO_2 dilution, preheat temperature, and pressure," *Combust. Flame*, vol. 151, no. 1–2, pp. 104–119, 2007.

[85] D. Lapalme and P. Seers, "Influence of CO_2, CH_4, and initial temperature on H_2/CO laminar flame speed," *Int. J. Hydrogen Energy*, vol. 39, no. 7, pp. 3477–3486, 2014.

[86] J. Andersen, C. L. Rasmussen, T. Giselsson, and P. Glarborg, "Global combustion mechanisms for use in CFD modeling under oxy-fuel conditions," *Energy and Fuels*, vol. 23, no. 3, pp. 1379–1389, 2009.

Vitae

Name: Salaudeen Shakirudeen Alade

Nationality: Nigerian

Date of Birth: 30th January, 1986

Email: Shakrudeen@gmail.com, g201303450@kfupm.edu.sa

Address: 4, Iyewa street, off Kogberegbe street,

Isolo, Lagos state, Nigeria.

Academic Qualifications:

- Master of Science (MS) Mechanical Engineering, King Fahd University of Petroleum and Minerals, Saudi Arabia.
- Bachelor of Technology (B.Tech) Mechanical Engineering, Ladoke Akintola University of Technology, Nigeria.

Journal Publications and Conference Presentations:

- Mohamed A Habib, Shakirudeen A. Salaudeen, Medhat A. Nemitallah, Esmail M.A Mokheimer, and Rached Ben-Mansour, "Numerical investigation of syngas oxy-combustion inside a LSCF-6428 oxygen transport reactor membrane". Accepted by Energy.
- K.A. Khalid, S.A. Salaudeen, A.S. Yassen, and M.A. Antar, "Experimental investigation on the performance of a cross flow air heated humidifier" ASME 2015 International Mechanical Engineering Congress & Exposition (IMECE-2015), Houston, Texas, USA.

- Shakirudeen A. Salaudeen, Medhat A. Nemitallah, and Mohamed A. Habib, "Syngas Oxygen Transport Reactor", 5th Annual Meeting of the Saudi Arabian Section of the Combustion Institute, KACST, Riyadh, Saudi Arabia (2015).
- Bamidele Olufemi Eyitope, Salaudeen Shakirudeen Alade, Mohamed Ifras Zubair, Araoye Abdulrazaq Adeniyi, and Luai Al-Hadhrami, "Numerical Analysis of Spray Coating Processes". International Journal of Modern Engineering Research, Vol. 5 Issue: 5 pp: 1-13, (2015).